1983-06

The effects of environment and dwell on high temperature fatigue crack growth of 2 1/4 Cr - 1 Mo steel.

Kamen, John S.

Monterey, California. Naval Postgraduate School

NAVAL POSTGRADUATE SCHOOL
Monterey, California

THESIS

THE EFFECTS OF ENVIRONMENT AND DWELL
ON HIGH TEMPERATURE FATIGUE CRACK GROWTH
OF 2 1/4 Cr - 1 Mo STEEL

by

John S. Kamen

June 1983

Thesis Advisor: K. D. Challenger

REPORT DOCUMENTATION PAGE		READ INSTRUCTIONS BEFORE COMPLETING FORM
1. REPORT NUMBER	2. GOVT ACCESSION NO.	3. RECIPIENT'S CATALOG NUMBER
4. TITLE (and Subtitle) The Effects of Environment and Dwell on High Temperature Fatigue Crack Growth of 2 1/4 Cr - 1 Mo Steel		5. TYPE OF REPORT & PERIOD COVERED Master's Thesis; June 1983 6. PERFORMING ORG. REPORT NUMBER
7. AUTHOR(s) John S. Kamen		8. CONTRACT OR GRANT NUMBER(s)
9. PERFORMING ORGANIZATION NAME AND ADDRESS Naval Postgraduate School Monterey, California 93940		10. PROGRAM ELEMENT, PROJECT, TASK AREA & WORK UNIT NUMBERS
11. CONTROLLING OFFICE NAME AND ADDRESS Naval Postgraduate School Monterey, California 93940		12. REPORT DATE June 1983 13. NUMBER OF PAGES 117
14. MONITORING AGENCY NAME & ADDRESS(if different from Controlling Office)		15. SECURITY CLASS. (of this report) Unclassified 15a. DECLASSIFICATION/ DOWNGRADING SCHEDULE

16. DISTRIBUTION STATEMENT (of this Report)
Approved for public release; distribution unlimited.

17. DISTRIBUTION STATEMENT (of the abstract entered in Block 20, if different from Report)

18. SUPPLEMENTARY NOTES

19. KEY WORDS (Continue on reverse side if necessary and identify by block number)
2]/4 Cr -] Mo Steel , Creep - Fatigue Interaction
High Temperature Fatigue Crack Growth
Environment Effects on Fatigue Crack Growth
Oxidation Effects on Fatigue Crack Growth

20. ABSTRACT (Continue on reverse side if necessary and identify by block number)
The effects of the environment and dwell periods on fatigue crack growth rates at 525°C for both annealed and normalized and tempered 2 1/4 Cr - 1 Mo steel in High Strain Fatigue (HSF) and Linear Elastic Fracture Mechanics (LEFM) regimes in air and in vacuum have been examined using optical and scanning electron microscopy techniques. Fatigue crack propagation rates were determined and were found to vary with

(20. ABSTRACT Continued)

the environment and the loading waveform used in the tests. At small crack depths in HSF, oxidation in air increased cyclic crack growth rates by over an order of magnitude compared with vacuum. For continuous cycling tests at a frequency of 0.01 Hz, and tests with a peak tension, compression, or tension plus compression dwell cycling, the rates were similar. The fastest crack growth in air occurred during cycles having both tension and compression dwell periods. Fractographs were analyzed in attempts to understand the reasons for the different propagation rates. Evidence suggesting partial rewelding of the crack surfaces during compressive dwell periods in vacuum and a change in fracture mode from transgranular to a branching "intergranular-like" fracture when the environment was changed from air to vacuum were observed.

Approved for public release, distribution unlimited.

The Effects of Environment and Dwell on High Temperature Fatigue Crack Growth on 2 1/4 Cr - 1 Mo Steel

by

John Sander Kamen
Lieutenant, United States Navy
B.S.M.E., United States Naval Academy, 1977

Submitted in partial fullfillment of the
requirements for the degree of

MASTER OF SCIENCE IN MECHANICAL ENGINEERING

from the

NAVAL POSTGRADUATE SCHOOL
June 1983

ABSTRACT

The effects of the environment and dwell periods on fatigue crack growth rates at 525°C for both annealed and normalized and tempered 2 1/4 Cr - 1 Mo steel in High Strain Fatigue (HSF) and Linear Elastic Fracture Mechanics (LEFM) regimes in air and in vacuum have been examined using optical and scanning electron microscopy techniques. Fatigue crack propagation rates were determined and were found to vary with the environment and the loading waveform used in the tests. At small crack depths in HSF, oxidation in air increased cyclic crack growth rates by over an order of magnitude compared with vacuum. For continuous cycling tests at a frequency of 0.01 Hz, and tests with a peak tension, compression, or tension plus compression dwell cycling, the rates were similar. The fastest crack growth in air occurred during cycles having both tension and compression dwell periods. Fractographs were analyzed in attempts to understand the reasons for the different propagation rates. Evidence suggesting partial rewelding of the crack surfaces during compressive dwell periods in vacuum and a change in fracture mode from transgranular to a branching "intergranular-like" fracture when the environment was changed from air to vacuum were observed.

TABLE OF CONTENTS

LIST OF TABLES

LIST OF FIGURES

I. INTRODUCTION

2 1/4 Cr - 1 Mo alloy steel has been used extensively as a structural material in elevated temperature applications by the power generation industry. Recently, it has been chosen as the steam generator material for the Clinch River Liquid Metal Fast Breeder Reactor (CRLMFBR). In Naval applications, 2 1/4 Cr - 1 Mo is used in 1200 psi boiler systems, tubing, fittings, steam lines, and valves. The excellent heat transfer characteristics of advanced heat exchanger systems (liquid sodium cooled in the CRLMFBR system) can introduce thermal transients; when these combine with flow induced vibration, and equipment service and repair time, large cyclic strain ranges result as a consequence. Therefore, the elevated temperature fatigue behavior that involves long constant strain dwell periods in the loading wave forms of this material must be defined.

Over the past several years, a large research program has been conducted to analyze this material's behavior in order to develop viable design criteria for long term high temperature service. However, uncertainties still exist particularily regarding long term prediction of material behavior out to projected component lifetimes of 30 to 40 years. In all this work, mechanical testing has been accelerated so that these predictions can be made using

data from tests of much shorter duration. The extrapolation used in this process, therefore, incorporates rather severe assumptions concerning the long term metallurgical stability of these alloys and the mechanisms of deformation and fracture. It has been recognized that the environment plays an important and perhaps dominant role in governing the elevated temperature fatigue behavior of this and other materials. This role, however, has not been investigated thoroughly in relation to the various loading conditions in different environments that could be experienced. The current ASME (American Society of Mechanical Engineers) Boiler and Pressure Vessel Code approach to elevated temperature fatigue assumes that the lower endurances noted in tests were dwell introduced in the fatigue cycle results from creep damage, not environmental damage (oxidation). Hence their methods to extrapolate laboratory data to long term service conditions use a creep model as their basis. If environment-related damage is the dominant damage mechanism, then the extrapolation methods are in error, and environmental effects should be incorporated into the design criteria.

It is the intent of this thesis to investigate the environmental effects on the elevated temperature fatigue behavior of annealed and normalized and tempered 2 1/4 Cr - 1 Mo steel in High Strain Fatigue (HSF) and Linear Elastic Fracture Mechanics (LEFM) regimes, and in

particular to determine the effects of different loading waveforms in air and in vacuum. Fatigue tests specimens were examined using metallographic and fractographic techniques with optical and scanning electron microscopy to evaluate the mode of fracture. Fatigue crack growth rates were plotted as a function of peak crack depth for different plastic strain ranges and frequencies to determine crack growth equations.

II. BACKGROUND INFORMATION

In the past, exhaustive studies have been completed on the mechanisms of fatigue crack growth in high temperature structural materials, however, these studies usually concerned themselves with the microstructural aspects of fatigue in metals, or creep-fatigue interaction [Ref. 1,2]. Relatively little work has been devoted to explain the environmental mechanisms and their effects on elevated temperature fatigue crack growth. Recently there have been developments of plausible mechanisms for this elevated temperature fatigue damage phenomenon, and the research reported here outlines previous investigations in this area.

Early work concerning the influence of the environment on elevated temperature fatigue crack propagation of metals investigated many aspects [Ref. 3], however, most work fell into two categories: high frequency fatigue and low frequency fatigue. In high frequency fatigue tests, stress was usually controlled over a small cyclic strain range; low frequency fatigue was usually strain controlled. In various high frequency fatigue tests, the endurances in air and vacuum or "inert" environments produced interesting results. In high frequency reversed bend tests on lead performed by Snowden [Ref. 4] there were two orders of

magnitude difference in fatigue life between vacuum, air, and pure oxygen. At all strain levels, endurances in a vacuum environment exceeded those in air. This behavior was observed by Naghitgull [Ref. 5] in the Co-base alloys S-816 and the Ni-base alloy Inconel 550, although the effect was smaller. Endurances for the Ni-base alloy converged at low stresses indicating the possible strengthening effect of air. Similar convergence of air and vacuum data was noted for AISI 316 steel at 837°C and a crossover occurred for nickel, where it was suggested that the oxide in cracks could prolong life in air at low stresses. A crossover was also noted in a ferritic stainless steel. Metallographic observations by Coffin [Ref. 6] on fatigue tested austenitic steel at 500°C, showed that oxidation formed preferentially on grain boundaries, and that the width of the heavily oxidized zone increased as strain range was reduced. This suggested that cyclic strain caused cracking of the oxide along grain boundaries, and thus accelerating subsequent oxidation.

In tests involving low frequency fatigue, the high strain amplitudes incorporated with hold times produced different effects than those noted at high frequency. White [Ref. 7] conducted low frequency (1 cycle/m) reverse bend tests on a low alloy steel at 500°C and found that fatigue endurances differed with the environment and the loading form. Endurances in an argon environment were twice those

in air. Also, introduction of a 30 minute hold time at zero stress in air did not affect endurance, but hold times of 30-300 minutes in tension progrsesively reduced it. The contribution of creep damage and oxidation under stress was assessed by testing a 1/2% Mo steel in vacuum and in air at 500°C. A 30 minute tension hold reduced the fatigue endurance relative to the continuously cycled specimens in vacuum indicating a creep component of damage. However, specimens cycled in air continuously, or with 30 minute hold periods displayed even lower endurances than comparative tests in vacuum. Thus White concluded that both oxidation and creep during hold periods in fatigue lowered endurance; however, from endurance curves it was shown that oxidation had more serious effect than did creep.

Metallography performed by White on these high temperature fatigue specimens in air revealed trangranular and oxidized cracks on the continuously cycled test. With hold times of 30 to 300 minutes at maximum strain, the surface which was in tension during the hold time displayed a mixture of intergranular and transgranular cracking. The surface that was in compression during the hold time had short, wide, transgranular cracks with blunt ends. In vacuum, some light oxidation of the crack surface appeared but it was far less than the air test. In the continuous cycling test, fine transgranular cracking occurred; the 30 minute hold time tests had intergranular cracks on the

tension side with trangranular cracks on the compression side.

Further study of elevated temperature low cycle fatigue behavior with hold times was conducted by Lord and Coffin [Ref. 8] on Cast Rene-80, an aircraft engine turbine bucket alloy. The purpose of their study was to: (1) determine whether a complex wave form involving tensile and compressive strain hold periods gave different predictions of life from those based on extrapolation of continuously cycled, triangular waveforms, fully reversed, results; and (2) whether the fracture mode was altered by the wave shape under these long hold time conditions. Lord and Coffin observed that when the hold times were equal in tension and compression, the fatigue life agreed closely with those predicted from continuous cycling results. A pronounced difference in life was found, however, when the loading wave form involved tension only or a compression only cycling. Surprisingly, compression only hold periods reduced the fatigue lives from those found in continuous cycling, while tension hold periods increased the fatigue life. Metallographic examination displayed transgranular crack propagation through the material, with an oxide layer coating the crack.

It is thus clear that the behavior of materials cannot be generalized as to its response to elevated temperature fatigue, but are different for each material.

Haigh, Skelton, and Richards [Ref. 9] investigated the oxidation-assisted crack growth during high cycle fatigue of a 1 Cr-Mo-V steel at high temperatures. Crack growth rates were described by Linear Elastic Fracture Mechanics (LEFM), and they were found to be highly dependent on oxidation.

Further work by Skelton [Ref. 10] investigated the crack growth during high strain fatigue of 0.5 Cr-Mo-V steel at 500°C. This paper discussed the effects of oxidation on fatigue crack growth with regards to hold periods, and also attempted to separate the initiation and propagation stages of fatigue fracture to give a more reliable explanation of each.

In this work, push-pull specimens were machined out of material trepanned from a large turbine casting and fatigue tested in air and vacuum environments. Some of the push-pull specimens were heat treated from a ferritic microstructure with approximately 5% pearlite to a granular bainitic microstructure. In continuous cycling tests, Skelton observed that for a given strain range and crack length, the crack propagation rate under vacuum was less than in air except at large crack depths and the lowest strain range ($\varepsilon p = 0.002$). In both cases, cracks were transgranular however those tested in air contained an oxide layer. For the tests conducted with half hour dwells in

tension at the lower strain ranges, the cracks propagated faster in both air and vacuum as compared with those continuous cycled, and the mode of fracture was intergranular. Several fatigue tests were also performed with a 7 hour dwell in tension; for both air and vacuum, the cyclic crack propagation rates were close to the half hour dwell test. This saturation of crack growth after long dwell periods at elevated temperatures hints that the dominant mechanism is environmentally controlled and not creep.

In other work on elevated temperature fatigue, Teranishi and McEvily [Ref. 11] investigated the effect of oxidation on both tension and compression hold time fatigue behavior of 2.25 Cr - 1 Mo steel. Their observations also indicated that hold periods heavily influenced high temperature fatigue behavior; however, they directly related fatigue behavior to the oxide that formed during the hold periods. Teranishi and McEvily noted that on going into compression after a tension hold, the oxide formed during the hold period spalled off. In contrast, on going into tension after a compression hold, the oxide cracked but did not spall off. Teranishi and McEvily postulated that by the oxide cracking and not spalling, local stress and strain concentrators are created which facilitate nucleation of fatigue cracks. This suggested that in the absence of oxidation effects, a tension hold may be more deterious

than a compression hold for this alloy. Although Teranishi and McEvily's work concerned itself mostly with crack initiation, their theory can be related to crack growth and crack branching.

In complementary work, Skelton and Haigh [Ref. 12] reported on fatigue crack growth rates and thresholds in steels under different environmental conditions. In their work, the effect of R (minimum load/maximum load) and loading frequency on fatigue crack growth in tests on Cr-Mo-V steels at 550°C was investigated under oxidizing and vacuum conditions. The results were described by linear elastic fracture mechanics (LEFM) using just the tensile loading to calculate the stress intensity amplitude ΔK.

At R = 0, zero to tension loading in air, lowering the frequency from 1.0 to 0.01 Hz generally increased the rate of crack propagation. For equal tension and compression loading in air (R = 1), crack growths were always higher, and the thresholds ΔK_o were also reduced. Thus it was possible to restart cracks stopped at R = 0 by the addition of equal compression loading. At R = 0, tension to tension loading in air, it was found that crack growth rates increased with increasing R up to a plateau. Under a vacuum environment, the results were somewhat different. Haigh and Skelton compared crack growth rates in air and under vacuum and noted that the propagation rates were

larger in air than under vacuum. Also there was a smaller effect of fatigue frequency with a vacuum environment.

In work concerning nuclear steam generator design; Brinkman, et al. [Ref. 13], investigated time dependent strain controlled fatigue behavior of annealed 2 1/4 Cr - 1 Mo steel. Brinkman's results related closely to Skelton's and White's research in low alloy steel but differed from those of Lord and Coffin on Cast Rene 80. Fully reversed strain-controlled push-pull fatigue tests of specimens from several heats of isothermally annealed commercial 2 1/4 Cr - 1 Mo steel were conducted in air at elevated temperature. Brinkman, et al., found that the fatigue life depended on the strain range, temperature, strain rate, cyclic wave form, and the particular heat of the material used. The fatigue life was reduced when either tension or compression strain hold periods were introduced in each cycle. Compressive hold periods had the more pronounced effect, and a further reduction in fatigue life occurred when duration of the compressive hold period was increased.

The most recent work on 2 1/4 Cr - 1 Mo steel was reported by Challenger et al. [Ref 14]. They addressed the question of whether creep fatigue interaction or environmental fatigue interaction was responsible for the greatly reduced fatigue life for specimens tested with various waveforms (tension, compression, or tension plus compression

hold periods at maximum strain) compared with the continuously cycled specimens at the same temperatures. Challenger et al. showed that the waveform effects in an oxidizing environment dominate crack initiation and that initiation can be considered to have occurred as soon as a circumferential crack in the oxide occurs. This idea was the basis for a model developed by Challenger, Miller, and Langdon [Ref. 15]. In their work on environmental fatigue, however, certain deficiencies in their model exist due to uncertainties regarding the effect of waveform on crack growth, and this was the primary motivation for this research.

Concerning the fractography of fatigue investigations, in 1951 Zapple and Worden [Ref. 16] observed an effect that seemed characteristic of some fatigue fracture surfaces, namely the appearance of fine striations. It was not until 1960 when the classic paper correlating fatigue crack growth rates and striation spacing was written by Forsyth and Ryder [Ref. 17], and later substantiated by them in 1961 [Ref. 18]. They observed a one to one correspondence between the number of loading cycles experienced by the material and the number of striations present in a precracked specimen. Also noted was that larger fatigue strain ranges produced wider striation spacing in the same material.

Fatigue striations can assume many forms and it is not absolutely clear why there are different morphologies.

Often associated with the different morphologies during crack propagation is the difference in testing environments. Fatigue striations tend to assume a cleavage-like appearance when formed in an aggressive environment, but appear more ductile when formed in an inert environment. Exposure to oxidizing and high temperature environments have resulted in completely obliterating fatigue striations making it difficult to detect them [Ref. 19].

III. EXPERIMENTAL

A. MATERIAL AND HEAT TREATMENT

The specimens of 2 1/4 Cr - 1 Mo steel examined in this work are specimens from high temperature fatigue tests performed by R. P. Skelton and K. D. Challenger at the Central Electricity Research Laboratories (CERL), Leatherhead, Surrey, United Kingdom. Two heats of steel were tested. The first heat, demoted XLM, was supplied as 32mm diamter bar. It was annealed by heating to 950°C for 1 hour, cooled to 700°C in 3 hours, held for 2 hours at 700°C, and then furnace cooled. The other heat was supplied by the UKAEA as normalized and tempered (N&T) plate. The original forging was held at 960°C for 6 hours and water quenched; tempering followed with the steel being held at 690°C for 12 hours, and then cooled at 23°C per hour. The compositions of the two heats of 2 1/4 Cr - 1 Mo steel are given in Table I.

B. FATIGUE TESTING

The cylindrical shaped specimens machined for testing in high strain fatigue (HSF) had a diameter and gauge length of 12.7mm (0.5in). A shallow starter notch, approximately 0.3mm deep, was cut as a chord in the center of the gauge to forego crack initiation effects in the testing. Rectangular specimens for the Linear Elastic

Fracture Mechanics tests were cut to 8 x 25mm cross sections and were notched approximately 5mm; maintaining a specimen depth to width ratio of 0.2.

The specimens were all subjected to fully reversed, axial push-pull cyclic loading using servo-controlled closed loop electrohydraulic or servo-electric fatigue testing machines. All experiments were performed at 525°C in either air or vacuum. The vacuum was maintained at 1.3 mPa (10^{-5} torr). The testing frequency during continuous cycling was approximately 10^{-2} Hz for the HSP and LEFM tests; the HSF tests used a triangular strain controlled waveform and the LEFM tests used a sinusoidal load controlled waveform. On most HSF specimens, 1/2 hour dwell periods were imposed at the maximum strains in tension (T), compression (C), or tension plus compression (T+C). These half hour dwell tests were conducted at 0.2% cyclic plastic strain. The continuous cycled HSF tests were conducted at cyclic plastic strain ranges of 0.2, 0.1, 0.02 percent for each increment of crack growth; with several strain ranges being possible on a single specimen. Figure 1 shows typical strain vs. time plots and stress/strain hysteresis loops for each of the four types of tests made. In the continuous cycling tests on the LEFM specimens the alternating gross stress was initially kept at ±115 MPa in vacuum resulting in cyclic stress intensity range ΔK (tensile value only) variation from 12 - 20 MPa $m^{1/2}$ as the crack increased in depth.

After about 7mm of crack growth, air was admitted into the system and corresponding growth rates were determined with similar ΔK ranges which required a reduced stress of ± 60 MPa.

To measure the crack growth rates for both the HSF and LEFM tests, D.C. potential drop methods were used to measure crack depths up to approximately 6mm in HSF and 15mm in LEFM tests. For the rectangular specimens (LEFM) there was a direct correspondence with crack depth and potential drop calibration. For the thumbnail shaped cracks observed in the cylindrical specimens (HSF), the calibration was verified by using a measurement of peak depth from obvious marking on the fracture surface which resulted from large strain changes during testing in air or changes in the wave shape in vacuum and comparing that crack length to the calculated crack length from the calibration curves.

Because of the vacuum chamber, conventional extensiometry could not be employed, so the dwell tests in HSF were not carried out at constant total strain. Instead, displacement control was affected remotely, resulting in some elastic follow up in the gauge. Figure 2 shows a typical hysteresis loop and indicates that these tests are a compromise between dwells at constant total strain and constant stress.

After significant crack propagation, the specimens were cut perpendicular to the crack surface. Half of the specimen was mounted for optical microscopy to show the total shape

of the crack and the oxide formation. After mounting, the specimens were polished and then etched in 2% Nital solution for 8 seconds. The optical metallography was performed on a Zeiss research optical microscope. The other half of the specimen was pulled apart and separated; these fracture surfaces were mounted for fractographic examination. A Cambridge Stereoscan scanning electron microscope was used for all examinations. Fracture surfaces with thick layers of oxide were partially cleaned with cellulose acetate replicating tape. However, the oxide was so thick and adherent that an inhibited HCL solution was frequently used to remove the oxide. All the fracture surfaces were reviewed for comparison of the different loading regions. The exact location of the fracture surface under observation was determined from the positioning calipers in the stage of the scanning electron microscope. Where striations were distinguishable, striations spacing was measured. The procedures for these measurements follows: several photographs of the fracture surface with distinguishable striations were taken using the scanning electron microscope at magnifications of approximately 500 - 1000X. Measurements of the striation spacings were then made using a line intercept technique. Averages of these measurements were tabulated for comparison.

IV. RESULTS

A. HSF CRACK PROPAGATION

The crack growth rates have been plotted as a function of peak crack depth for the continuous cycled and dwell period tests in air and in vacuum for the annealed and the normalized and tempered material.

1. Continuous Cycling in Air

The results for the continuous cycled in air for the annealed material are given in Figure 3, and for the normalized and tempered material in Figure 4. The crack growth rates for the two different heat treatments are compared in Figure 5. From Figures 3-5 it is seen that the growth rate is a function of plastic strain range, $\Delta\varepsilon_p$. At the largest plastic strain range, 0.2%, the growth rates for the N+T (normalized and tempered) material were greater than those for the annealed material, however, this effect was reversed at the smallest strain range investigated, 0.02%.

For both heats, the cracks were transgranular with a layer of oxide coating the crack surface. Figures 6 and 7 show unetched views of the cracks. Both cracks were relatively straight, and propagation occurred perpendicular to the straining direction. The crack of the annealed material had a jagged appearance (see Figure 6), and upon

further investigation at higher magnifications the oxide was found to occasionally grow outward away from the crack in small protrusions. These protrusions varied from small pockets of oxide to sharp lines of oxide perpendicular to the propagation direction (see Figure 8) possibly indicating crack branching. Initially from the pattern of these branches, it was thought that they had formed near inclusions, however this was not the case. The branches did not favor either intergranular or transgranular growth. No change in the crack propagation path due to changing strain range was observed.

The crack for the normalized and tempered material was wider than that of the annealed material, possibly indicating a greater tendency for oxidation under these conditions (see Figure 7). Higher mangification photos of the N+T material are given in Figure 9. These photos indicate a slight tendency for crack branching with small thin lines of oxide extending away from the crack. Major branching was also observed, Figure 9. The crack morphology is dependent upon the plastic strain range, where at larger strains, the crack had more oxide branching and a rougher appearance.

Fractography results are given in Figures 10-12 for the annealed heat, and 13 and 14 for the N+T heat. For the annealed material, Figure 10 displays different zones in the fracture surface where the plastic strain range was changed. It is evident from the zone lines that the crack

progressed with a "finger-nail" type crack front away from the starter notch. Ridges extend radially from the starter notch and are noted by the white lines on the surface in Figure 10. Oxide was removed from the majority of the fracture surface, however, some of the thick oxide formed early in the test could not be removed. Higher magnification fractographs of the annealed fracture surface are given in Figures 11 and 12. The surfaces coinciding with the larger plastic strains were slightly rougher than the smaller strain regions (see Figure 11). The ridges noted earlier tended to progress across different plastic strain zones in a continuous manner. Striations characteristic of cyclic fatigue were noted in this material in each zone where the oxide was removed or thin enough not to totally mask the striation pattern. Striation spacing was found to increase with increasing plastic strain as first suggested by Forsyth in Reference 18. This is shown in Figure 12a, where a transition from 0.1 to 0.02% plastic strain is displayed. Striation spacing as a function of crack growth rates is given in Figure 15. The striation spacing from all tests was found to be directly proportional to the crack growth rate, and closely fit a perfect correlation curve.

Fractographs for the normalized and tempered material are given in Figures 13 and 14. Figure 13 shows the total fracture surface and the pronounced transitions between different plastic strain zones. The darker zones represent

areas subjected to smaller plastic strains; these areas are flatter than the higher strained zones. Radial ridges are also noted in this heat, however, they are most prevalent in the larger strain regions and tend to smooth out with low strains. Figure 12(b) displays a transition region where the oxide has been removed. The difference in surface roughness and striation pattern is observed. Due to the heavy oxide layer, striation measurements were limited.

2. Continuous Cycling in Vacuum

The results for the continuous cycling tests in vacuum for the annealed, and normalized and tempered materials are given in Figures 16 and 17, respectively. Figure 18 compares the data of the two heat treatments given in Figures 16 and 17. Vacuum results present the same trend in growth rates as a function of plastic strain range; however at small crack depths, crack growth rates in vacuum were considerably less than corresponding values in air and only approached them at crack depths of about 4mm (near the end of the crack (see Figure 19). This behavior suggests a marked contribution to growth made by oxidation at low crack growth rates (short cracks).

Microscopy revealed that no oxide was present on the crack surface for both the annealed, and the normalized and tempered materials. The cracks for the vacuum tests are shown in cross section unetched in Figures 20 and 21 with the continuous cycled areas of the crack noted. Higher

magnification crack profiles are shown in Figures 22 and 23. Figure 22 shows the ferritic grain structure of the annealed material and a relatively smooth crack that continuously changes direction slightly and propagates in a transgranular/ intergranular-like manner. Limited crack branching was observed. Figure 23 shows the bainitic microstructure of the N+T material and a crack that propagates trangranularly through the prior austenite grains. Figure 23 also displays a series of fine cracks which cooperatively propagated in the crack direction. This division in the crack path indicates a strong tendency for branching; the fine cracks suggest the possibility of reweldment or partial reweldment of the crack, slowing the crack growth rate.

Fractography results are given in Figures 24-27, with Figures 24 and 25 showing the complete fracture surfaces. It should be noted here that Figures 24 and 25 are the fracture surfaces of the vacuum tests for all loading conditions in HSF, and that the continuous cycling regions are only portions of the total fracture surface. Figures 26 and 27 compare the fracture surfaces of both heat treatments in continuous cycling at the two different levels of plastic strain tested. The topography of the fracture surfaces in vacuum are much more varied and irregular compared with those of air. Sharp ridges that are oriented radially away from the starter notch are observed similar to those in air.

Striation patterns are recognizable, but much less distinct than those tests in air; the striation spacing could not be determined due to the irregularity and jagged appearance of the cyclic patterns. Possible crack branching was observed in Figure 27 on the normalized and tempered material at a transition point between the plastic strain ranges of 0.2% and 0.1%.

In general, the propagation rates in air and vacuum obeyed the relation:

$$da/dN = Ba^{Q} \qquad \text{eq. 1}$$

where a is crack length, N the number of cycles, and B and Q are constants for a given plastic strain range. The values of B and Q for the different cycling conditions are listed in Table II.

3. Cycles with 1/2 Hour Dwell in Air

The effects of an added 1/2 hour dwell in tension, compression, or tension and compression for the annealed, and the normalized and tempered in air are given in Figures 28 and 29, with a comparison of the two heats in Figure 30. For the N+T heat; the crack growth rates appear to be independent of whether a tension, compression, or tension plus compression type dwell was imposed. This trend is similar for the annealed heat, however the tension plus compression dwell clearly shows an increase in crack growth rate, Figure 30. The oxidation component had apparently

saturated and there was no evidence either of additional creep damage contribution imposed by the 1/2 hour dwell periods. It is important to emphasize that the air data in Figures 28, 29 and 30 were step tests on a single specimen so that the observations do not result from specimen to specimen scatter.

Microscopy results are shown in Figures 31 and 32. Unetched total crack profiles are compared in Figures 20(a) and 21(a). At this low magnification, the cracks appear to be similar, showing major oxidation along the edge of the crack. Etched crack sections at higher magnifications are shown in Figures 31 and 32; these show that both cracks tend to propagate transgranularly. For the annealed material, a difference is noted in the appearance of the oxide in sections of the crack that had dwell periods of tension, compression, and tension plus compression (see Figure 31). The oxide in the tension dwell period section remained largely intact, whereas the oxide in the compression dwell section was mostly cracked. In the tension plus compression dwell section, the oxide was in patches, seemingly not adherent to the surface; this possibly suggests why cycling with tension plus compression dwell periods produced larger crack growth rates. The normalized and tempered material (Figure 32) has a thick oxide layer along the crack surface with an occasional tendency for oxide branching. These

branches are similar to the branches noted in the continuously cycled specimen. No correlation could be made with the loading waveforms used in the test and the oxide formed at those sections of the crack. The tip of the crack is filled with a cracked oxide.

The fractography results for both heats are given in Figures 33-36. Figure 33 displays half the total crack surface of the annealed material and the thick layer of oxide (the darker area) that could not be removed. The different loading regions cannot be discerned as in the continuous cycled fracture surface (see Figure 10). Figure 35 shows three areas of the fracture surface that are coincident with the different loading wave forms with dwell periods. Relatively little difference in surface characteristics is noted in these photographs; all the areas were smooth in appearnace with some oxide remaining. Rough striation patterns were also observed.

The normalized and tempered fracture surface is given in Figure 34. Here different loading waveform regions are recognized, however, they are not as pronounced as the continuous cycled surface (see Figure 13). For this specimen the oxide was very thick and only could be removed near the end of the crack, therefore only limited surface observation could be performed. Figure 36 shows the fracture surface of areas of different waveform loading. Limited striation counting was performed however.

4. Cycles with 1/2 Hour Dwell in Vacuum

Crack growth results in vacuum with a 1/2 hour dwell are given in Figures 37 and 38. These results are somewhat surprising. (Here again it should be noted that these results were based on single specimen tests.) In both the annealed and the normalized and tempered steel a tension type dwell caused the highest cyclic growth rate.

During a compression dwell stage, the N+T material showed a lower, reduced crack growth rate; and with the annealed material, crack growth ceased. Tension plus compression dwell cycling produced an intermediate propagation rate. Overall, the crack growth rates in vacuum for the annealed material were greater than the N+T material. The complete halting of the crack in the annealed material suggested that rewelding was occurring during the compression dwell period.

Figures 39 to 41 compare the crack morphologies for the 1/2 hour dwell specimens in vacuum. As noted earlier, Figures 20(b) and 21(b) show the total unetched crack profile for the vacuum tests; the various loading waveforms are annotated. For the annealed material, higher magnification photographs of the crack are given in Figure 39. These photographs show no oxide along the crack and a fracture mode that is intergranular-like; occasionally the crack follows along the grain boundaries. Intergranular and transgranular branching is also observed. There was no

increased tendency for branching to occur during any specific wave form imposed; they seemed to form randomly. Branches were very thin and extended a short distance away from the main crack. Tension dwell sections were slightly straighter and seemed to have more of a tendency for transgranular propagation.

The normalized and tempered cracking morphologies are given in Figures 40 and 41. After the continuously cycled crack initiation section of the crack where a wide crack opening displacement is noted, the crack seemed to propagate in a series of fine cracks that were closely clustered. Occasionally these fine cracks would branch away from the predominant crack direction, but would only proceed short distances from the main cluster. Figure 41 displays this fine crack branching. It is suggested that crack rewelding could possibly occur in these fine cracks in the compression dwell of a cycle.

The fractography results are quite interesting. The crack surfaces that were analyzed are shown in Figures 24 and 25. In Figure 24, the surface of the annealed material had a greyish-silver appearance, whereas in Figure 25, the normalized and tempered material had regions of different colors that depended on the loading waveform applied.

Fractographs for the annealed material are given in Figure 42. The fracture surfaces are similar for both the

tension, and the tension plus compression dwell cycling test (note: compression dwell cycling ceased crack growth) with sharp jagged contours lining the surface. The pocketed areas in Figure 42 resemble grains being ripped out of the surface as the crack passed through that area. This may be why the intergranular-like fracture mode was seen in Figure 22. Figure 42(c) possibly shows intergranular crack branching in a tension dwell region. Striation-like patterns were noted, however due to the rough jagged surface features striation spacing could not be calculated.

Fractographs for the normalized and tempered material are given in Figure 43. Generally, the fracture surfaces are similar in that a rough, jagged ridge-like appearance is present, but on closer examination, regions of different wave-form loading displayed different characteristics. In regions where 1/2 hour tension dwell cycling was applied, the surface was generally rough, but smooth between contours. In 1/2 hour compression dwell cycling these surfaces were dimpled, possessing a wet tacky paint appearance. The regions in which 1/2 hour tension plus compression dwell cycling was applied had a combination of both of the above mentioned characteristics. See Figure 44. This dimpling in the compression dwell region possibly could substantiate rewelding or partial rewelding of the fine crack surfaces.

5. Effect of Frequency in Air

To determine the effect of varying frequency on crack growth at a plastic strain range of 0.2%, a test on the annealed material was performed in air at progressingly higher cycling frequencies of 0.025, 0.05, and 0.25 Hz (triangular waveform). The results are given in Figure 45. It can be seen that the effect of frequency is minimal. The cyclic crack growth rate decreased slightly with increasing frequency. Figure 45 also compares the crack growth rates of the tests stated above to the continuous cycle tests in air where the plastic strain range was varied throughout the test and the test frequency was approximately 0.01 Hz. In Figure 45, only the 0.2% plastic strain data was plotted. No frequency effects were observed.

Microscopy of the frequency test specimen revealed a transgranular crack with a thin layer of oxide coating the crack surface. The total unetched crack profile is shown in Figure 46. Figure 47 shows the microstructure surrounding the crack and the slight oxide branching. In Figures 48 and 49 the fractography displays a relatively smooth surface with a prominent striation pattern.

B. LEFM CRACK PROPAGATION

1. Continuous Cycling in Air and Vacuum

The results for the LEFM tests in air and vacuum are given in Figure 50, where continuous cycling crack growth

rates as a function of ΔK are plotted. The annealed material shows only a small effect due to the environment change from vacuum to air halfway through the test. The normalized and tempered material, however, demonstrated a fourfold reduction in growth rates for vacuum compared with those in air. The air and vacuum data for the normalized and tempered material represent upper and lower bounds for the scatterband of data in these tests.

The propagation rates in air and in vacuum obey the general relation:

$$da/dN = C \Delta K^m \qquad \text{eq. 2}$$

where a is crack length, N the number of cycles, ΔK is the range of stress intensity measured in the tensile mode only, m is the slope of the log-log plot, and C a constant. The values for C and m for an upper bound relation are approximately 7.65x10±8 and 3.5 respectively.

The microscopy for the LEFM tests are given in Figures 51-55. Figures 51 and 52 show the crack profiles for both the reannealed and normalized and tempered material. The reannealed material displays a wide transgranular crack with a thin layer of oxide on the surface of the crack. In the section of the crack which was subjected to the vacuum environment for half of the test, the crack propagated in a very jagged manner. In this region only, long thin transgranular

branches extended from the crack, randomly growing into the base metal. The branches were filled with oxide. The totally air exposed section of the crack was straight and smooth; except for the end of the crack where the direction of the path altered.

The cracks are shown in cross section for the annealed and the normalized and tempered steel in Figures 53 and 54, respectively. The crack propagation path is very different in the sections of the crack where the crack propagated in vacuum from the region where the crack propagated in air. Both sections had an oxide layer covering the surface of the crack and the crack was transgranular. The vacuum section was rough and jagged, with the crack altering its direction often during propagation. When the crack altered significantly away from the straight path axis, small branches extended in the original direction of the path. The projections were full of oxide (presumably, oxidation occurred when air was admitted into the test chamber). In the air only section of the crack, the path was straight, smooth, and very narrow. The tip of the crack is very sharp and is filled with cracked oxide. Figure 55 shows the tip of the crack and the oxide present. Noted at the very tip of the crack is a short thin extension of the crack where oxide has not formed yet. This most likely is the next step in propagation of the crack. The cracked oxide at the tip suggests that a type of spalling mechanism is assisting the propagation of the crack.

The fractography results are given in Figures 56-59. The differences mentioned in the microscopy above are clearly shown in the fracture surface photographs in Figures 56 and 57. The vacuum areas are rough and irregular whereas the air areas are smoother and flatter. This is very evident in the normalized and tempered fracture surface in Figure 57; the mountainous vacuum region levels out to a planer air region.

Striation spacing data was taken from areas near the end of the crack in the air areas and was found to directly correlate with crack growth rates.

V. DISCUSSION

A. ENVIRONMENTAL EFFECTS

In HSF cycling, when the crack growth rate is approximately 2×10^{-3} mm/cycle, or for crack depths of approximately 4 mm, the continuous cycling propagation rates in vacuum approach the propagation rates in air (see Figure 19). This indicates a strong dependence on oxidation effects early in crack life, or at relatively low crack growth rates; the effect then diminishes with the crack advancing by mostly mechanical means and oxidation making only a minor contribution at high crack growth rates. The oxidation effects are best interpreted as a formation, spalling, and regeneration process of the oxide occurring at the crack tip. Figure 55 shows evidence of this. In Figure 55 the crack tip is full of cracked oxide, the cracks in the oxide extend to the oxide-metal interface. With cycling, the oxide that has formed on the surface, cracks and spalls. This allows that portion of the crack tip to be exposed to further oxidation and the cycle continues.

This effect decreases later in crack life as the crack growth rate increases with crack depth. The controlling damage mechanism shifts to a mechanical growth mechanism (as in the vacuum test) from an oxidizing mechanism, Figure 19. This oxidation effect is best displayed in

Figure 52, which shows the crack profile of the LEFM test where the test started in vacuum and then air was bled into the system half way through the test. The mechanism of crack growth clearly goes from a mechanical mode in vacuum where the crack changed directions continuously and is sharp and jagged, to an oxidation mode in air where the crack grows straight and smooth presumably driven by oxidation at the crack tip. Accelerated oxidation rates due to increased strain concentrations at the crack tip have been reported by Skelton and Bucklow [Ref. 20]. This must also be occurring in the present tests in order to explain the large difference between the crack growth rates in air and vacuum.

The loading waveforms, i.e. tension, compression, tension plus compression has very little effect on the crack growth rates in air, but a very large effect in vacuum. In air, the oxidation effect must saturate after a critical time (which is quite short at 525°C), no doubt when oxide layers growing from opposite faces of the crack meet. In vacuum, the substantial reduction of the crack rate when a 1/2 hour compression dwell was imposed in cycling for the N+T material, and the ceasing of the crack growth in the annealed material may be explained by partial reweldment or total reweldment of the crack tip. Fractographs of the N+T material in Figure 44 shows a flat faceted surface in the tension dwell area and a dimpled "sticky" appearance in the compression dwell area of the crack surface. It is thought

that this sticky appearance is caused by the welding of asperities on the crack surface during the hold period. Other evidence of rewelding is suggested in Table III where the crack closure data near waveform change points is tabulated. The transition time for the potential across the crack to attain V(min) from V(max) during each 1/2 hour compression cycle was greater for the N+T than the annealed, thus showing a greater opportunity for rewelding and hence a greater suppression of the crack growth during compression cycling for the annealed material.

No evidence of rewelding was noted in fractography of material exposed to an air environment. Oxidation on the crack surface must prevent rewelding.

The LEFM tests surprisingly showed no environmental effects for the annealed material, but demonstrated a substantial difference in crack growth rates between the air and the vacuum environments in the N+T material. Skelton and Bucklow [Ref. 20] showed that for 1/2 Cr-Mo-V steel at 500°C, for a given plastic strain range, surface oxidation rates per cycle are greater for bainitic (i.e N+T) material than for annealed material. In general this was found to be the case; surface cleaning for fractography was more difficult for the N+T material than the annealed material, crack profiles in Figures 6 and 7 clearly display this, and fractographis in Figure 36 also show the oxidation

characteristics. The more rapid the oxidation of the bainitic N+T material would also explain why the N+T crack growth rates for the LEFM tests are higher than the annealed and why there is a large effect of environment. However, an explanation for the lack of a significant effect of environment for the LEFM tests on the annealed material cannot be explained at this time.

B. CREEP EFFECTS

Creep effects are manifested by grain boundary damage ahead of the crack during a tension dwell. This leads to an increase in the overall cyclic crack growth rates either during the dwell itself, or in the subsequent stress reversals. Compression dwells may reverse the deformation and some "healing" will occur, but there will be some imbalance because the strain concentration at the crack tip disappears.

Due to limited data obtained from the tests in vacuum for the N+T material, only the creep behavior of the annealed material will be discussed here. Figure 60 compares tension dwell cycling and continuous cycling under vacuum and shows the effects of creep on crack growth rates. Tension dwell cycling produced propagation rates that increases at a constant rate when compared to the continuous cycling. Therefore, the effect of creep was small at low crack growth rates, but increased as crack growth rates increased. This

is what would be expected because as the crack gets longer, the strain intensity at the crack tip increased which would promote more creep damage per cycle.

The micrographs and fractographs from tension dwell cycling tests show no evidence of purely intergranular cracking under tension dwell cycling, in contrast to observations made by Skelton [Ref. 10] on 1/2 Cr-Mo-V steel at 500°C where increased crack growths also occurred with dwell. The results indicate an intergranular-like fracture mode with crack branching. It should be noted here that surface striation patterns were subtly recognizable but no striation spacings could be determined.

VI. CONCLUSIONS

1. Oxidation, not creep, is the major cause for the high fatigue crack growth rates of 2 1/4 Cr - 1 Mo steel in air at 525°C.

2. The loading waveform; i.e. tension only, compression only, or tension plus compression has very little effect on the crack growth rates in air, but has a large effect in vacuum. In vacuum the crack growth rate is always decreased by the imposition of a compression dwell period.

3. Crack path in air is transgranular and perpendicular to the loading direction, whereas, in vacuum the crack has a "intergranular-like" character and frequent branching is observed.

4. Fracture surfaces in air are flat and featureless with the exception of fatigue striations. In vacuum the characteristics of the fracture surface becomes dependent on the loading waveform and is always "intergranular-like" with a "sticky" appearance when compression dwell period is imposed.

5. Compression dwells in vacuum results in rewelding at the crack tip causing a dramatic reduction in crack growth rate, whereas in air, the oxide prevents this rewelding from occurring.

6. No frequency effects were noted in the annealed material test in air. Thus, the damaging effects of oxidation saturate quite rapidly at least at 525°C.

7. In LEFM regimes, crack growth rates are increased by a factor of 5 in an air environment over that for vacuum, for the normalized and tempered material. Surprisingly, no environment effect was noted for the annealed material.

VII. RECOMMENDATIONS

1. Conduct high strain fatigue (HSF) tests to greater growth rates and crack depths in air and vacuum environments to determine if mechanical effects completely overcome the damaging effects of oxidation.

2. Incorporate environmental fatigue factors in material design philosophy and equations to more accurately explain and predict mechanical behavior of materials.

3. Alter the environment from vacuum to air in individual HSF tests at different crack depths to accurately measure the effect of oxidation on crack growth rates.

4. Alter the duration of the tension dwell time in vacuum HSF tests to resolve the magnitude of creep damage to fatigue crack growth.

APPENDIX A

TABLES

TABLE I

Analysis (wt.%) of 2 1/4 Cr - 1 Mo Steels

Material	C	Si	Mn	P	S	Cr	Mo
XLM	0.11	0.33	0.50	0.013	0.021	2.31	0.93
UKAEA	0.11	0.25	0.58	0.008	0.009	2.32	1.09

TABLE II

Parameters Calculated for Equation 1 for Continuous Cycling

Material	Environment	ε_p	ε_t	Initial Stress Range (MPa)	Q	B
Annealed	Air	0.002	0.0049	446	0.72	1.06×10^{-3}
		0.001	0.0036	386	0.59	8.2×10^{-4}
		0.0002	0.0023	312	0.90	2.3×10^{-4}
N+T	Air	0.002	0.0056	534	0.82	1.42×10^{-3}
		0.001	0.004	450	0.67	9.2×10^{-4}
		0.0002	0.0021	288	1.08	7.0×10^{-5}
Annealed	Vacuum	0.002	0.0045	380	1.82	1.55×10^{-4}
		0.001	0.0032	332	1.69	6.5×10^{-5}
N+T	Vacuum	0.002	0.0055	531	1.14	3.7×10^{-4}
		0.001	0.0038	413	0.89	1.3×10^{-4}

TABLE III

Crack Closure Data Near Waveform Change Point
[Ref. 21]

Annealed				N+T			
TYPE	V(max) mV	V(min) mV	Transition Time, h	TYPE	V(max) mV	V(min) mV	Transition Time, h
T to C	0.21 0.21	0.18 0.17	0	T to C	0.38 0.36	0.28 0.22	10.0
T to C	0.56 0.50	0.35 0.17	3.0	C to (T+C)	0.44 0.45	0.22 0.36	7.0
C to (T+C)	0.53 0.56	0.17 0.30	8.0	T to C	0.69 0.65	0.49 0.23	28.0
(T+C) to T	0.60 0.61	0.30 0.40	0	C to (T+C)	0.76 0.81	0.23 0.45	20.0
T to (T+C)	0.63 0.63	0.40 0.30	0				

NOTE: In vacuum tests, the potential drop measurement was short-circuited during a compression dwell, indicating crack closure.

The minimum values (0.17 and 0.22 mV for annealed and N+T material respectively) corresponded to the potential at the beginning of the test, i.e. there was complete closure in a C dwell (unlike the case of (T+C)). The effect, however, was not immediate: N+T material took longer to attain V(min) during each 1/2 h C cycle owing to its greater creep strength and also demonstrated a greater transition time, adjusting to the new cycling conditions after a waveshape change. Annealed material thus has a greater opportunity for rewelding and hence suppressed growth during C cycling.

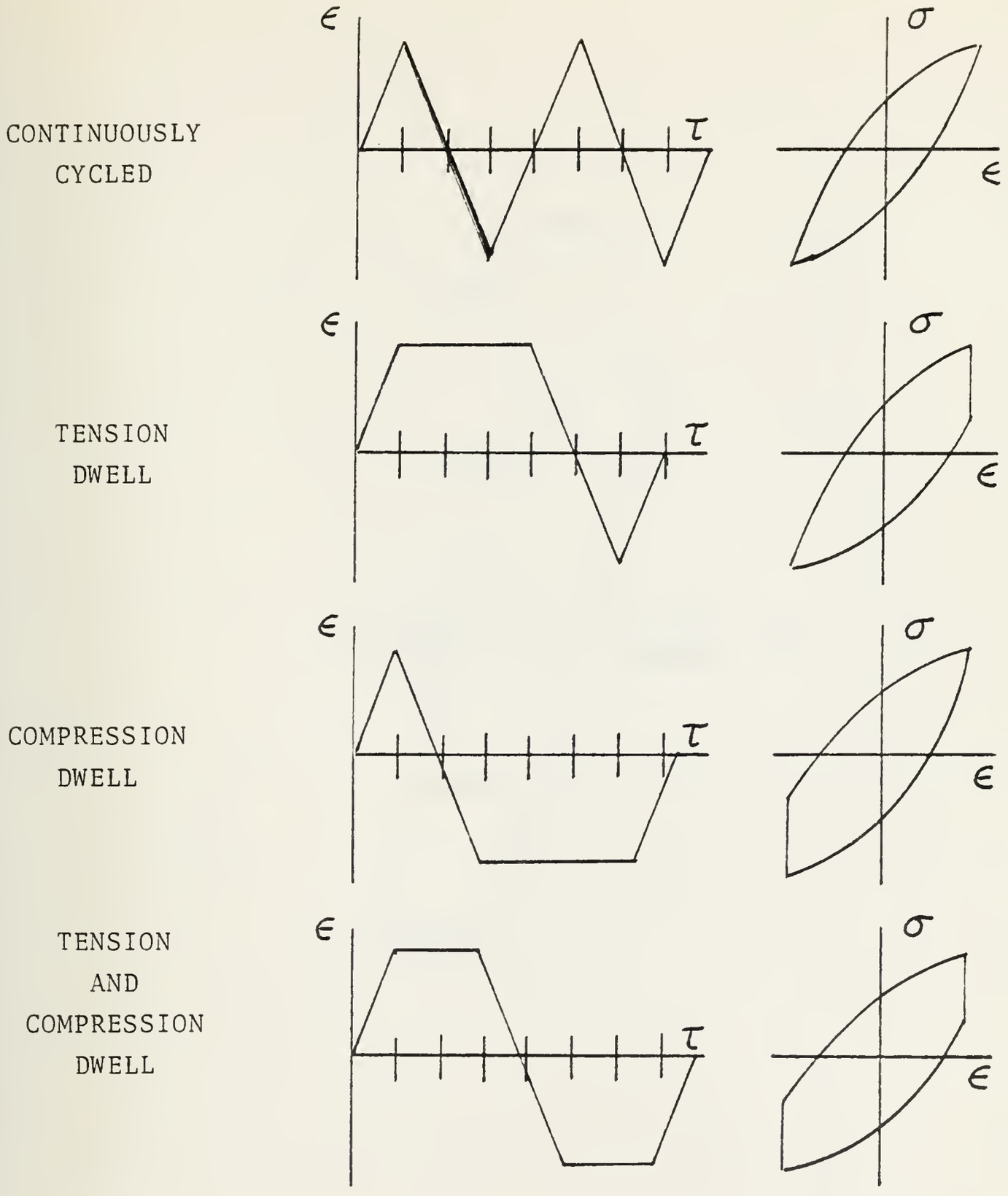

Figure 1. Loading Waveforms

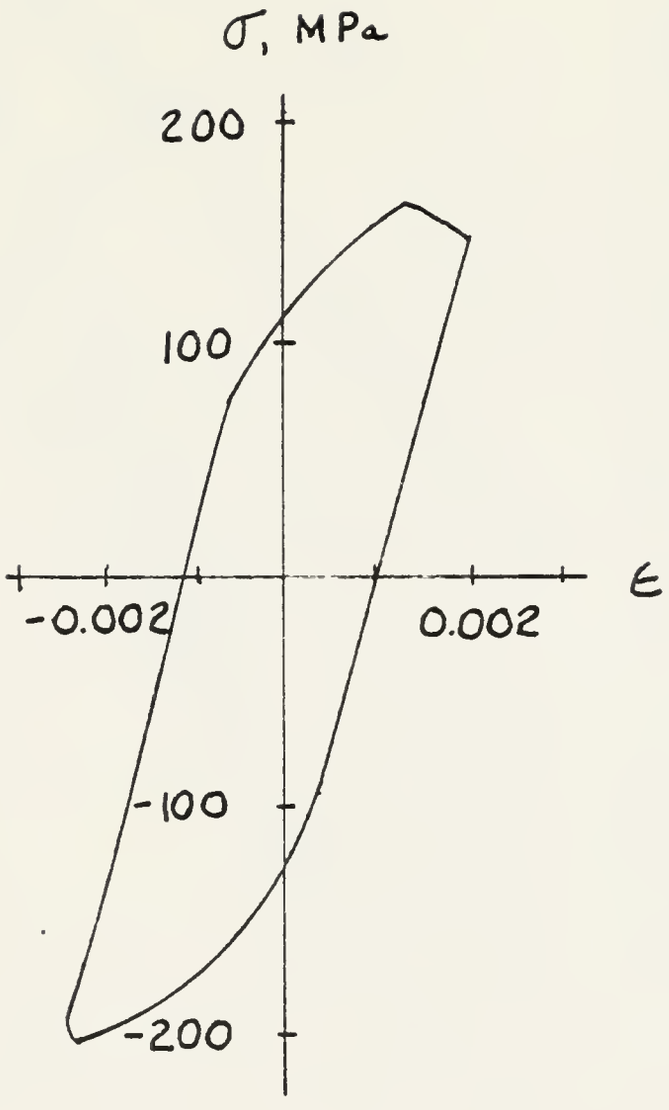

Figure 2. Typical Hysteresis Loop with Tension Dwell. Note Bias Toward Compression.

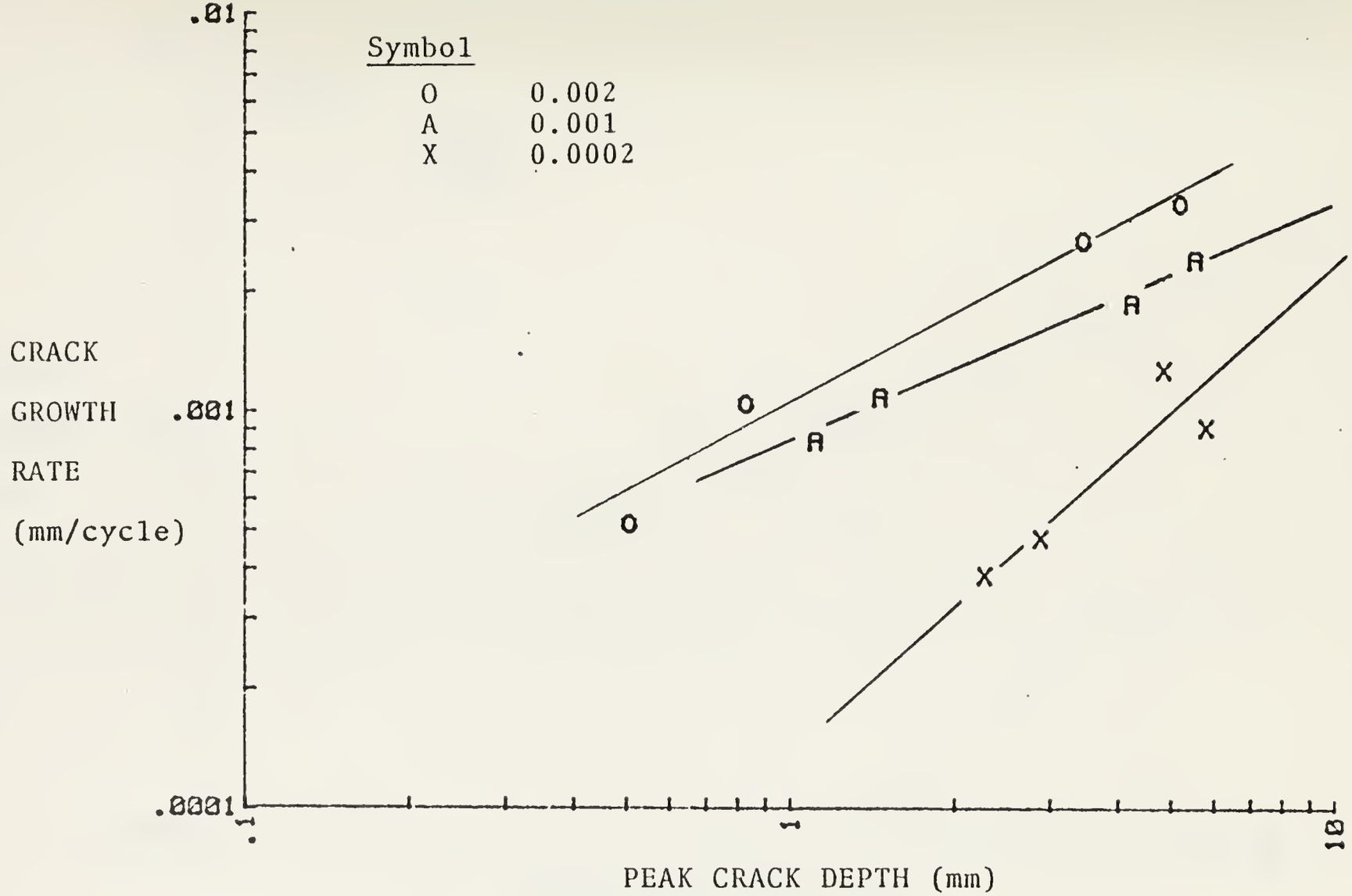

Figure 3. Continuous Cycling HSF Crack Growth Data for Annealed Material at 10^{-2} Hz in Air

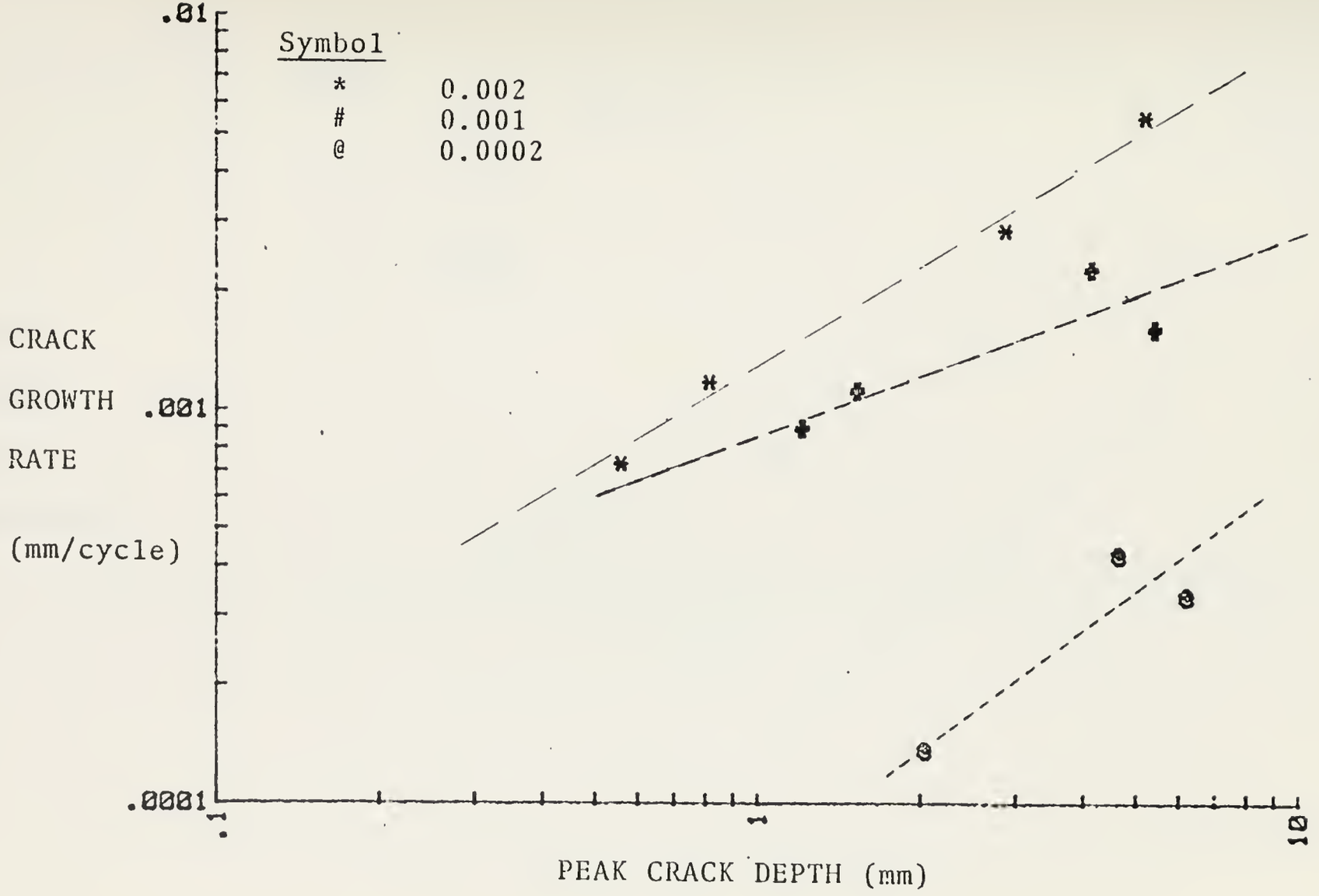

Figure 4. Continuous Cycling HSF Crack Growth Data for Normalized and Tempered Material at 10^{-2} Hz in Air

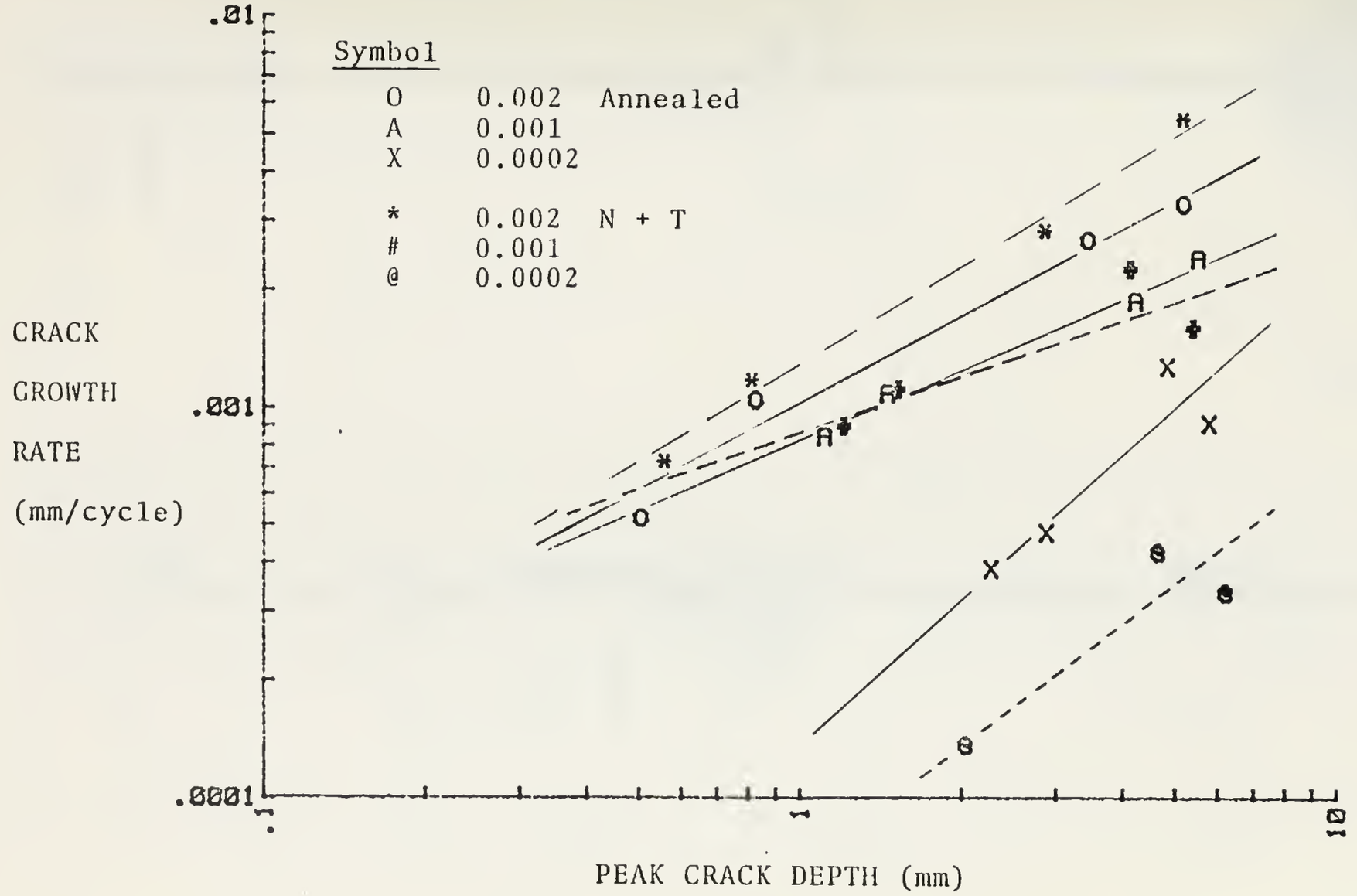

Figure 5. Continuous Cycling HSF Crack Growth Data at 10^{-2} Hz in Air

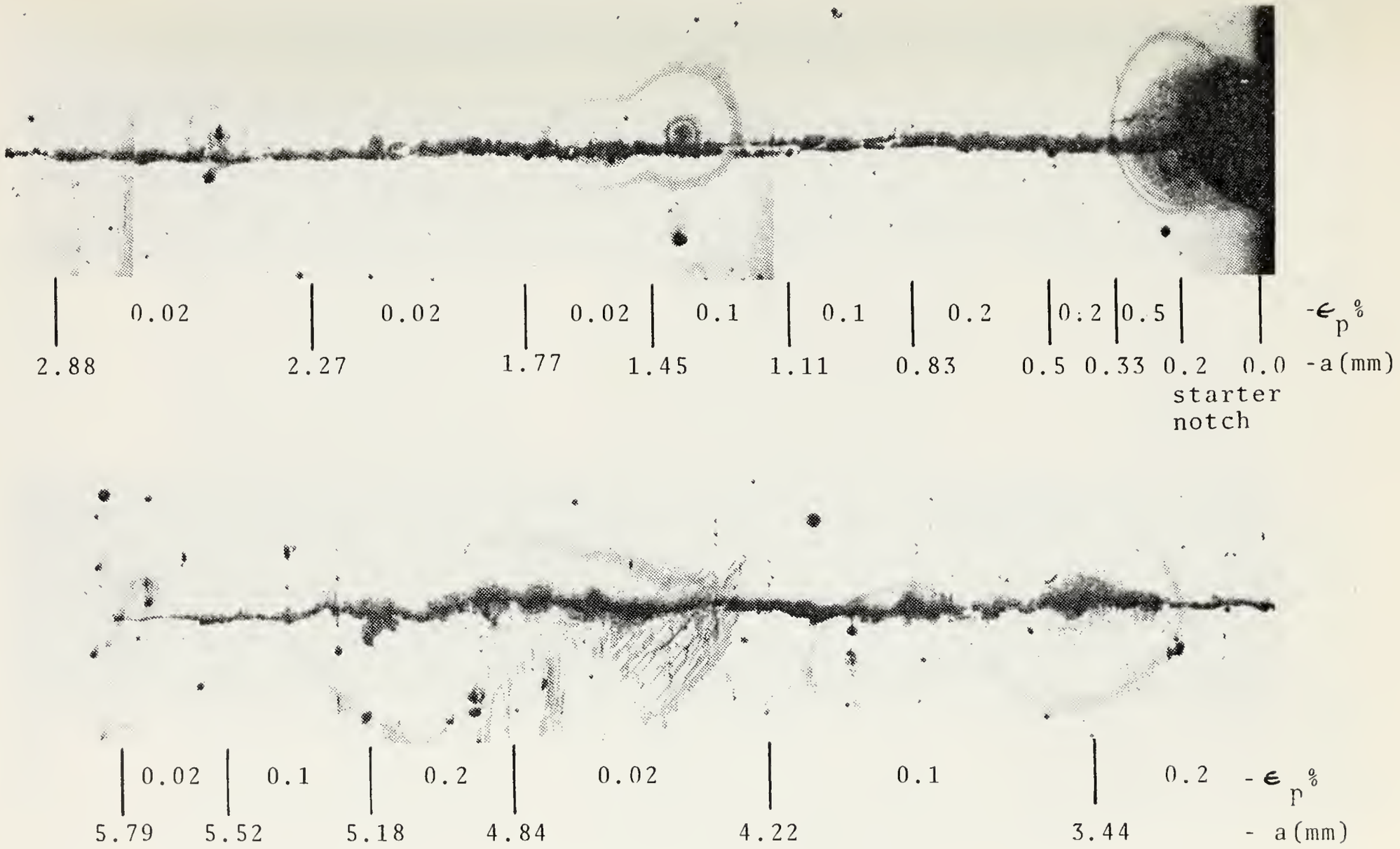

Figure 6. Profile of Continuous Cycling Crack in Annealed Material in Air (64x). Specimen No. 7

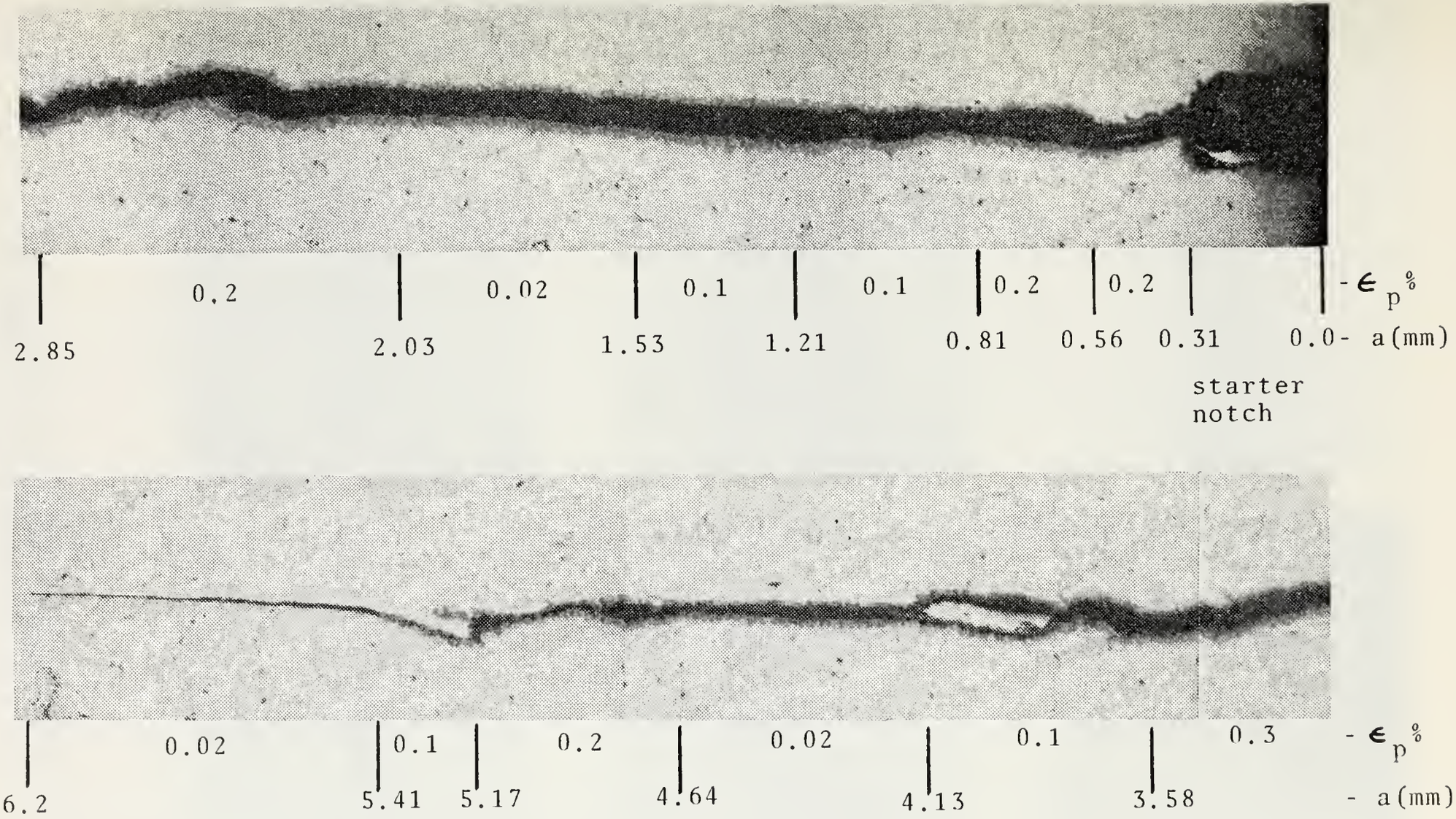

Figure 7. Profile of Continuous Cycling HSF Crack in Normalized and Tempered Material in Air (64x). Specimen No. 9

ε_p = 0.2%, (300x)

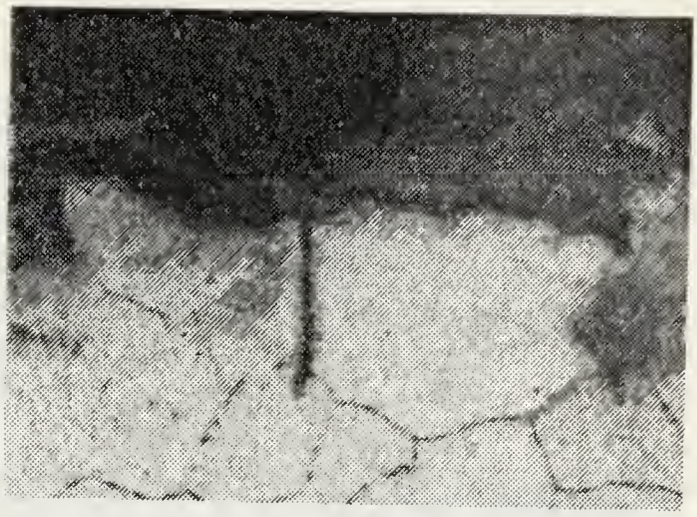

ε_p = 0.1%, (600x)

ε_p = 0.1%, (600x)

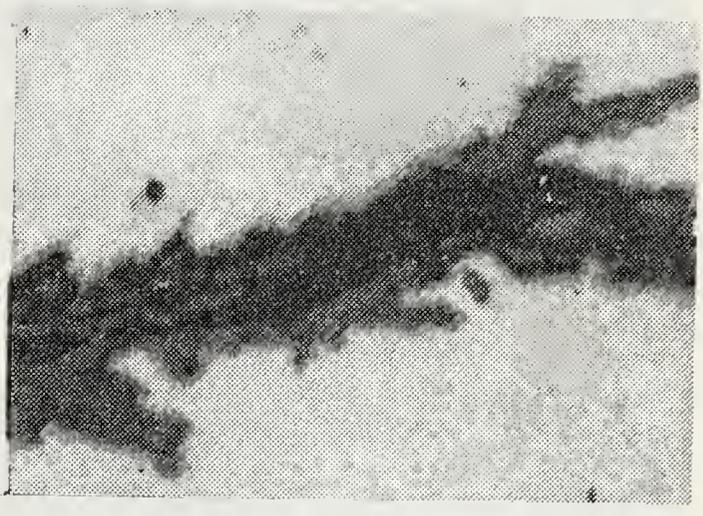

ε_p = 0.1%, (300x)

ε_p = 0.02%, (300x)

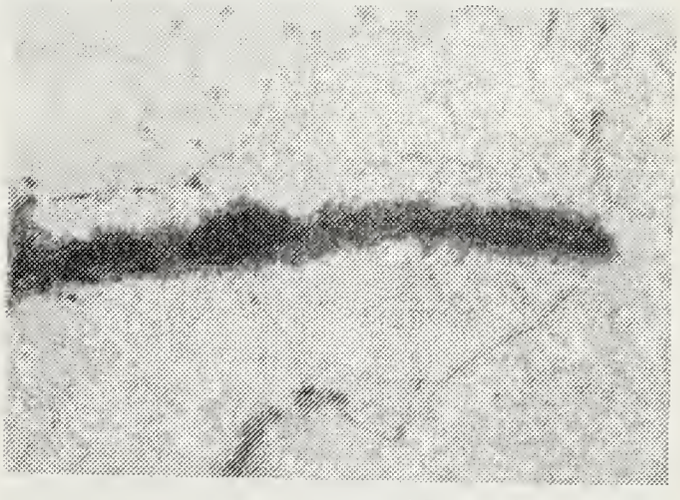

ε_p = 0.02%, (300x)

Figure 8. Micrographs of Continuous Cycling in Air of Annealed Material. Specimen No. 7

ε_p = 0.2% (320x)

ε_p = 0.2% (320x)

ε_p = 0.3% (320x)

ε_p = 0.1% (320x)

ε_p = 0.02% (320x)

ε_p = 0.2% (320x)

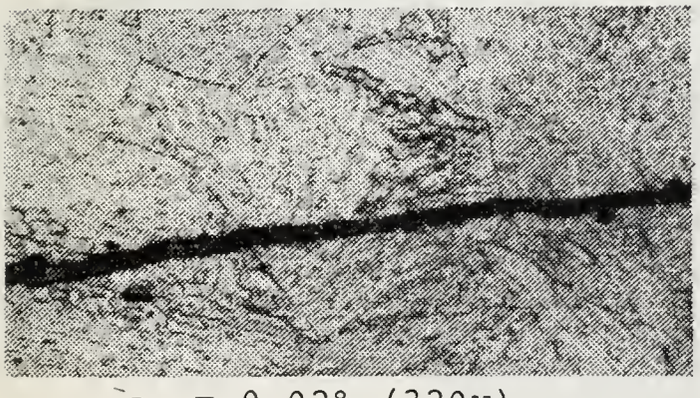

ε_p = 0.02% (320x)

ε_p = 0.02% (1500x)

Figure 9. Micrographs of Continuous Cycling in Air. Normalized and Tempered Material. Specimen No. 9.

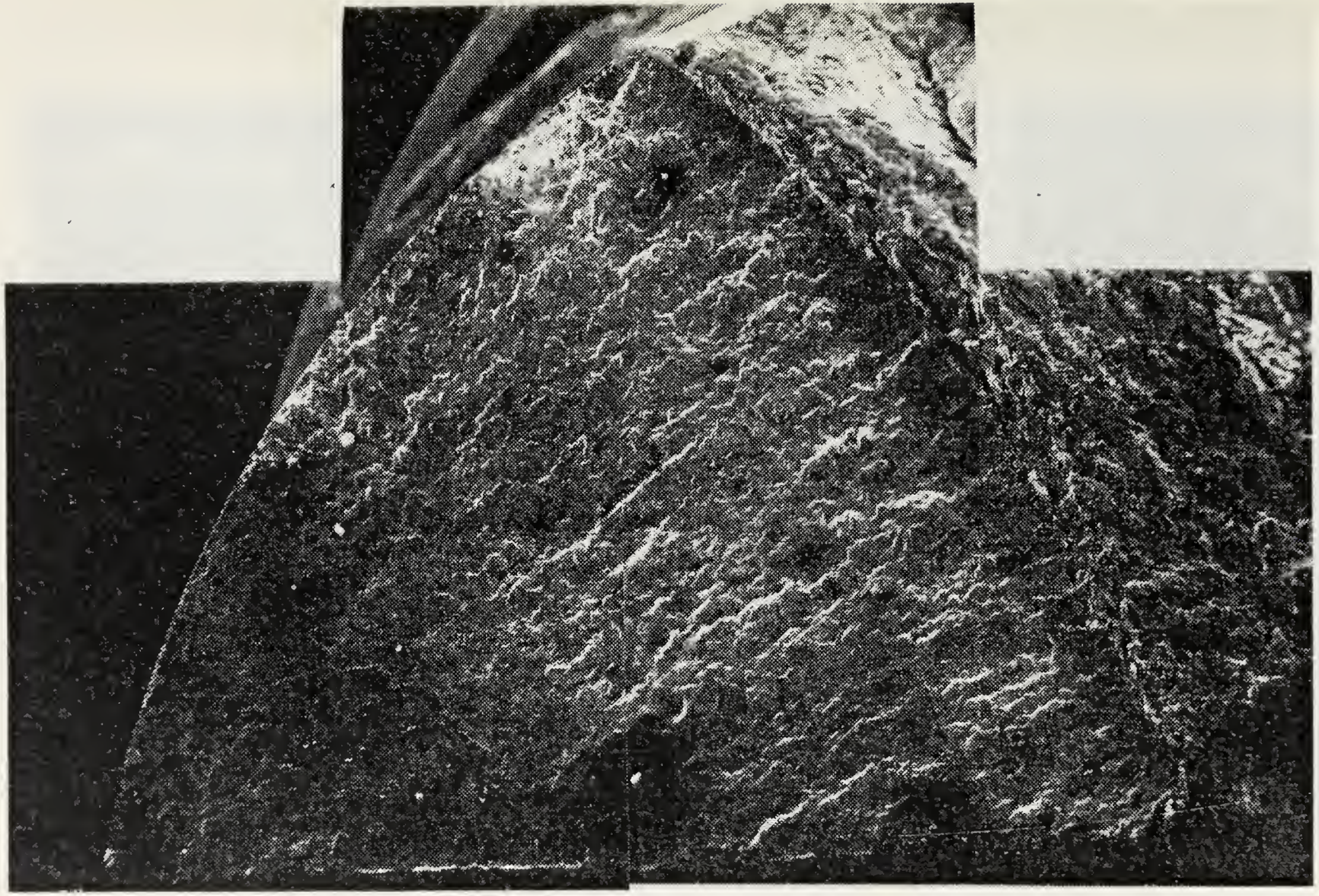

Figure 10. 1/2 Fracture Surface of Annealed Material. Continuous Cycling in Air (24x). Specimen No. 7

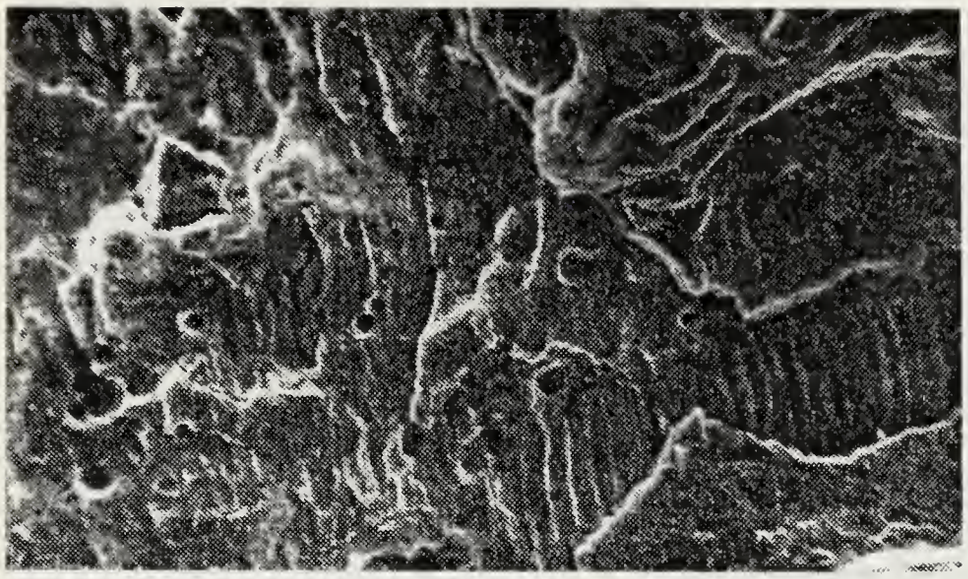

ε_p = 0.2% (600x)

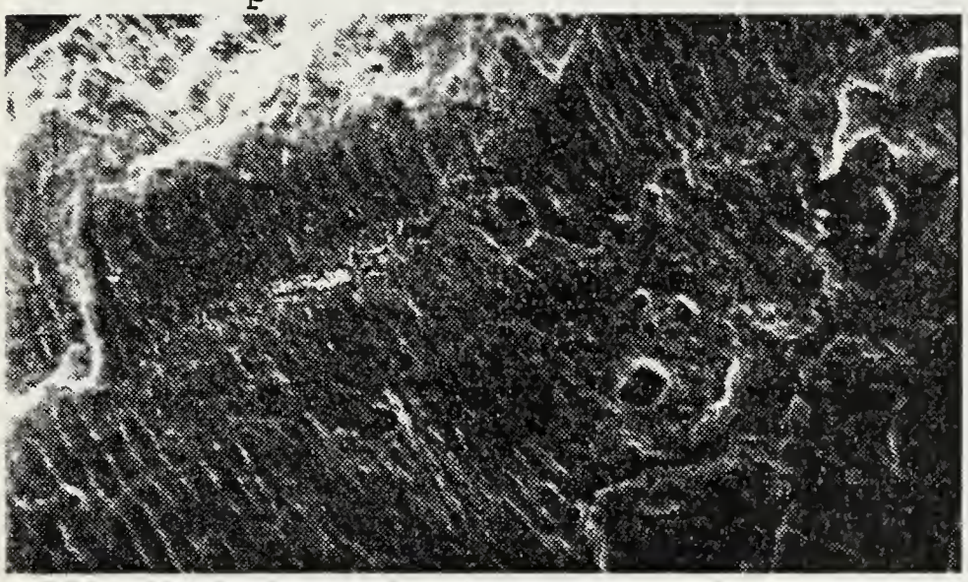

ε_p = 0.1% (690x)

ε_p = 0.02% (2440x)

Figure 11. Fractographs of Continuous Cycling Annealed Material in Air at 0.2, 0.1, 0.02% Plastic Strain Range. Specimen No. 7.

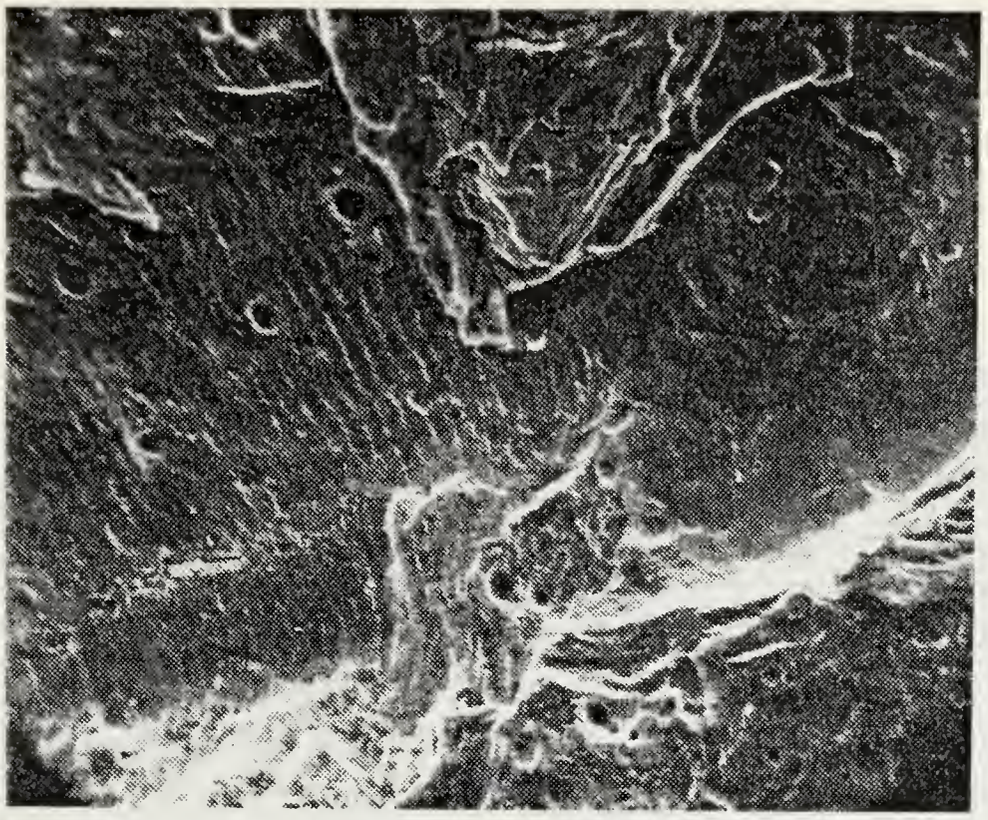

a) Annealed Material in Continuous Cycling, ε_p = 0.1 - 0.02%. Specimen No. 7.

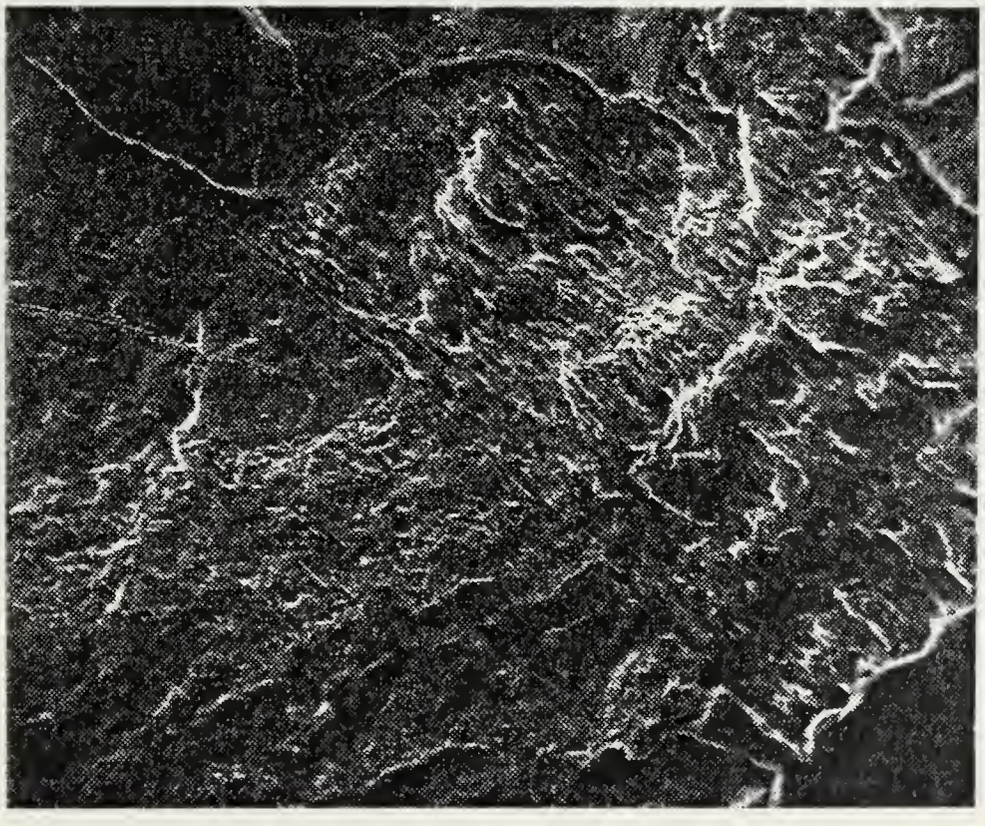

b) N+T Material in Continuous Cycling, ε_p = 0.02 - 0.2%. Specimen No. 9.

Figure 12. Fractographs of Plastic Strain Range Transitions in Continuously Cycled Material

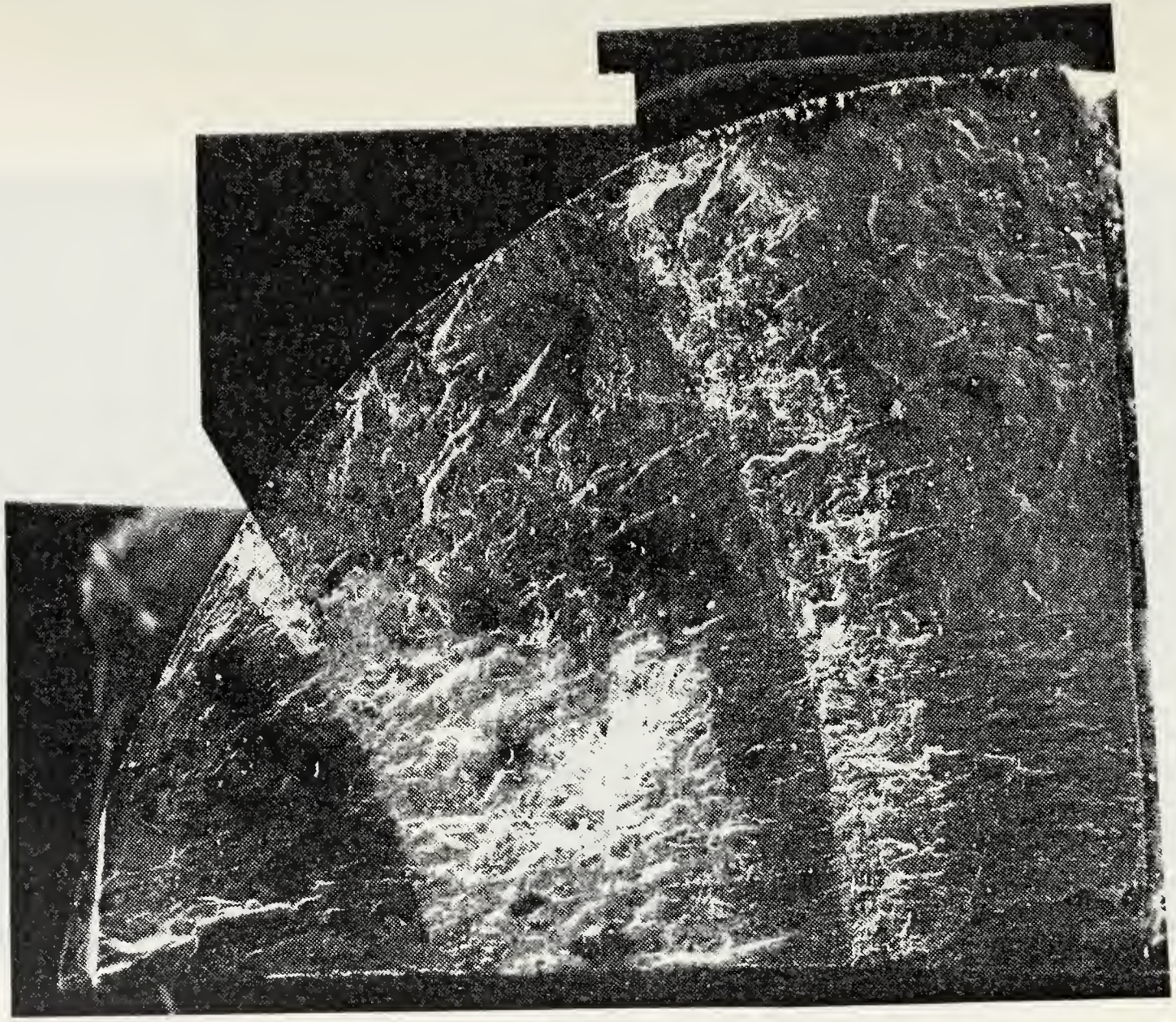

Figure 13. 1/2 Fracture Surface of Normalized and Tempered Material. Continuous Cycling in Air (26x). Specimen No. 9.

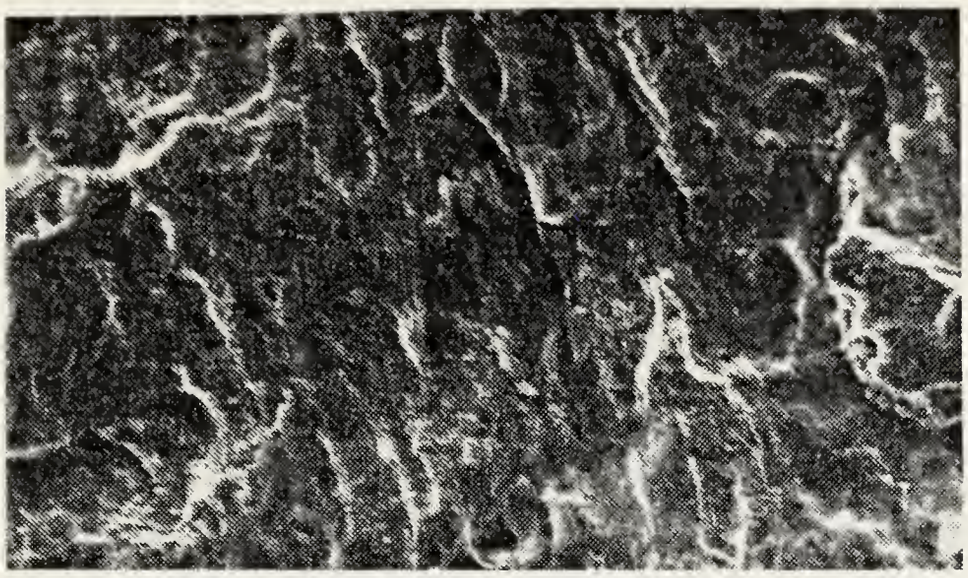

ε_p = 0.2% (665x)

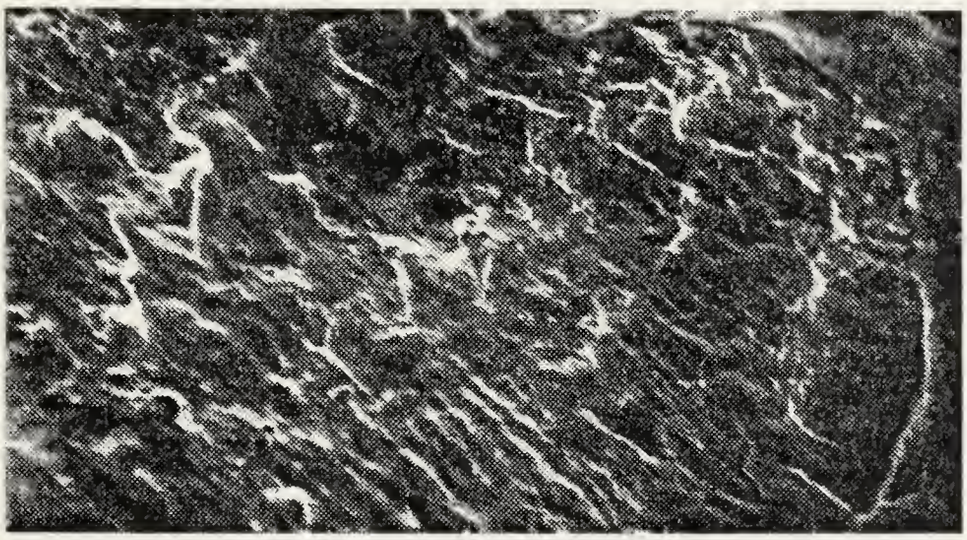

ε_p = 0.1% (660x)

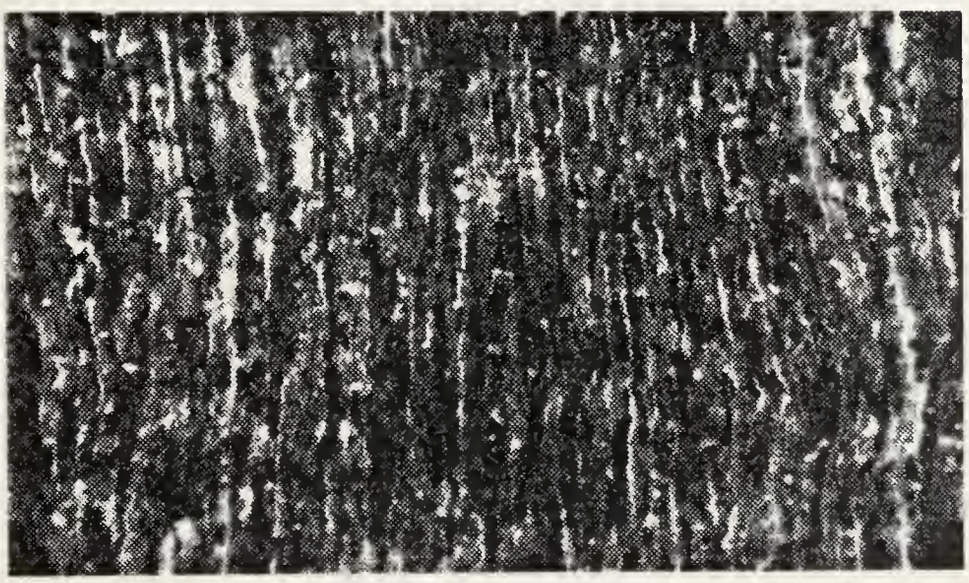

ε_p = 0.02% (3270x)

Figure 14. Fractographs of Continuous Cycling Normalized and Tempered Material in Air at Plastic Strain Ranges of 0.2, 0.1, 0.02%. Specimen No. 9.

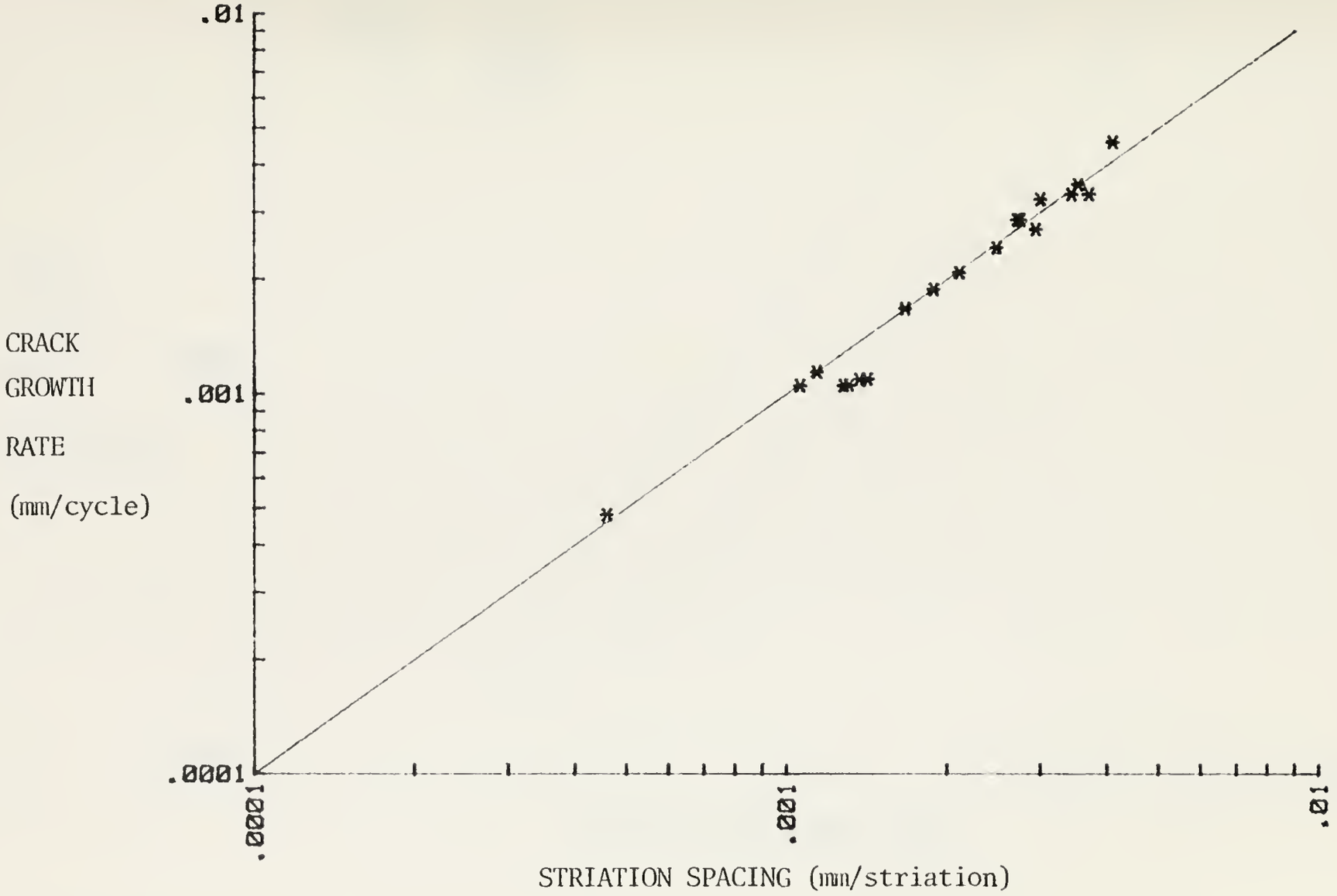

Figure 15. Striation Spacing for various HSF Testing in Air

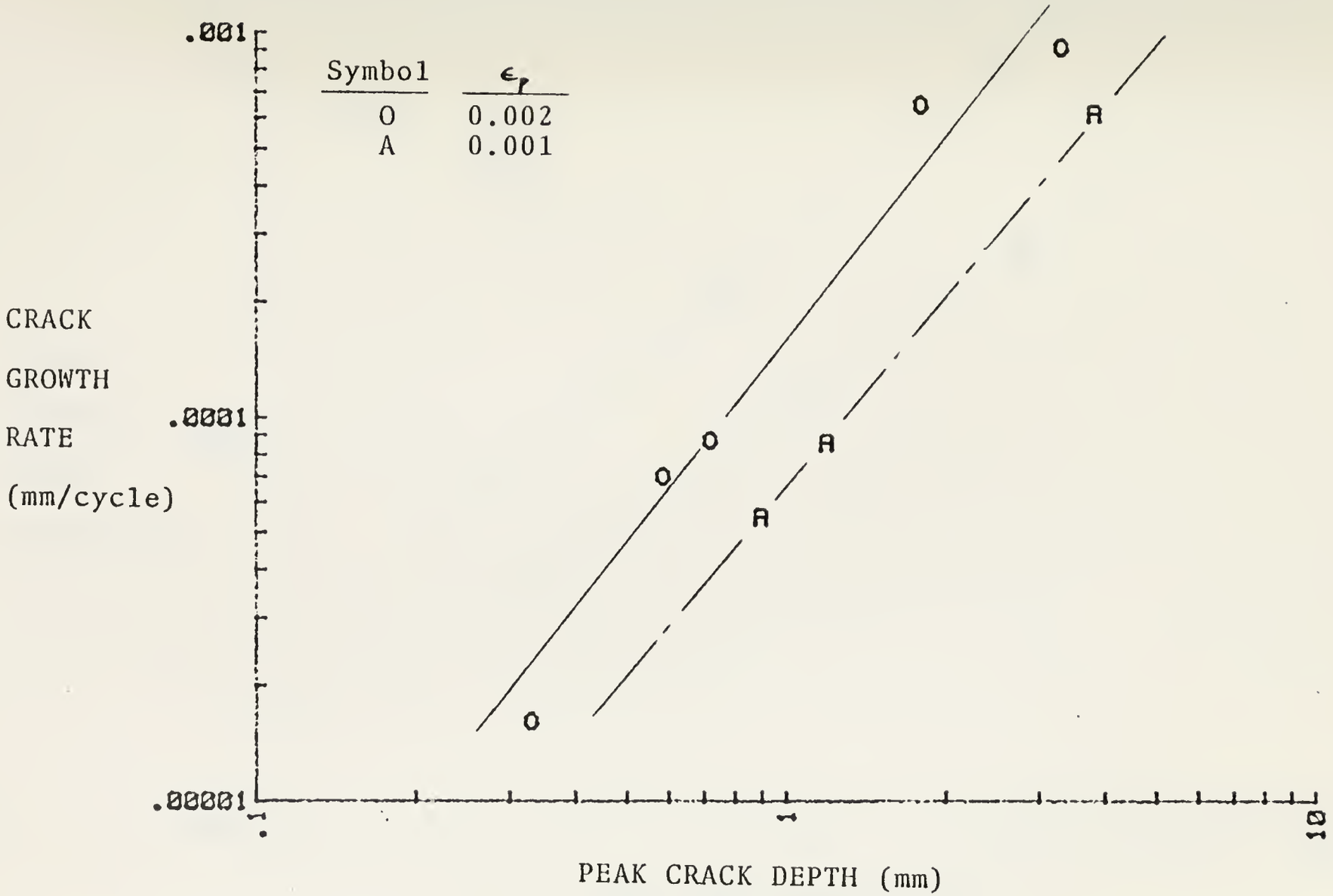

Figure 16. Continuous Cycling HSF Crack Growth Data for Annealed Material at 10^{-2} Hz in Vacuum

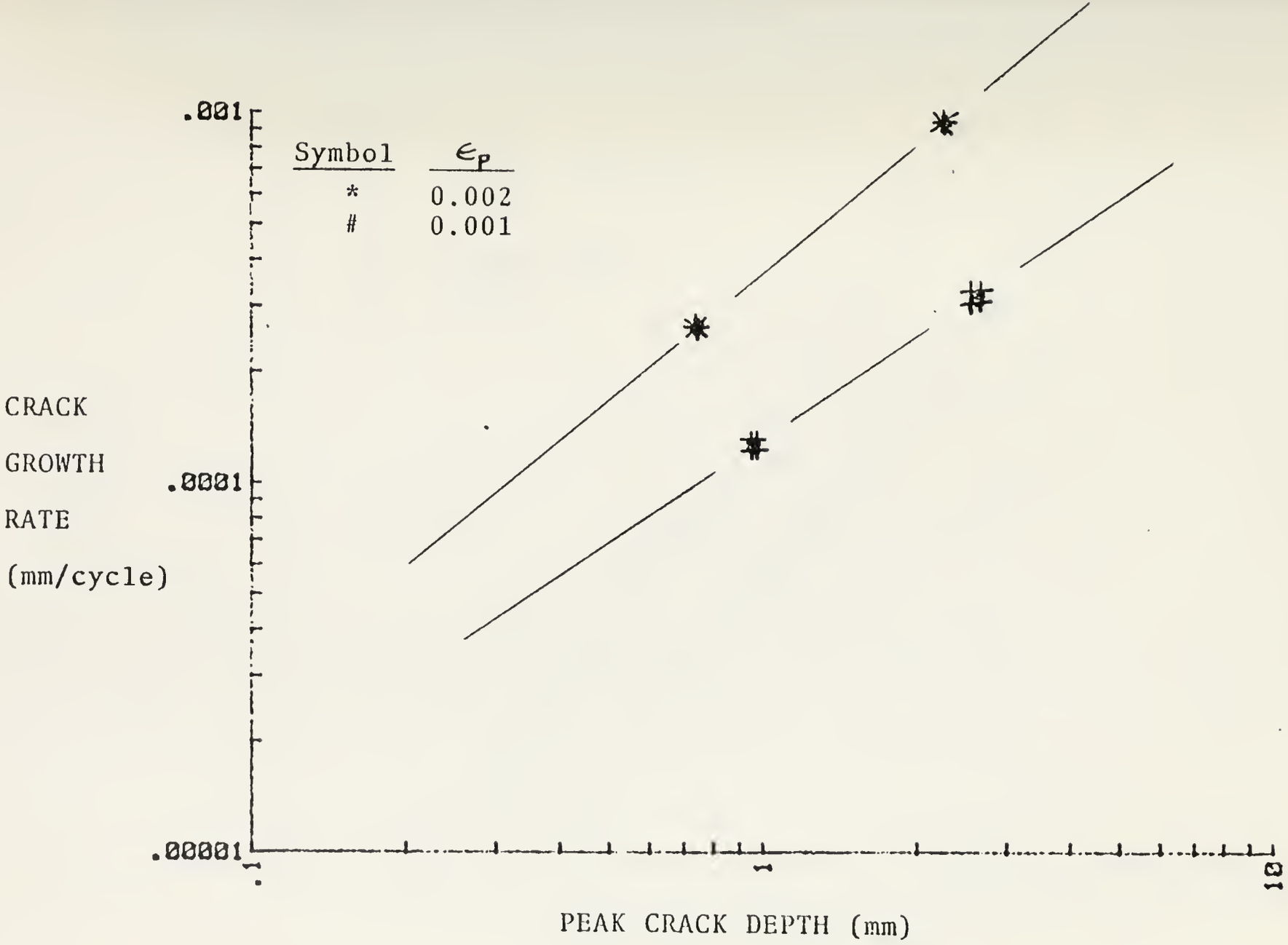

Figure 17. Continuous Cycling HSF Crack Growth Data for Normalized and Tempered Material at 10^{-2} Hz in Vacuum

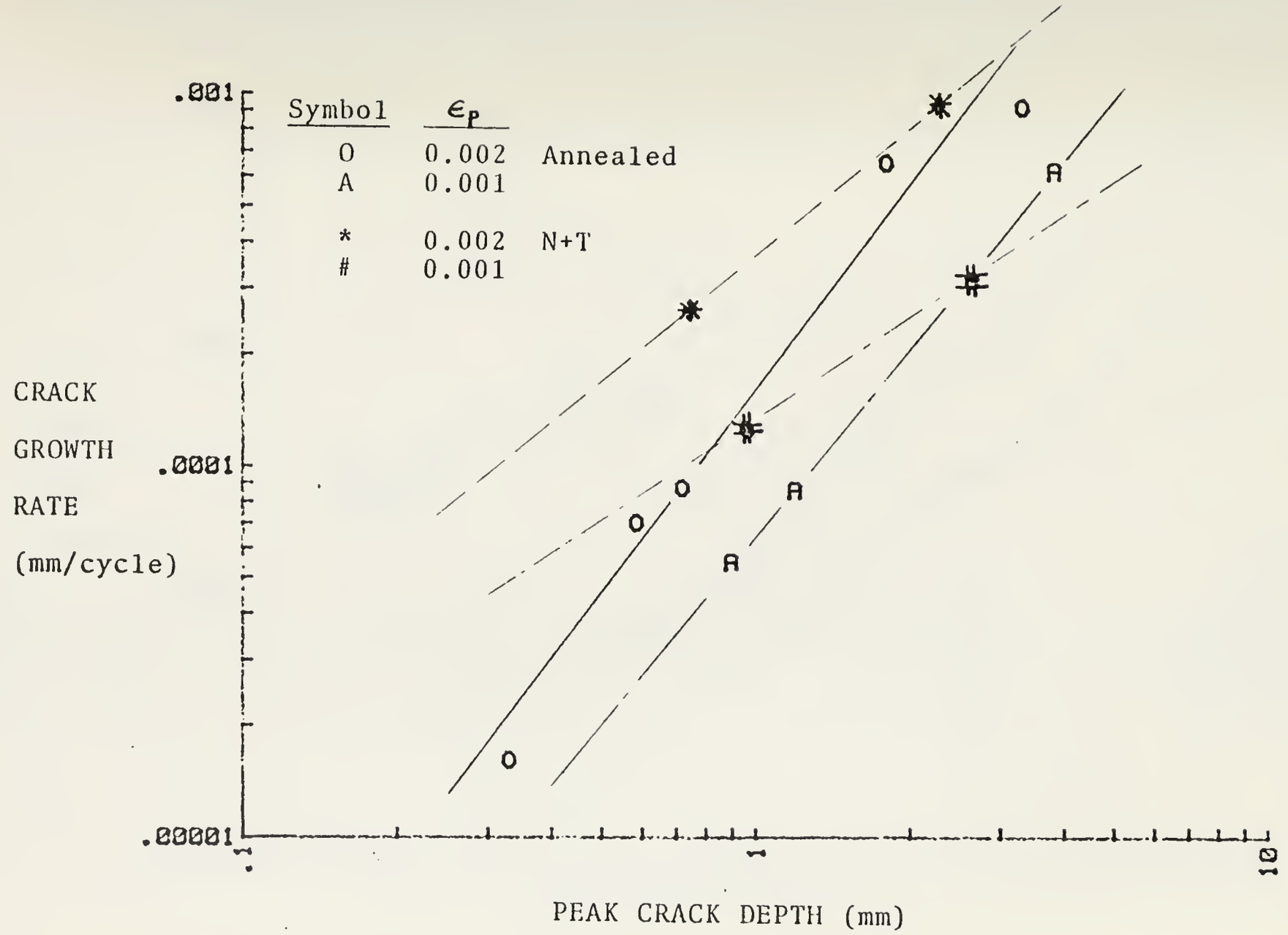

Figure 18. Continuous Cycling HSF Crack Growth Data at 10^{-2} Hz in Vacuum

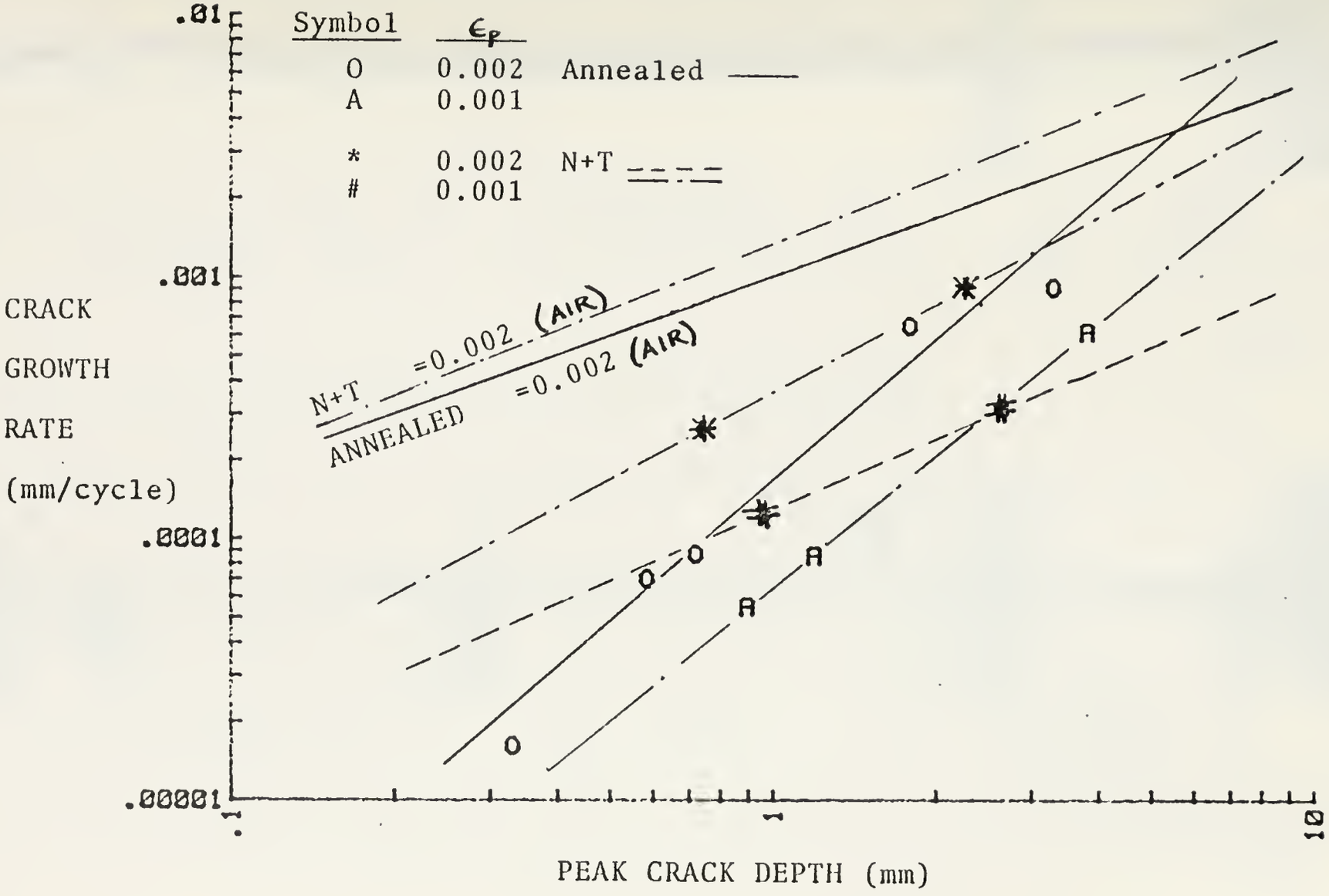

Figure 19. A Comparison of Continuous Cycling HSF Crack Growth Data at 10^{-2} Hz in Air vs. Vacuum

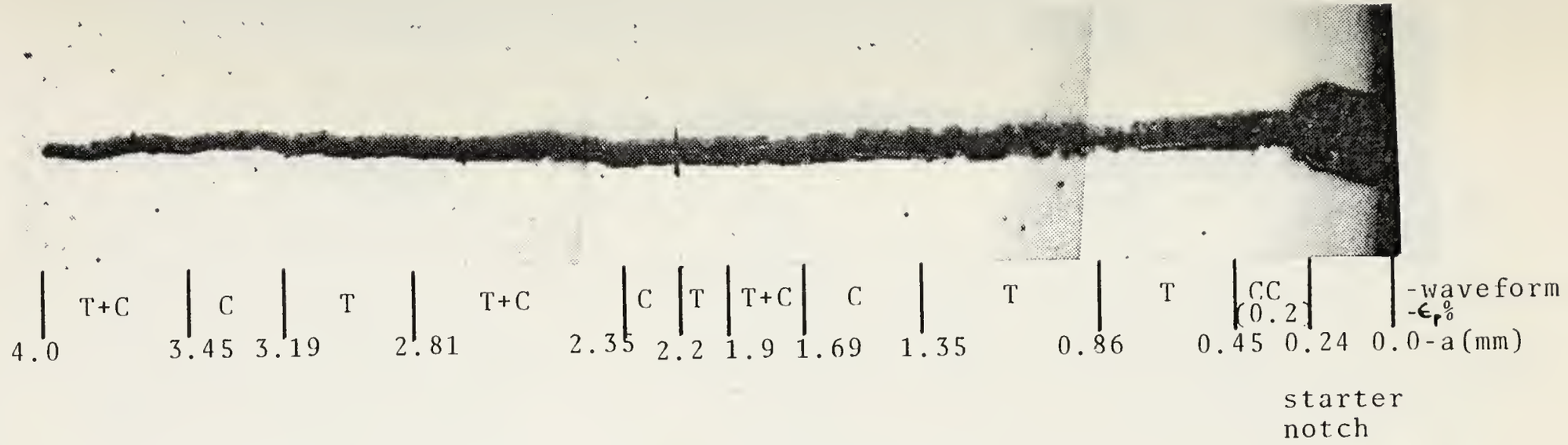

Note: T=Tension, C=Compression, CC=Continuous Cycling

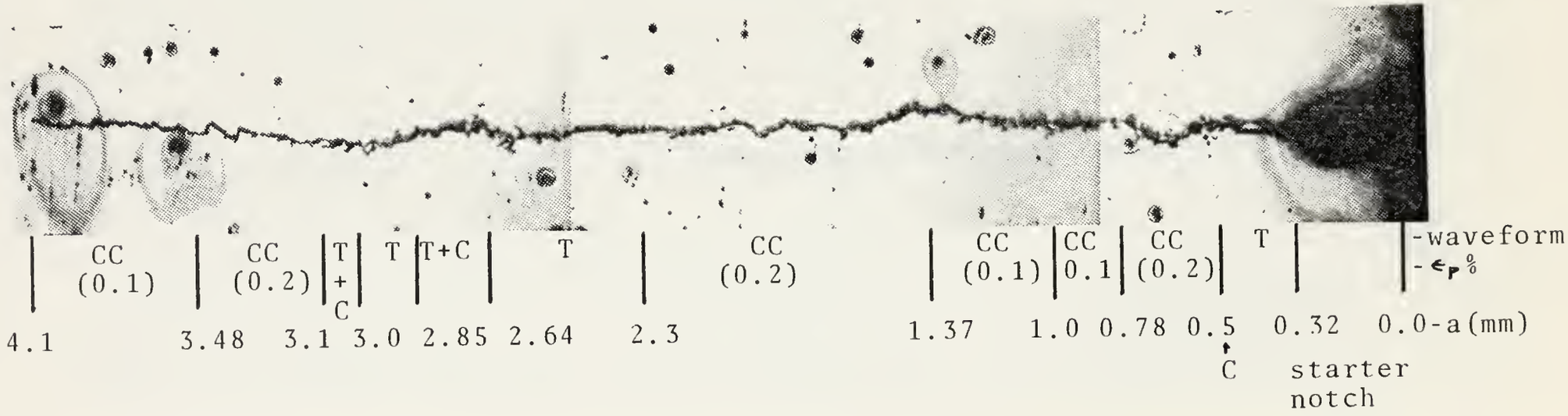

Figure 20. Crack Profiles Annealed Material in: a) Air, Subjected to 1/2 Hour Dwell Periods, b) Vacuum, Subjected to Continuous Cycling and 1/2 Hour Dwell Periods. Specimens 5 and 6, Respectively (64x)

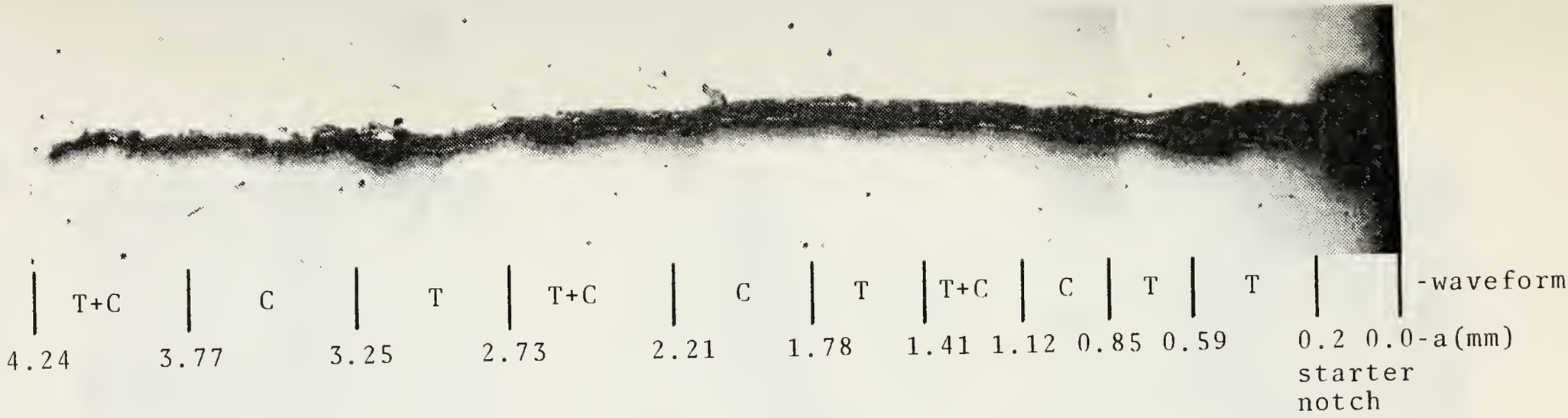

Note: T=Tension, C=Compression, CC=Continuous Cycling

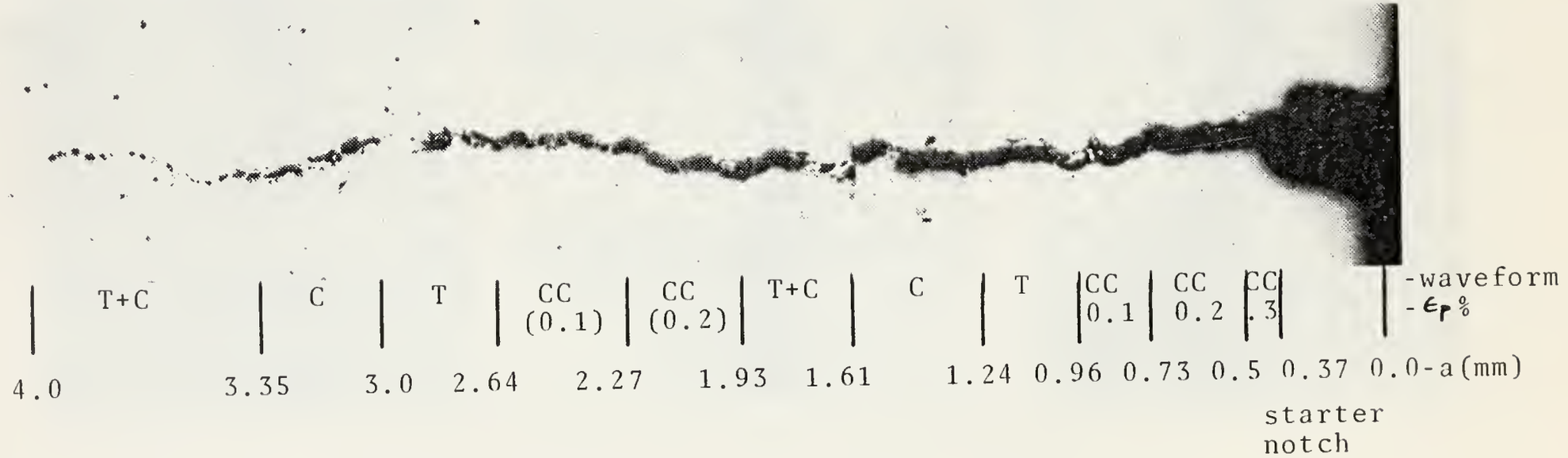

Figure 21. Crack Profiles of Normalized and Tempered Material in: a) Air, Subjected to 1/2 Hour Dwell Periods, b) Vacuum, Subjected to Continuous Cycling and 1/2 Hour Dwell Periods. Specimens 11 and 12, Respectively (64x)

a) ε_p = 0.2% (240x)

b) ε_p = 0.1% (240x)

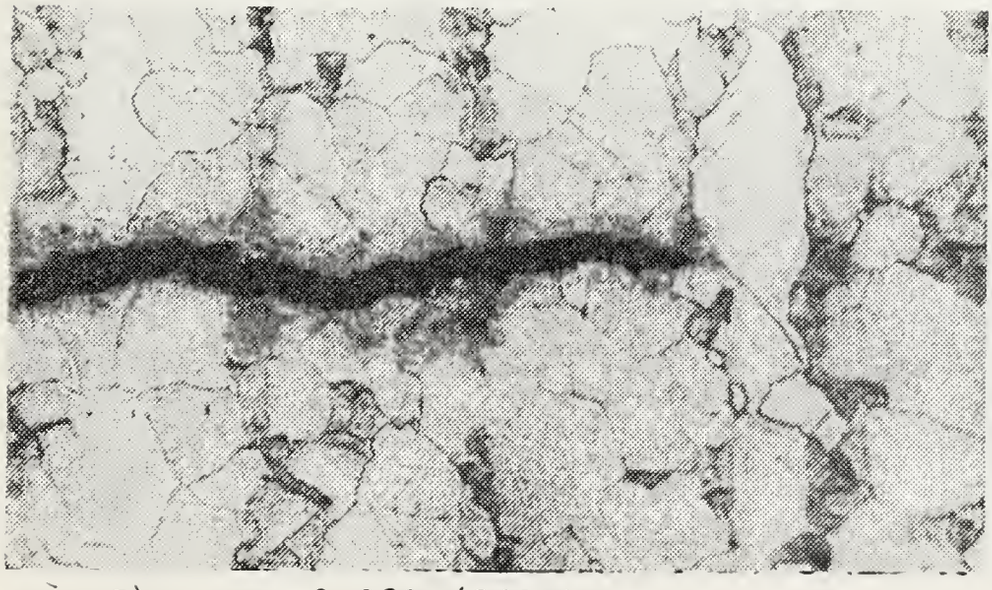

c) ε_p = 0.02% (240x)

Figure 22. Micrographs of Continuous Cycling in Vacuum. Annealed Material. Specimen No. 6.

a) ε_p = 0.1% (600x)

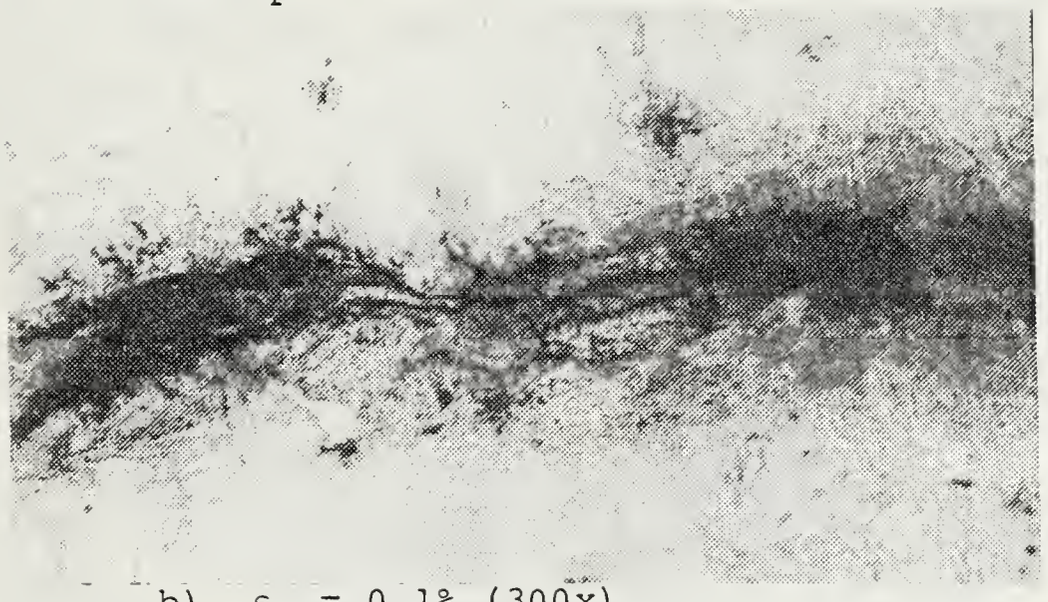

b) ε_p = 0.1% (300x)

c) ε_p = 0.2% (300x)

Figure 23. Micrographs of Continuous Cycling in Vacuum. Normalized and Tempered Material. Specimen No. 13.

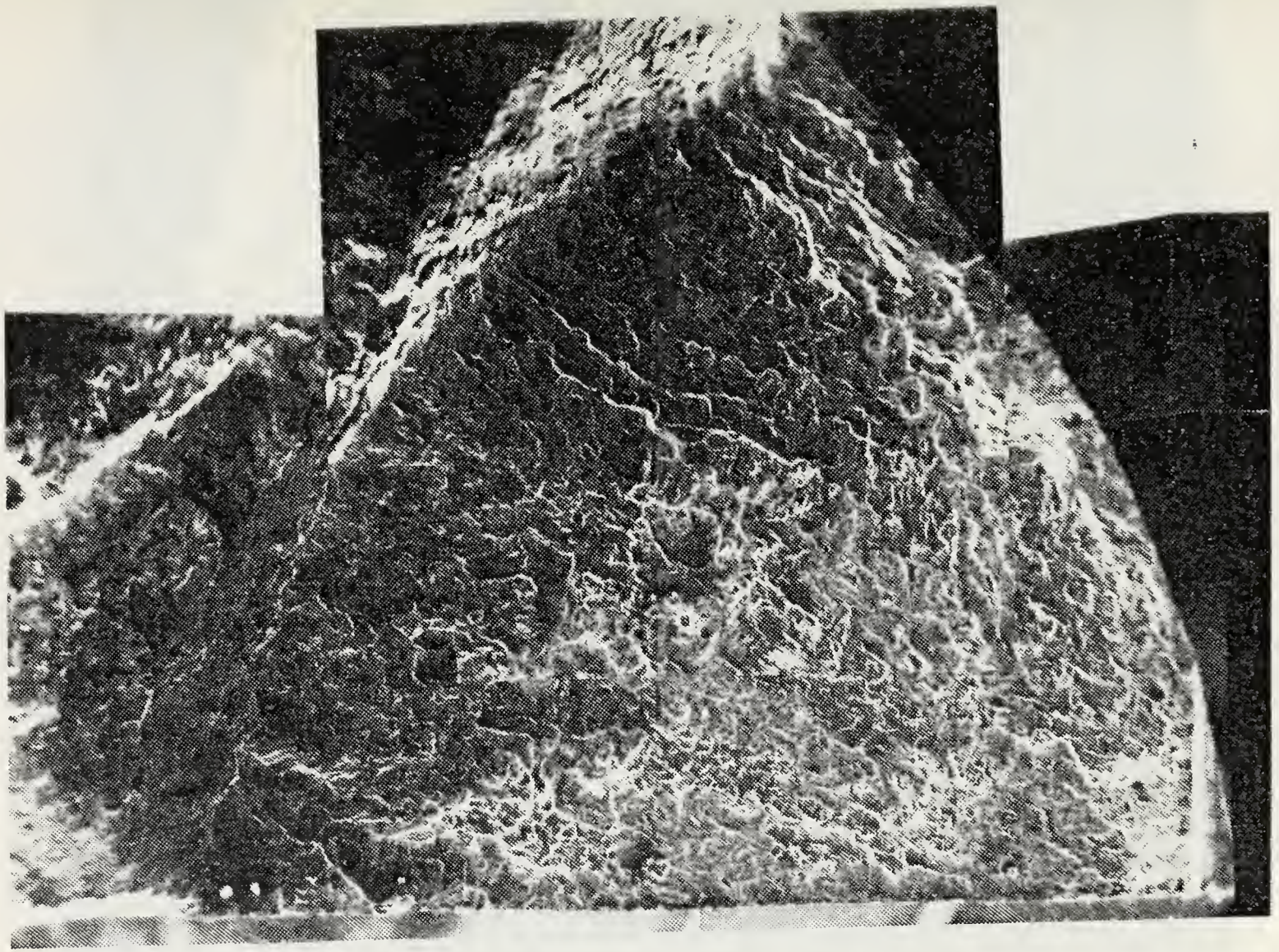

Figure 24. 1/2 Fracture Surface of Annealed Material Subjected to 1/2 Hour Dwell Periods and Continuous Cycling in Vacuum. Specimen No. 6 (31x)

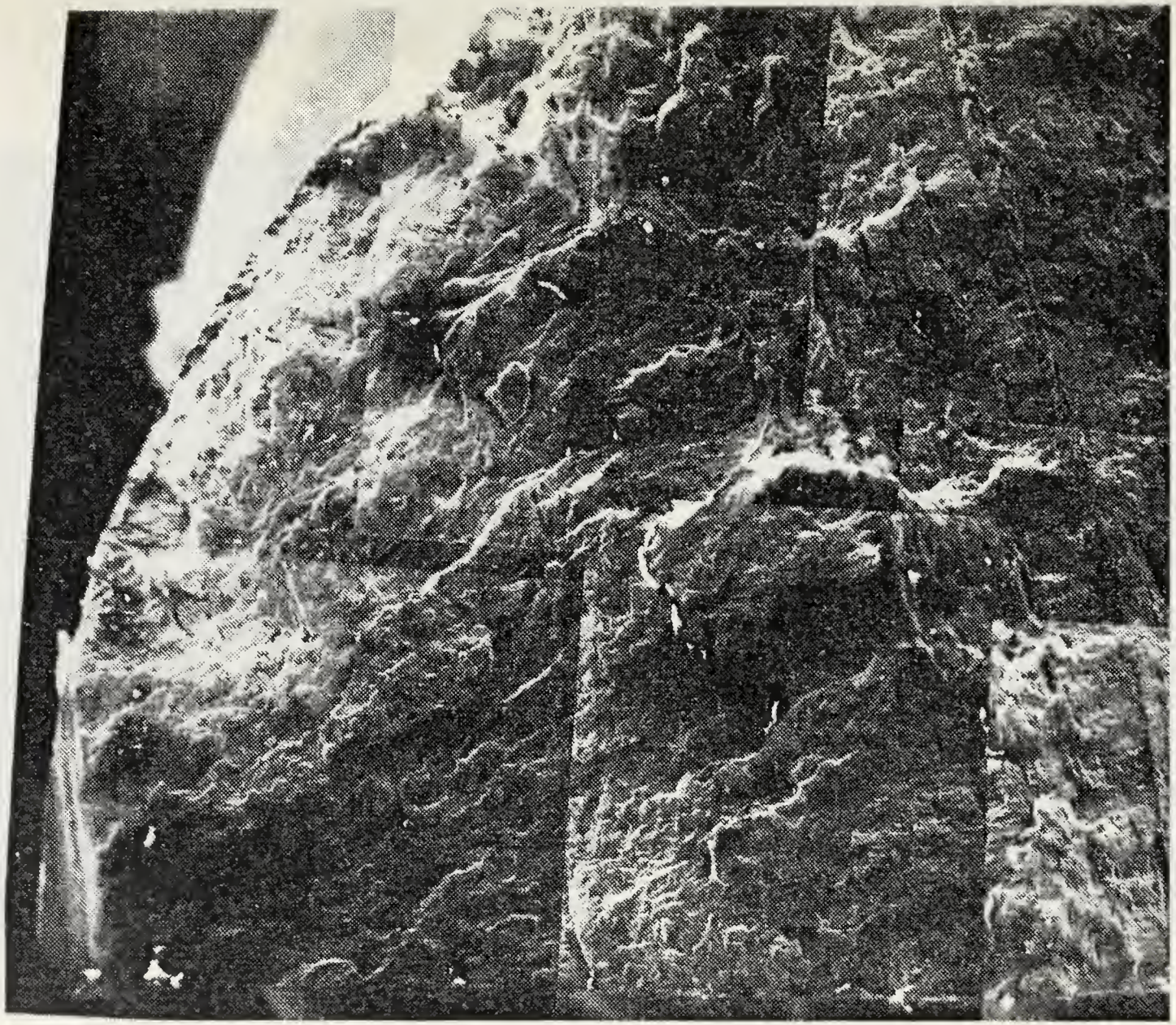

Figure 25. 1/2 Fracture Surface of Normalized and Tempered Material Subjected to 1/2 Hour Dwell Periods and Continuous Cycling in Vacuum. Specimen No. 12 (28x)

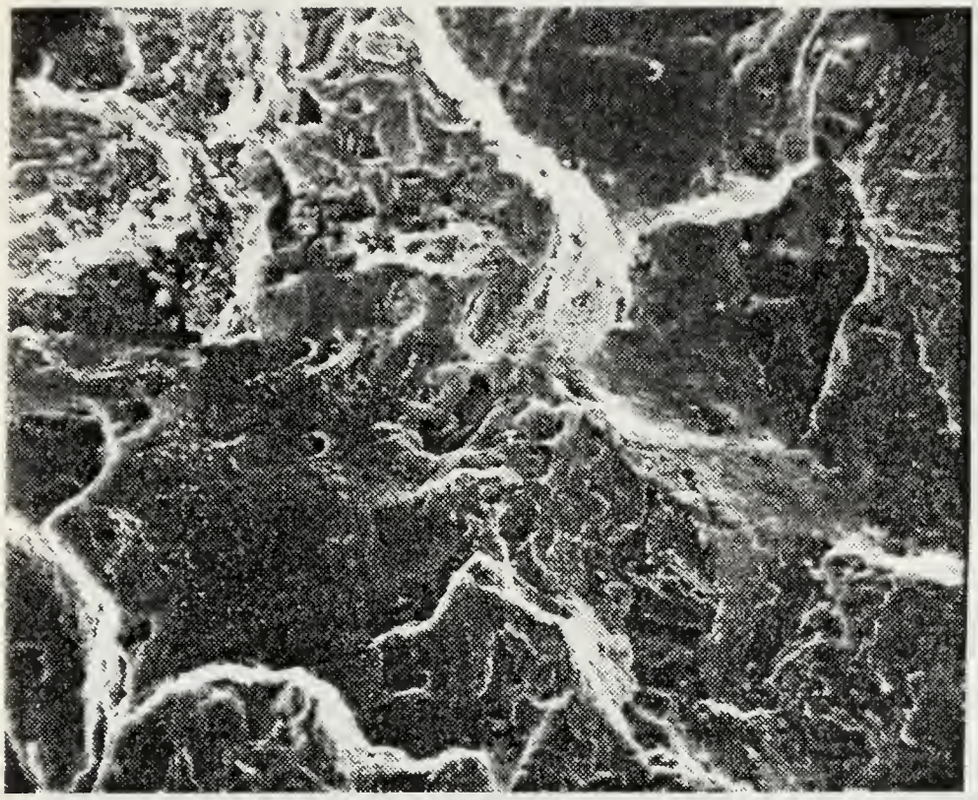

a) ε_p = 0.1% (680x)

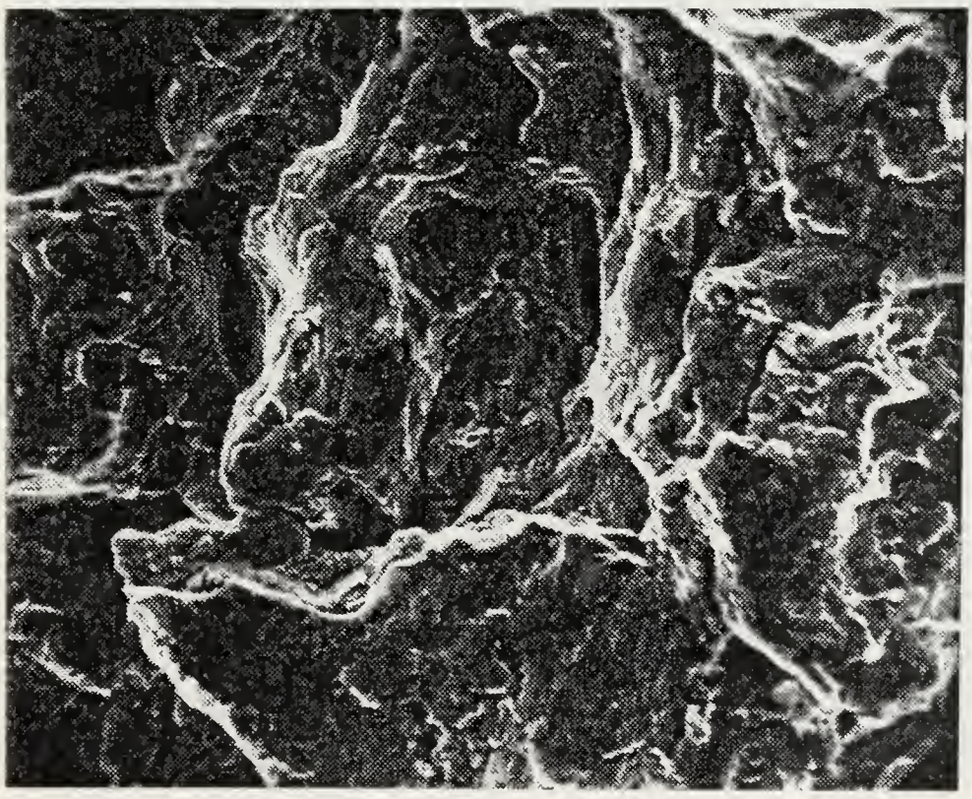

b) ε_p = 0.2% (690x)

Figure 26. Fractographs of Continuous Cycling in Vacuum of Annealed Material. Specimen No. 6.

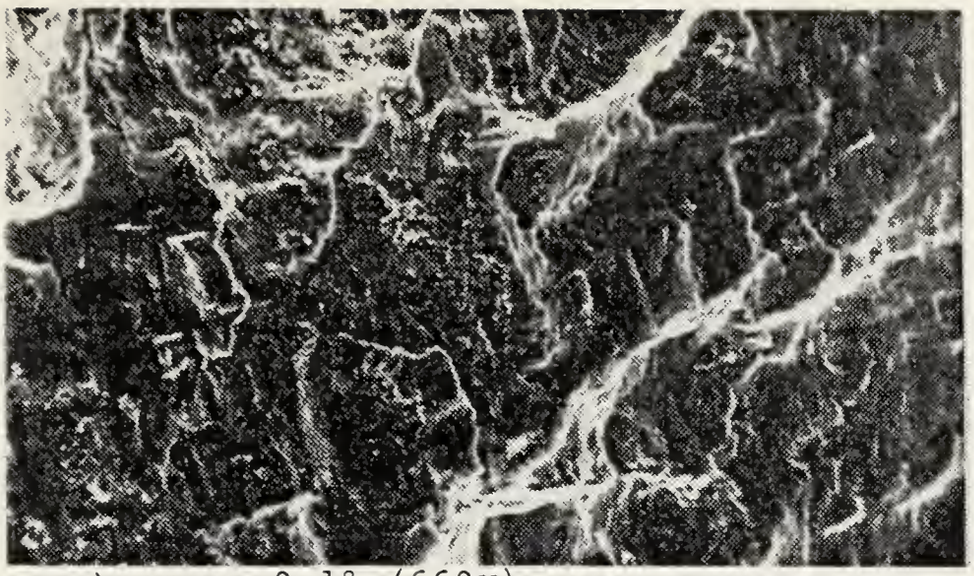

a) ε_p = 0.1% (660x)

b) ε_p = 0.2% (660x)

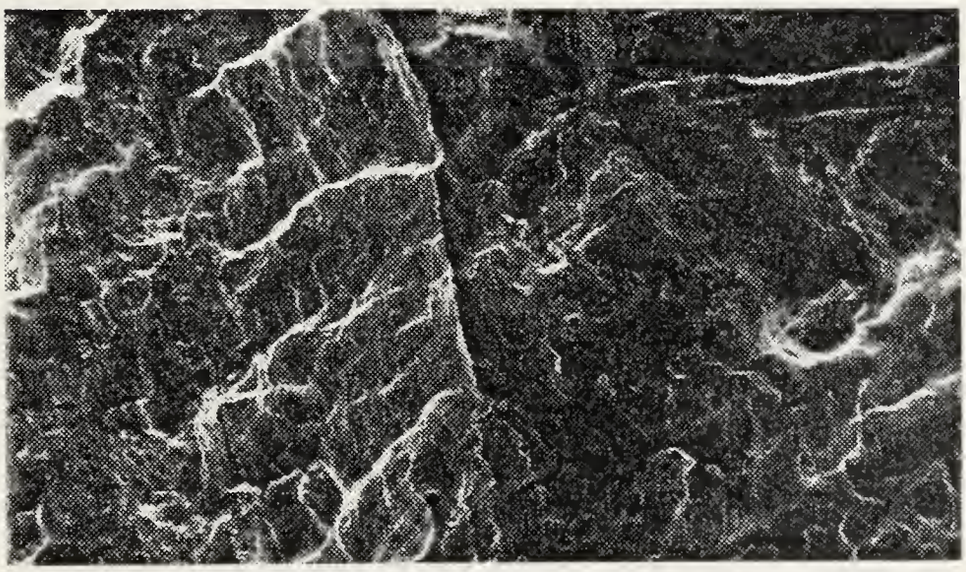

c) Transition ε_p = 0.2 - 0.1% (660x)

Figure 27. Fractographs of Continuous Cycling in Vacuum of Annealed Material. Note Transition in (c). Specimen No. 6.

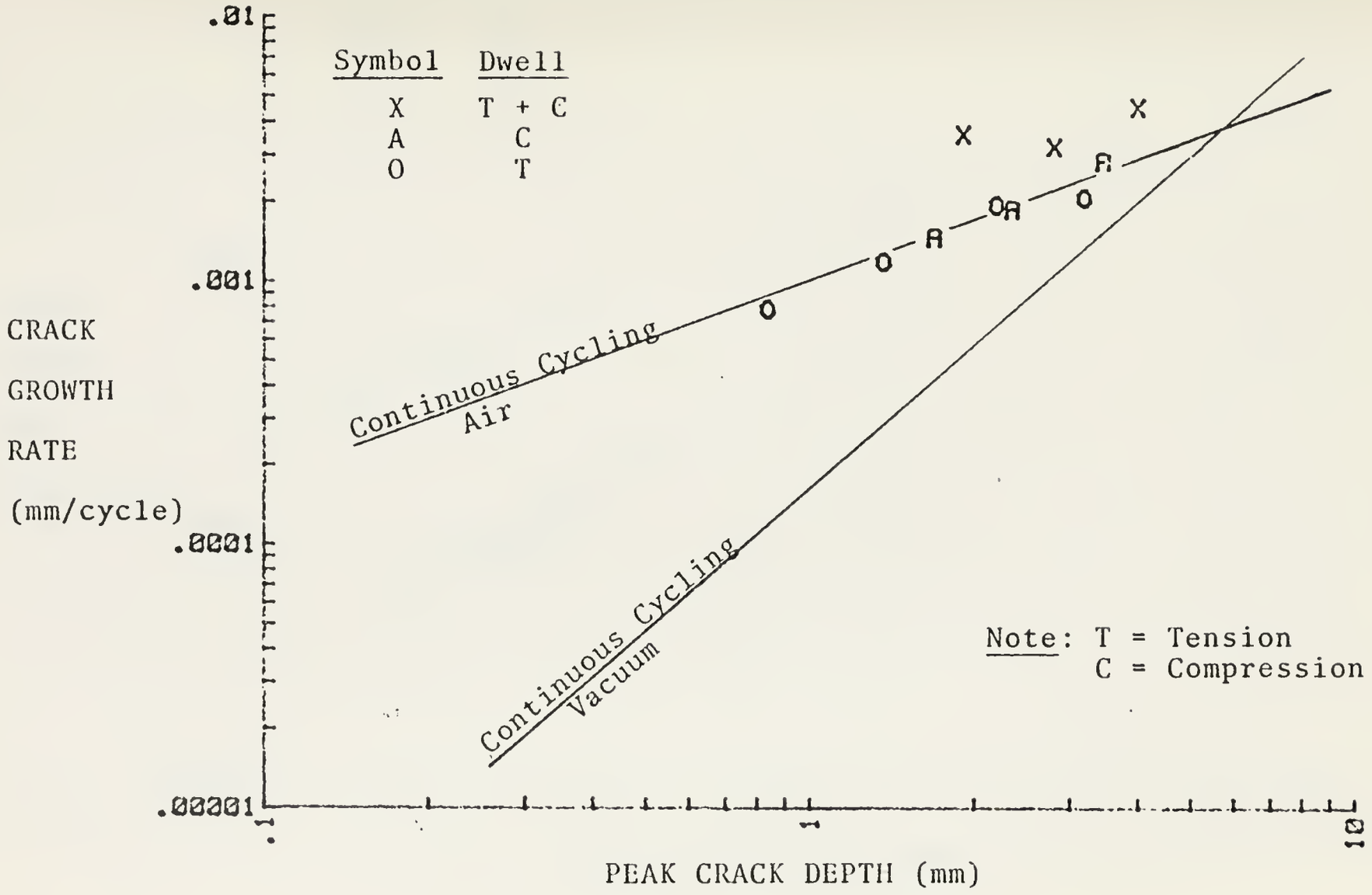

Figure 28. 1/2 Hour Dwell Data for Annealed Material at 0.2% Plastic Strain Range in Air

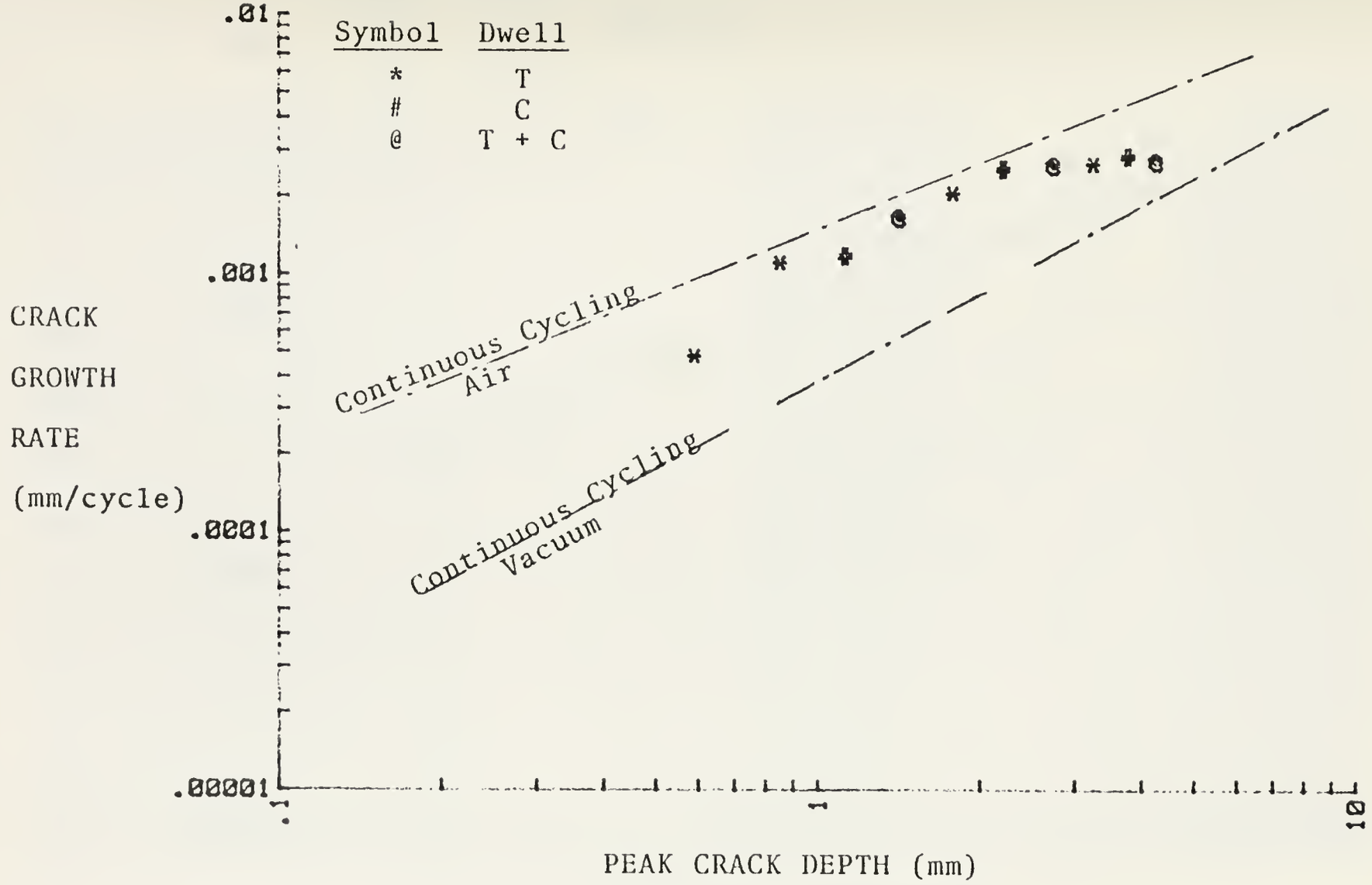

Figure 29. 1/2 Hour Dwell Data for Normalized and Tempered Material at 0.2% Plastic Strain Range in Air

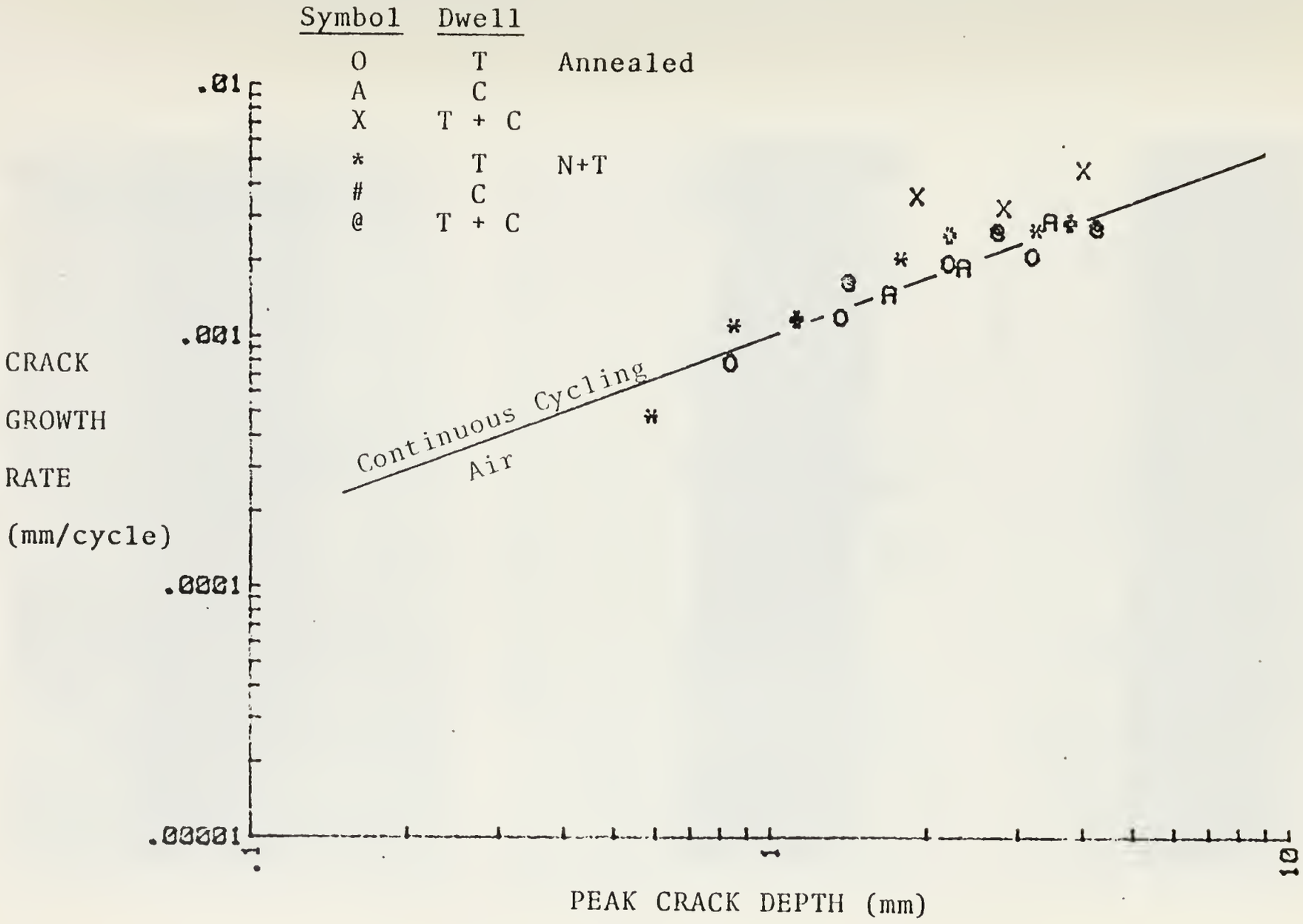

Figure 30. 1/2 Hour Dwell Data at 0.2% Plastic Strain Range in Air

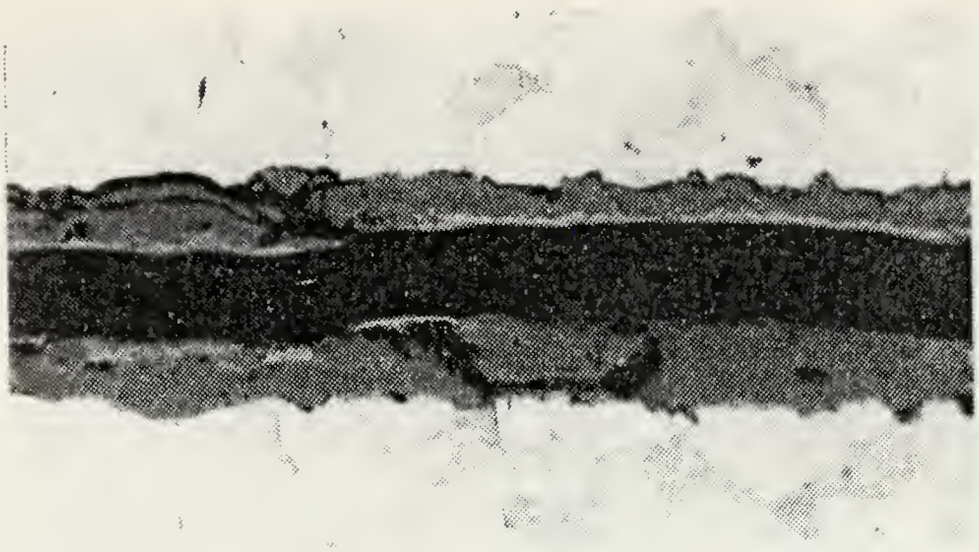

a) Tension (T) Dwell (320x)

b) Compression (C) Dwell (320x)

c) T+C Dwell (320x)

Figure 31. Micrographs of 1/2 Hour Dwell Cycling in Air, Annealed Material. Specimen No. 5.

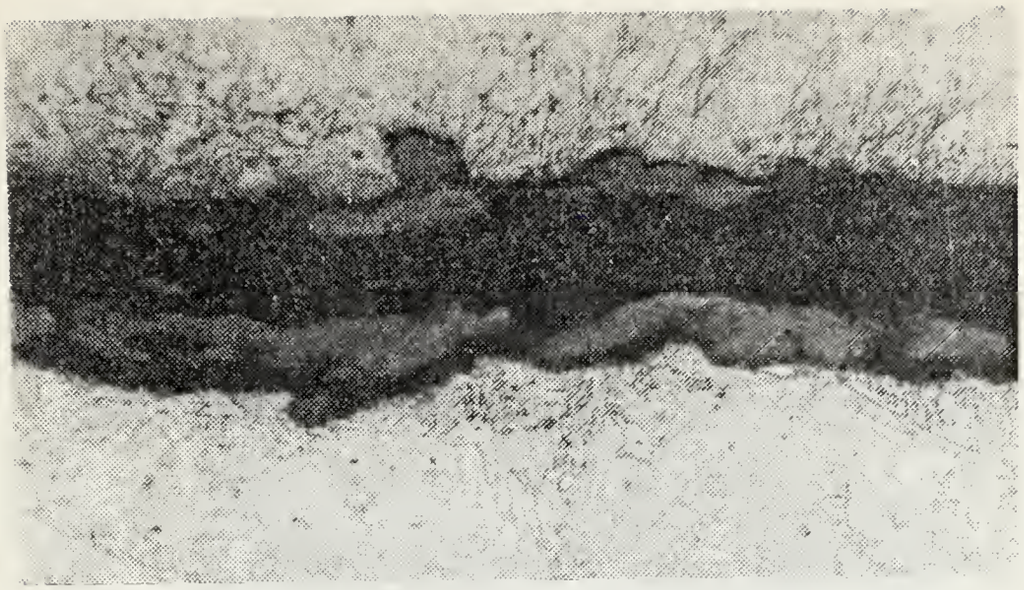

a) Tension (T) Dwell (190x)

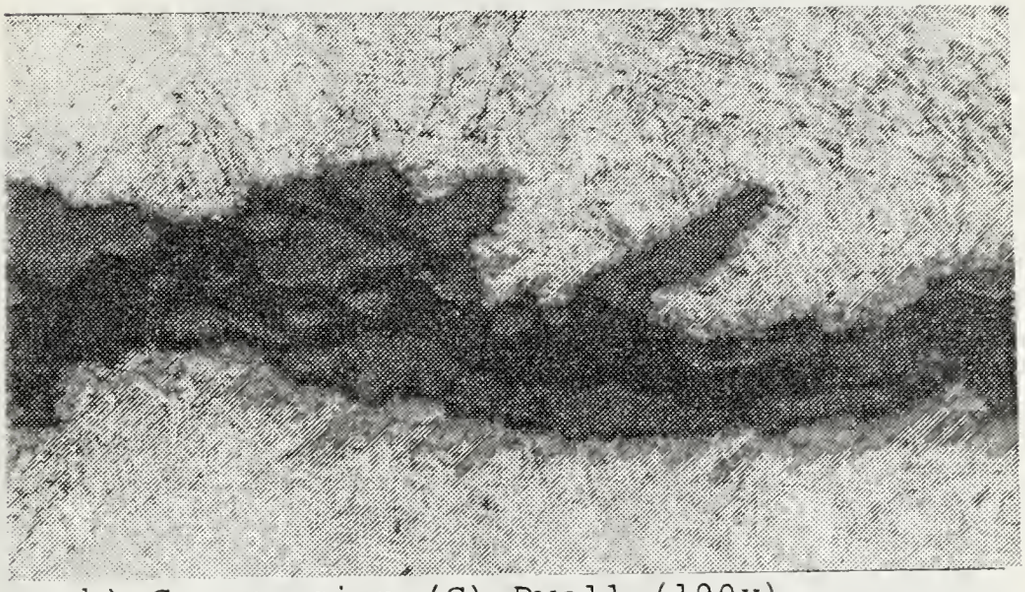

b) Compression (C) Dwell (190x)

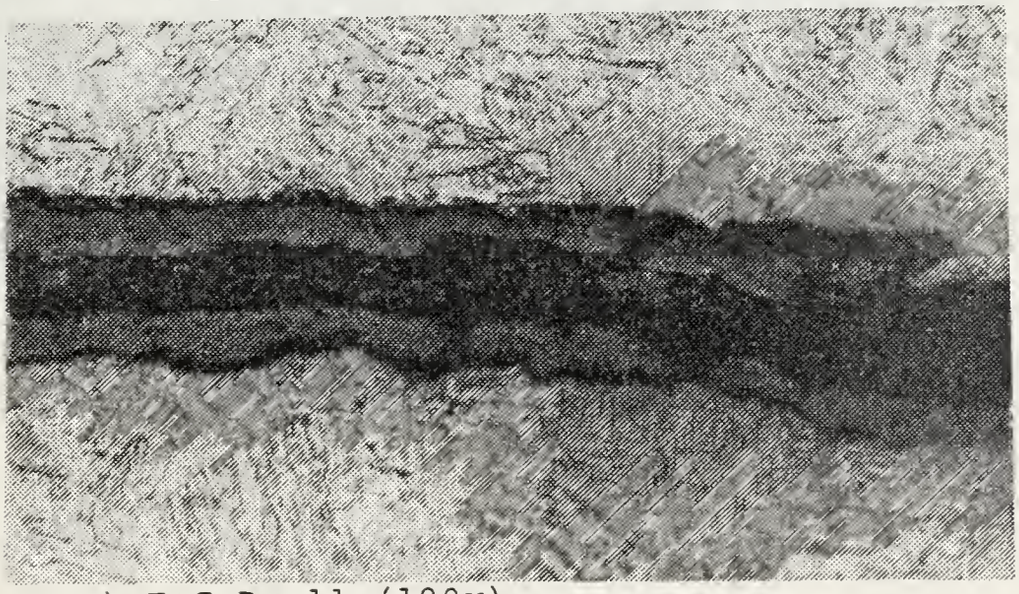

c) T+C Dwell (190x)

Figure 32. Micrographs of 1/2 Hour Dwell Cycling in Air. Normalized and Tempered Material. Specimen No. 11.

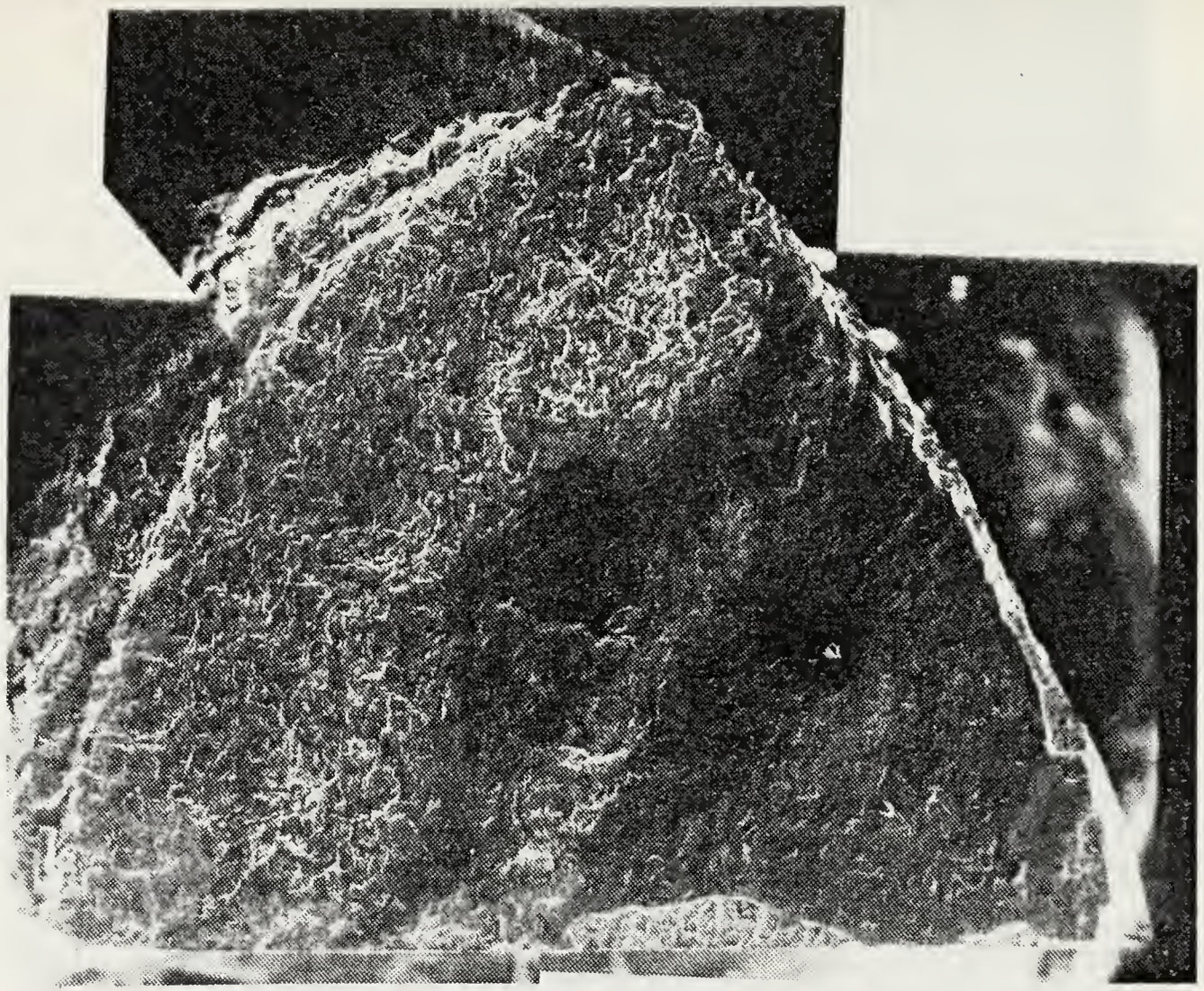

Figure 33. 1/2 Fracture Surface of Annealed Material Subjected to 1/2 Hour Dwell Cycling in Air. Specimen No. 5 (30x)

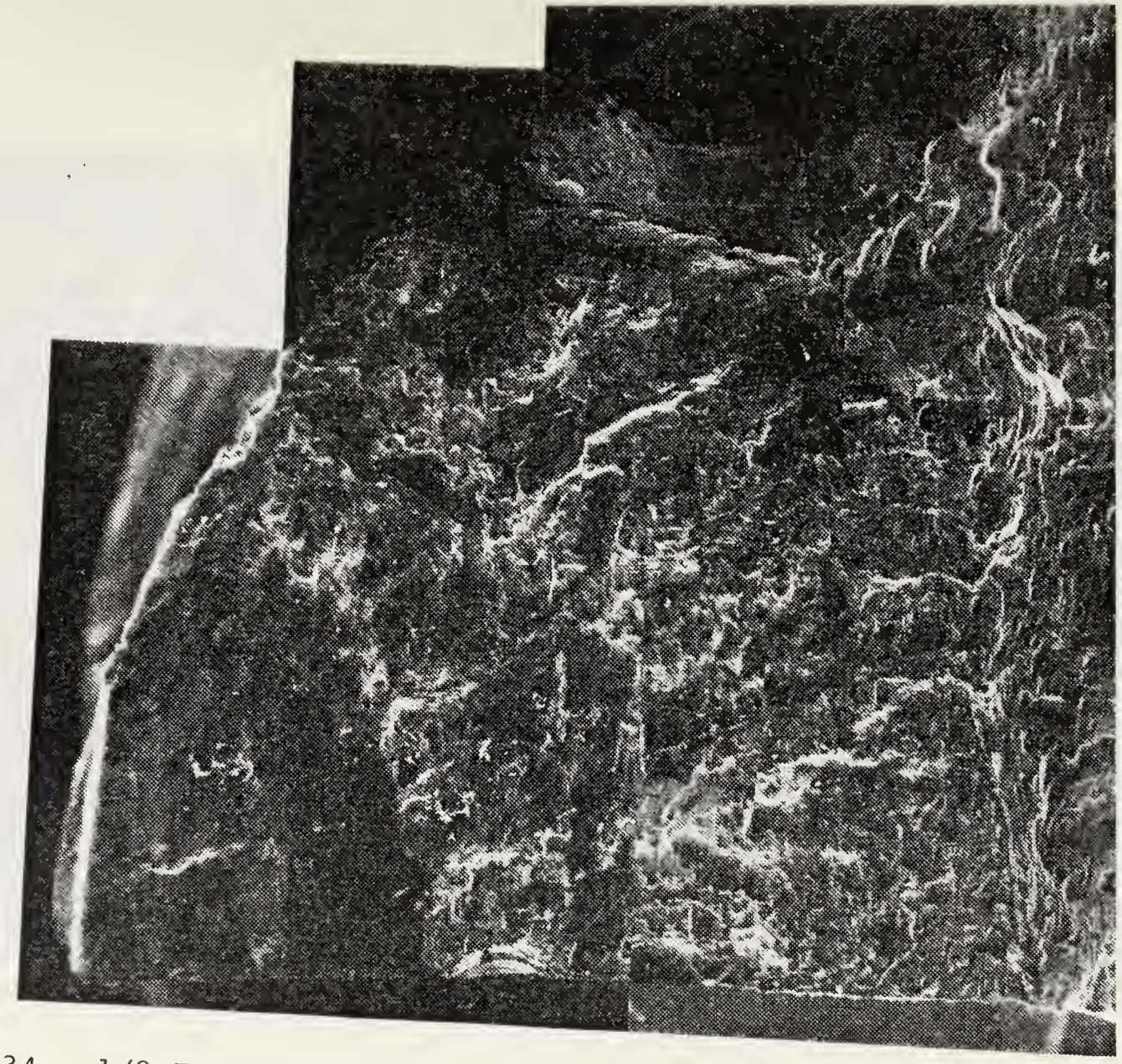

Figure 34. 1/2 Fracture Surface of Normalized and Tempered Material Subjected to 1/2 Hour Dwell Cycling in Air. Specimen No. 11 (26x)

a) Tension (T) Dwell (575x)

b) Compression (C) Dwell (575x)

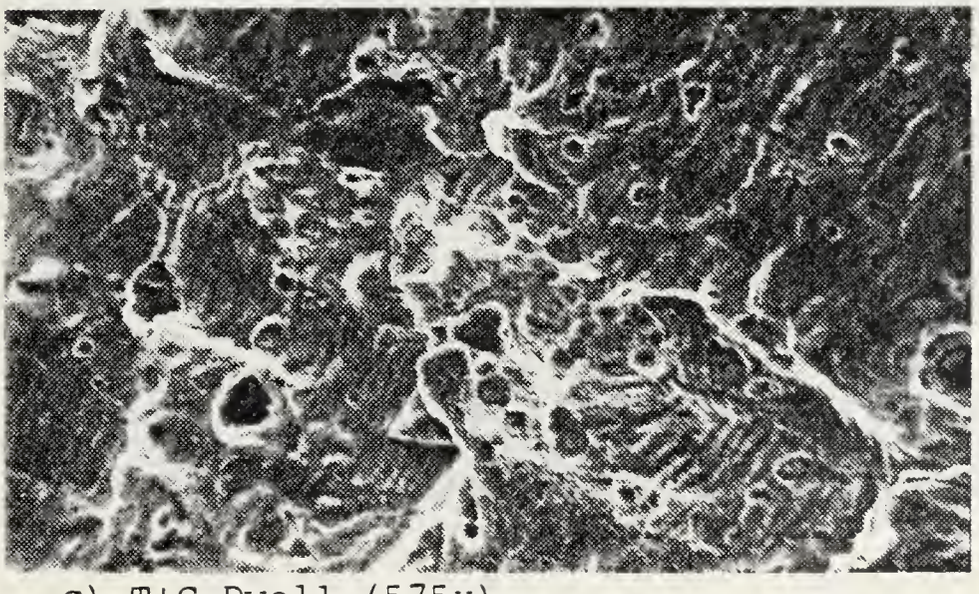

c) T+C Dwell (575x)

Figure 35. Fractographs of Annealed Material Subjected to 1/2 Hour Dwell Cycling in Air. Specimen No. 5.

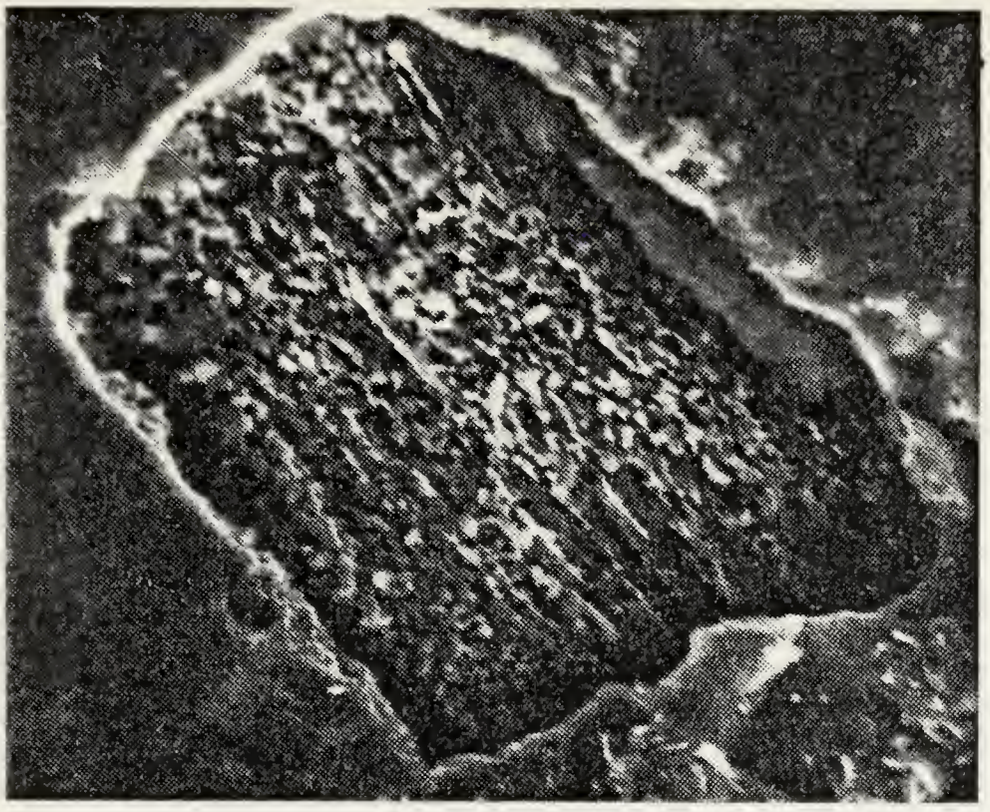

a) Tension Dwell (1300x) (Note: thick oxide layer)

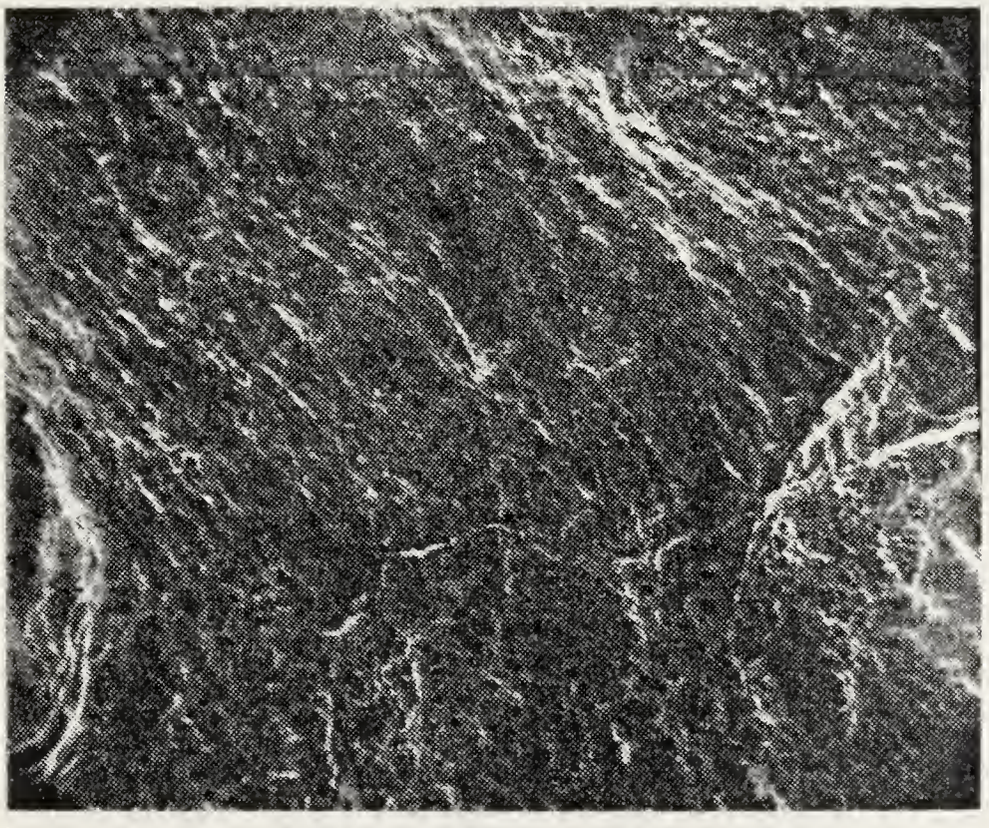

b) Tension + Compression Dwell (645x)

Figure 36. Fractographs of Normalized and Tempered Material Subjected to 1/2 Hour Dwell Cycling in Air. A compression fractograph could not be obtained due to the heavy oxide layer present.

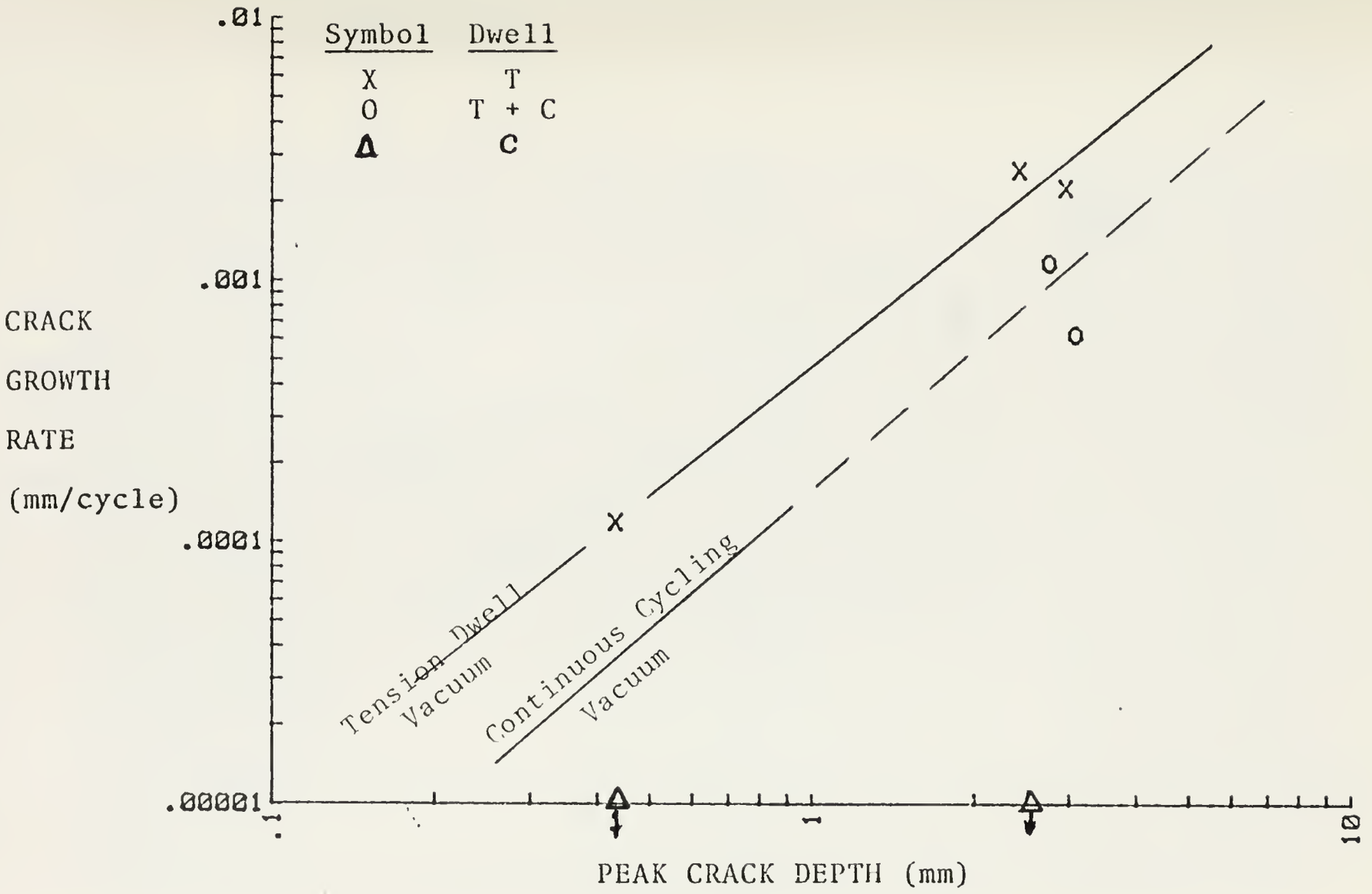

Figure 37. 1/2 Hour Dwell Data for Annealed Material at 0.2% Plastic Strain Range in Vacuum

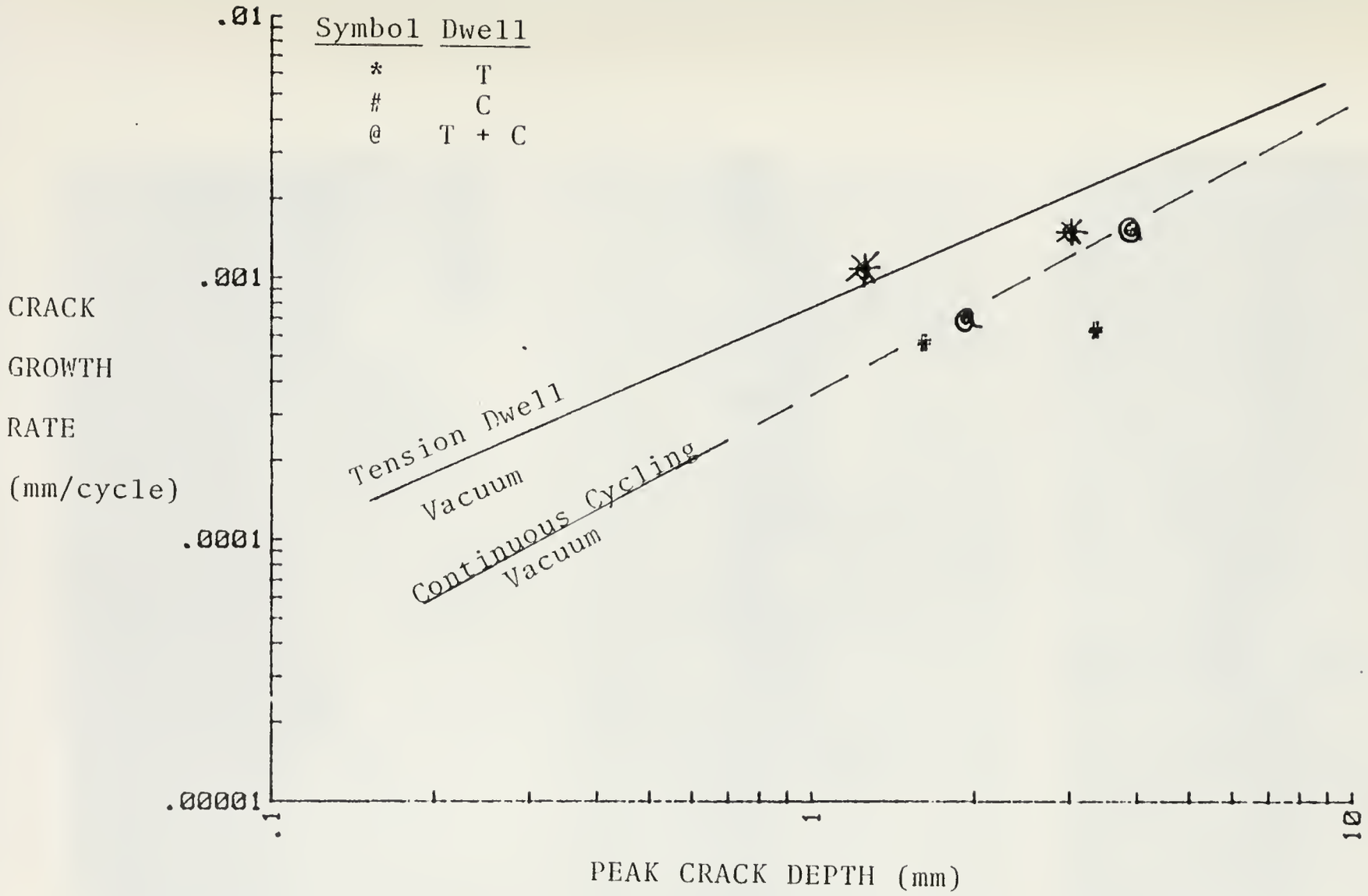

Figure 38. 1/2 Hour Dwell Data for Normalized and Tempered Material at 0.2% Plastic Strain Range in Vacuum

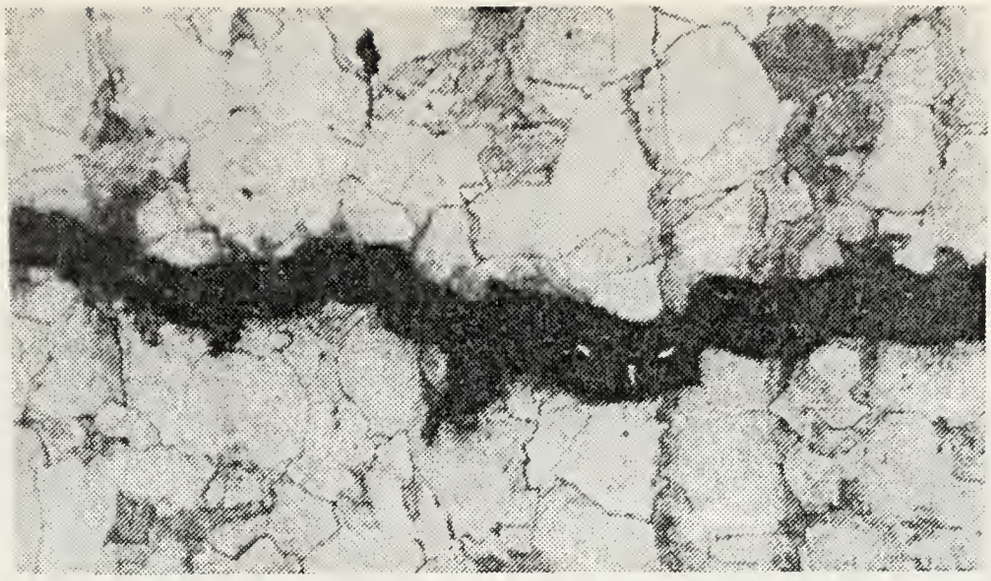

a) Tension Dwell (240x)

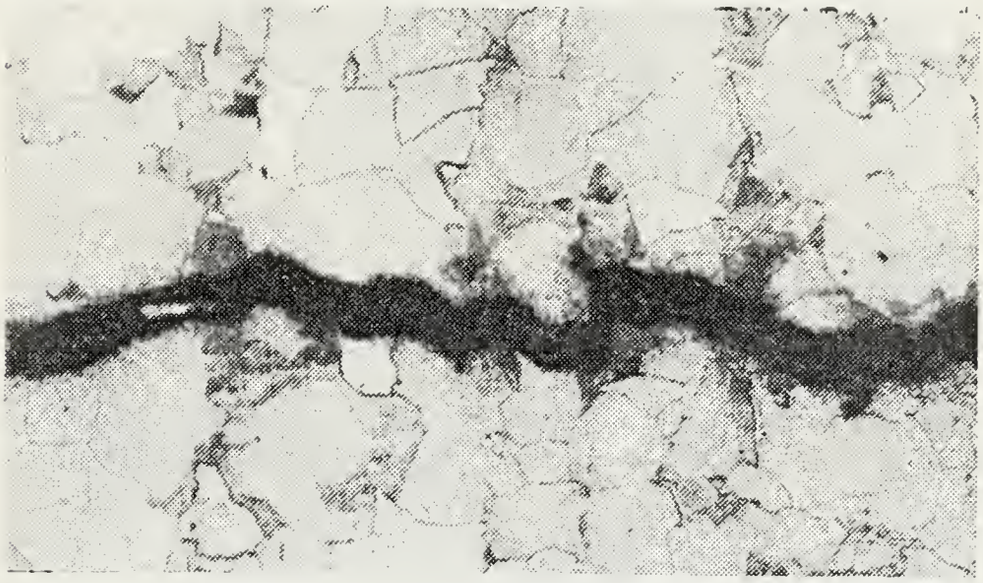

b) T+C Dwell (240x)

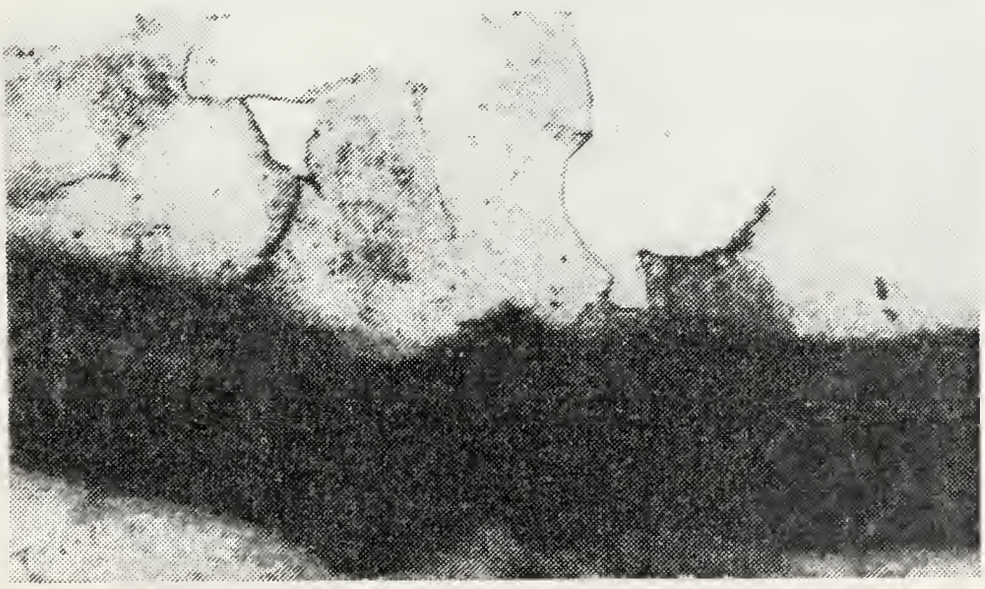

c) T/C/Continuous Cycling (600x)

Figure 39. Micrographs of Annealed Material with 1/2 Hour Dwell Cycling in Vacuum. Specimen No. 6. Note: There was no crack growth in compression.

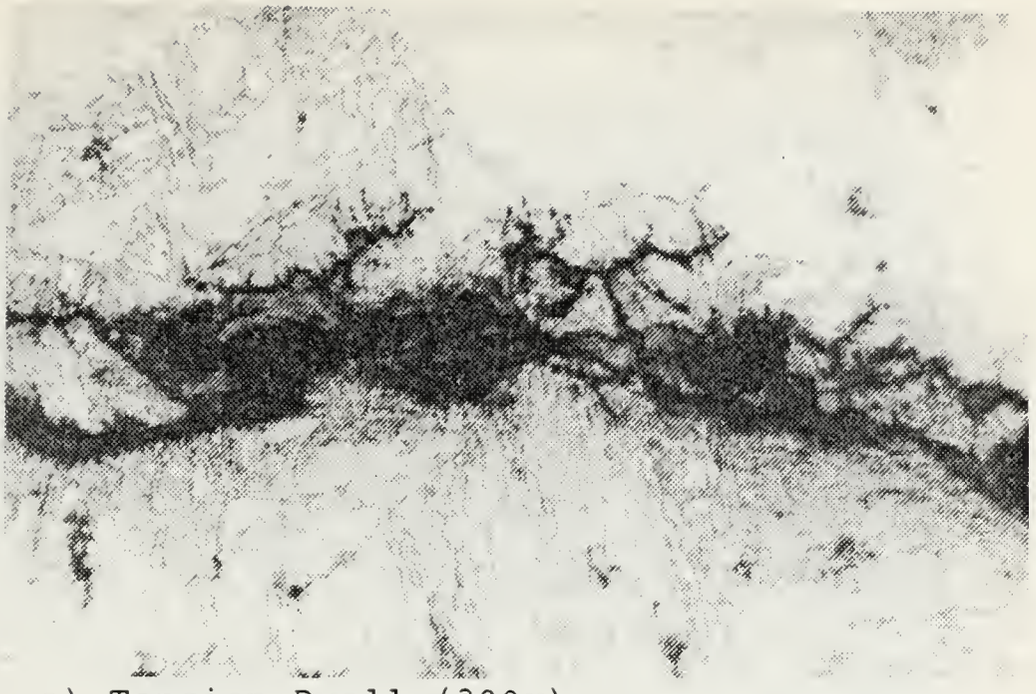

a) Tension Dwell (300x)

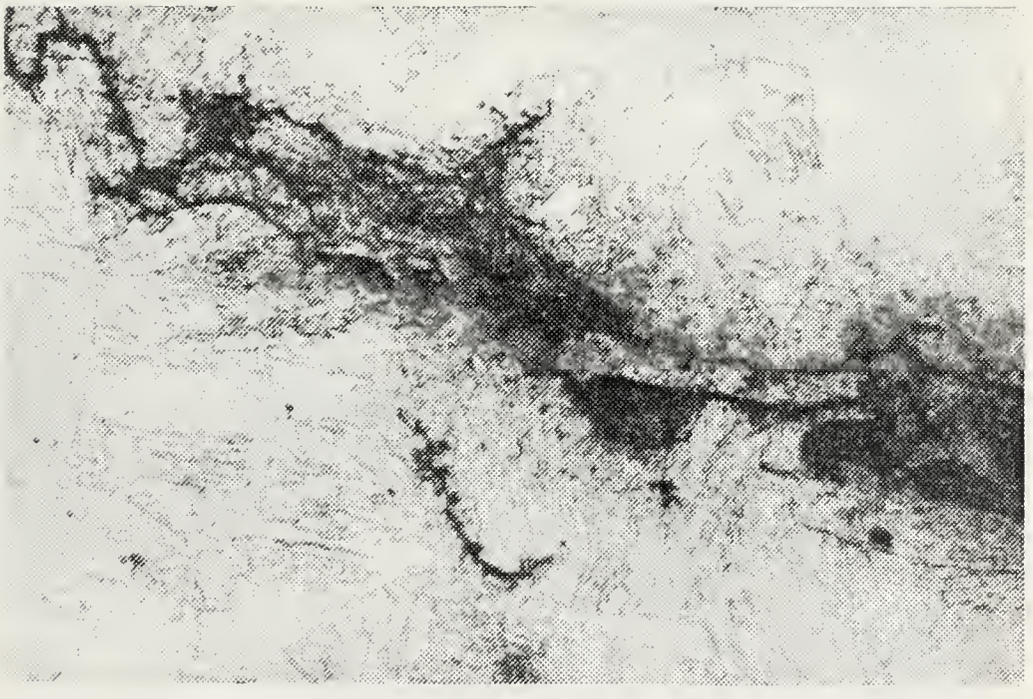

b) Compression Dwell (300x)

Figure 40. Micrographs of Normalized and Tempered Material with 1/2 Hour Dwell Cycling in Vacuum. Specimen No. 13.

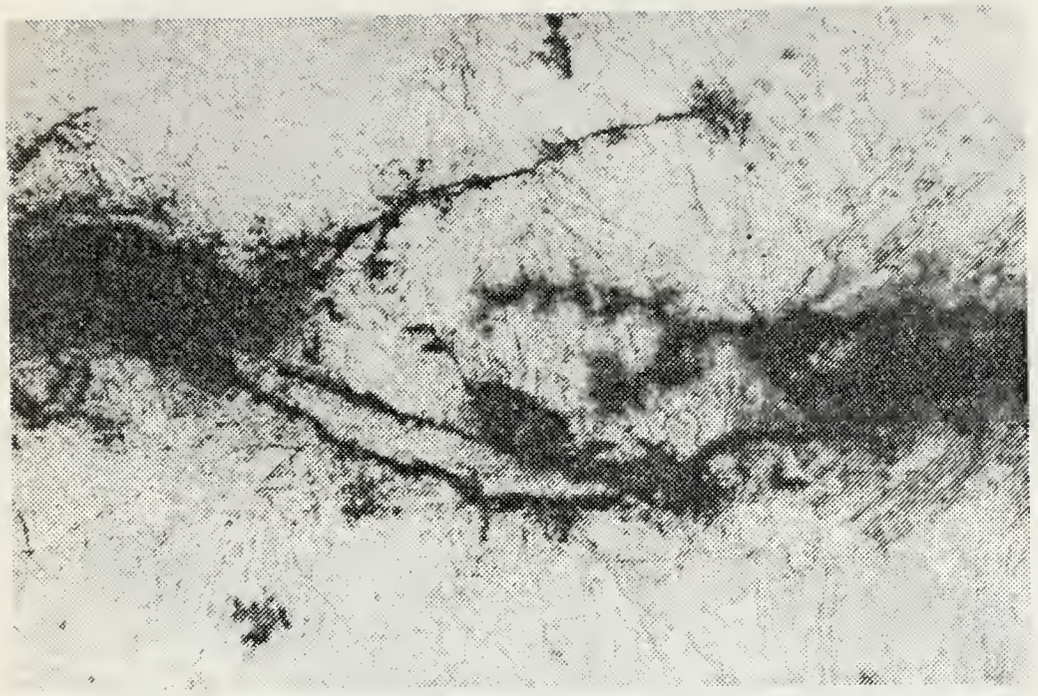

c) Tension + Compression Dwell (300x)

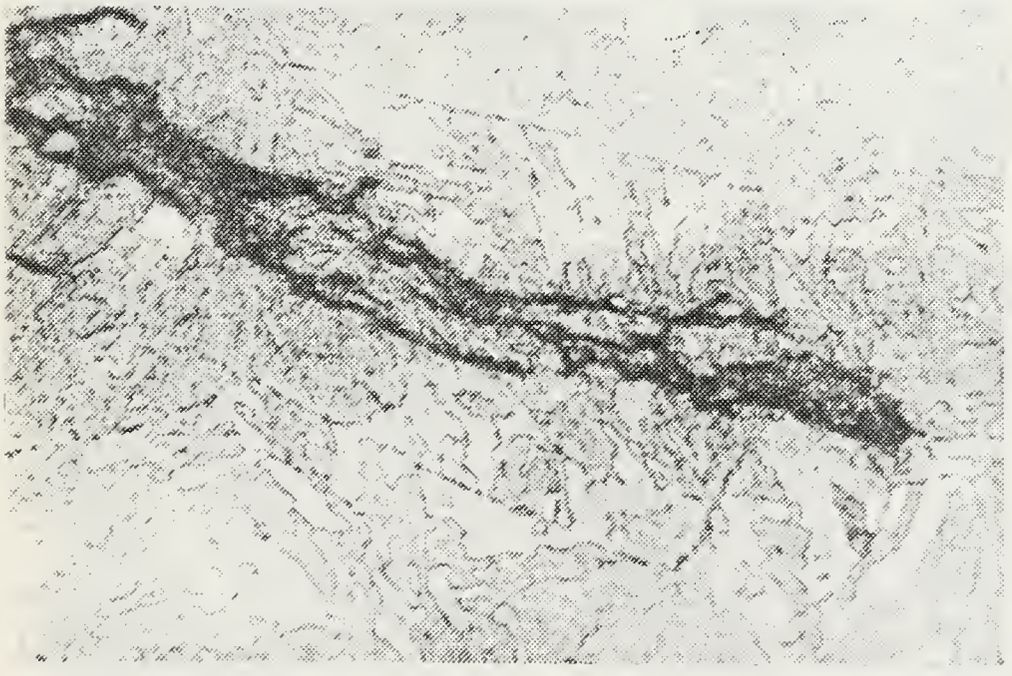

d) Tension + Compression Dwell (750x)
Tip of Crack shown.

Figure 41. Micrographs of Normalized and Tempered Material with 1/2 Hour Dwell Cycling in Vacuum. Specimen No. 13.

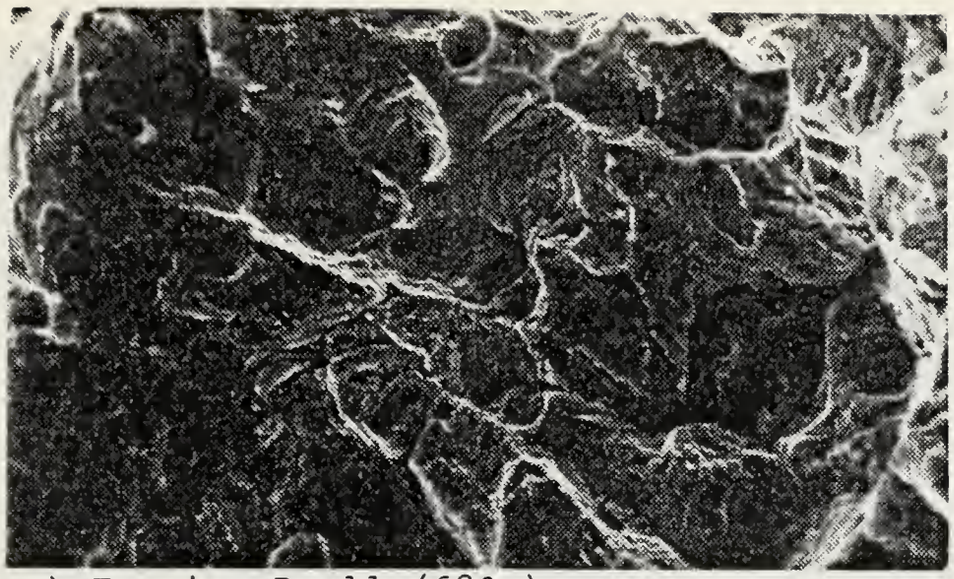

a) Tension Dwell (680x)

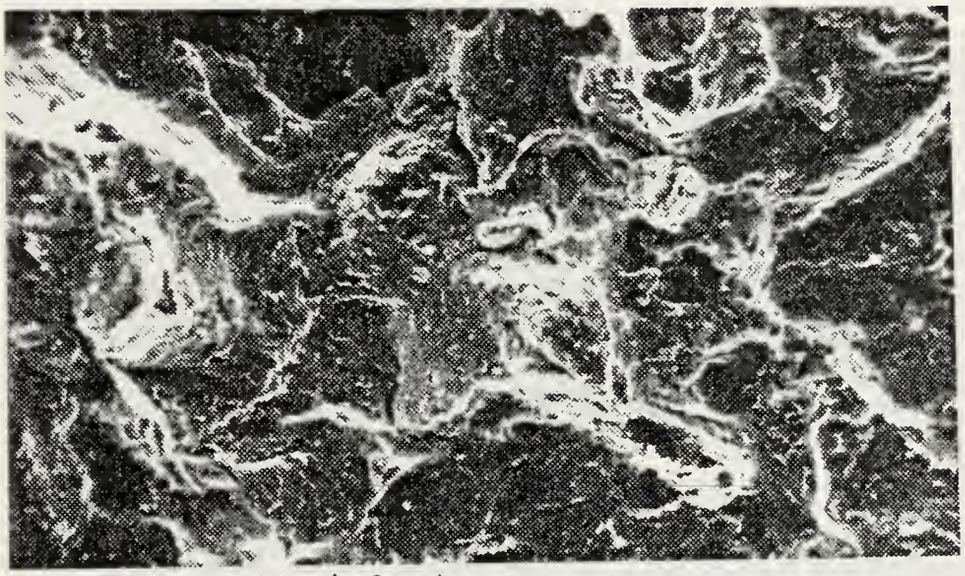

b) T+C Dwell (680x)

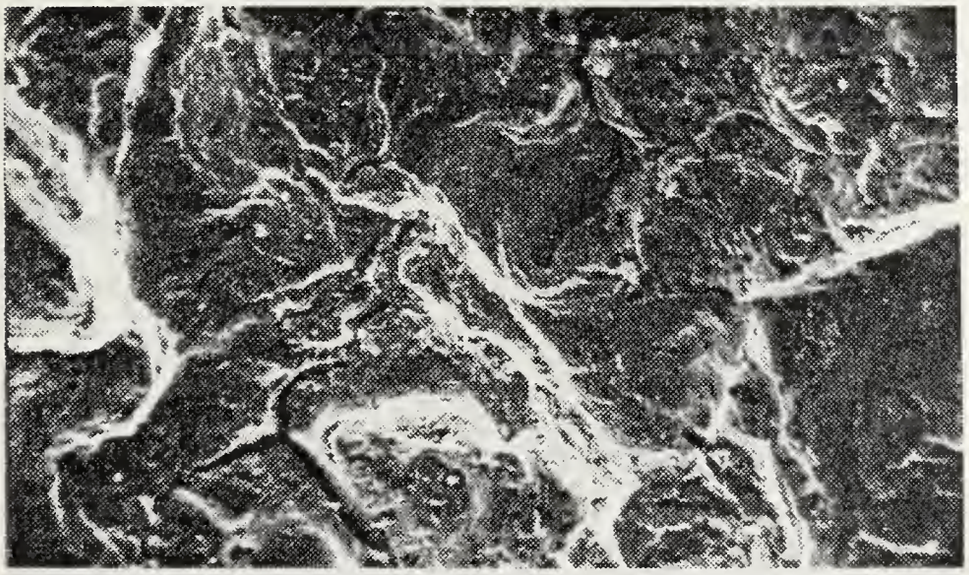

c) Tension Dwell (680x), Note Possible Intergranular Fracture

Figure 42. Fractographs of Annealed Material with 1/2 Hour Dwell Cycling in Vacuum. Specimen No. 6.

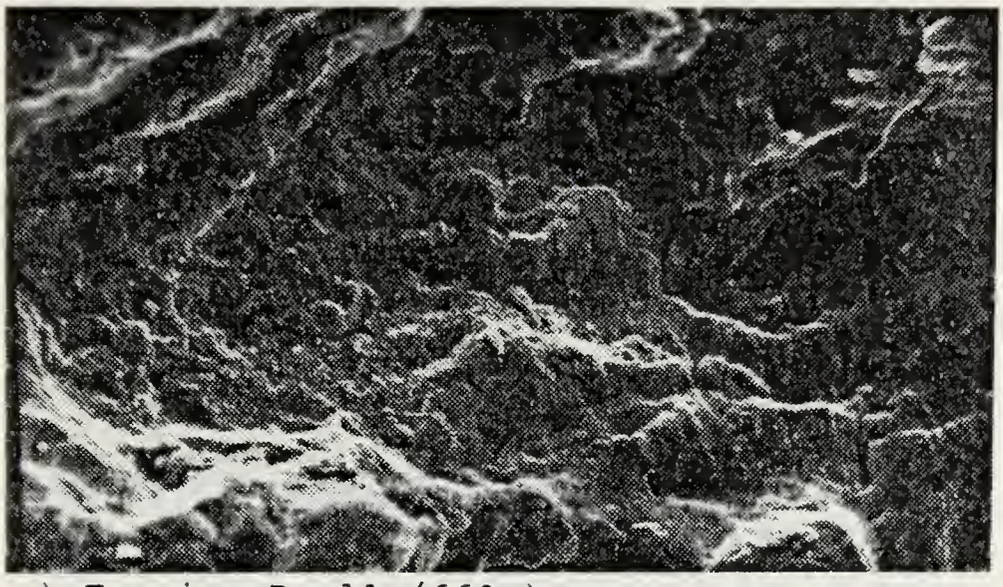

a) Tension Dwell (660x)

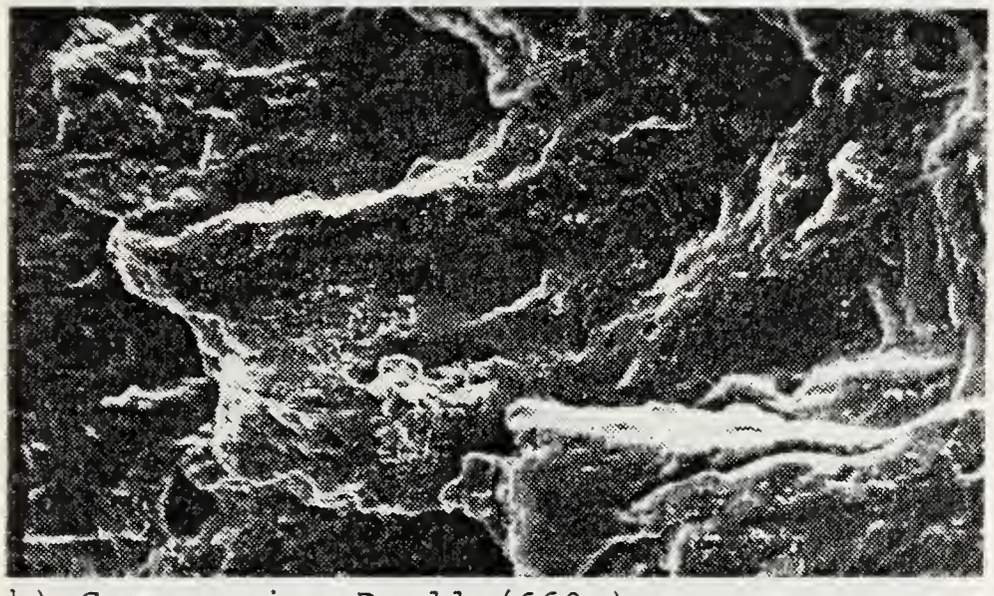

b) Compression Dwell (660x)

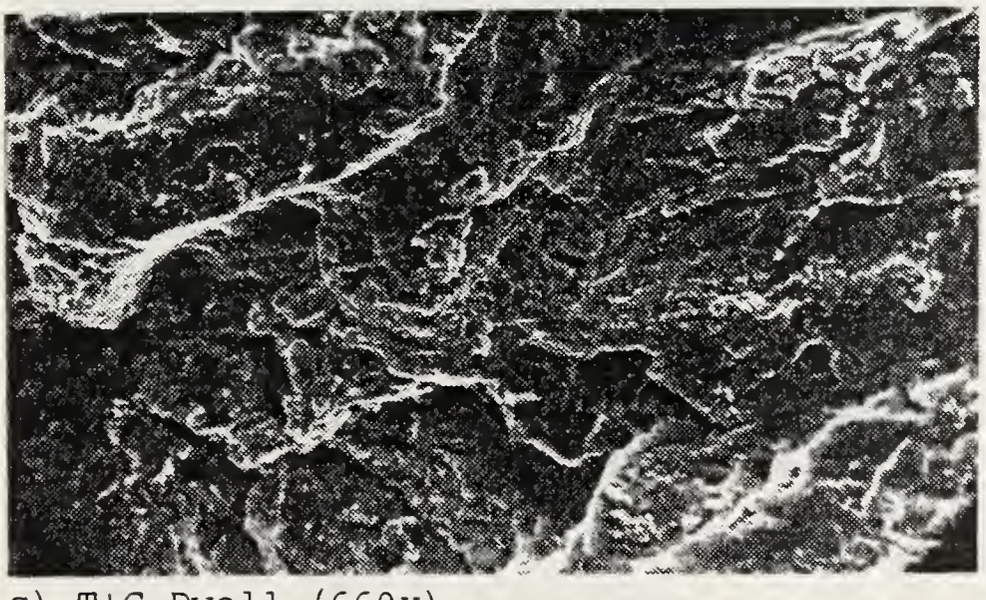

c) T+C Dwell (660x)

Figure 43. Fractographs of Normalized and Tempered Material with 1/2 Hour Dwell Cycling in Vacuum. Specimen No. 13.

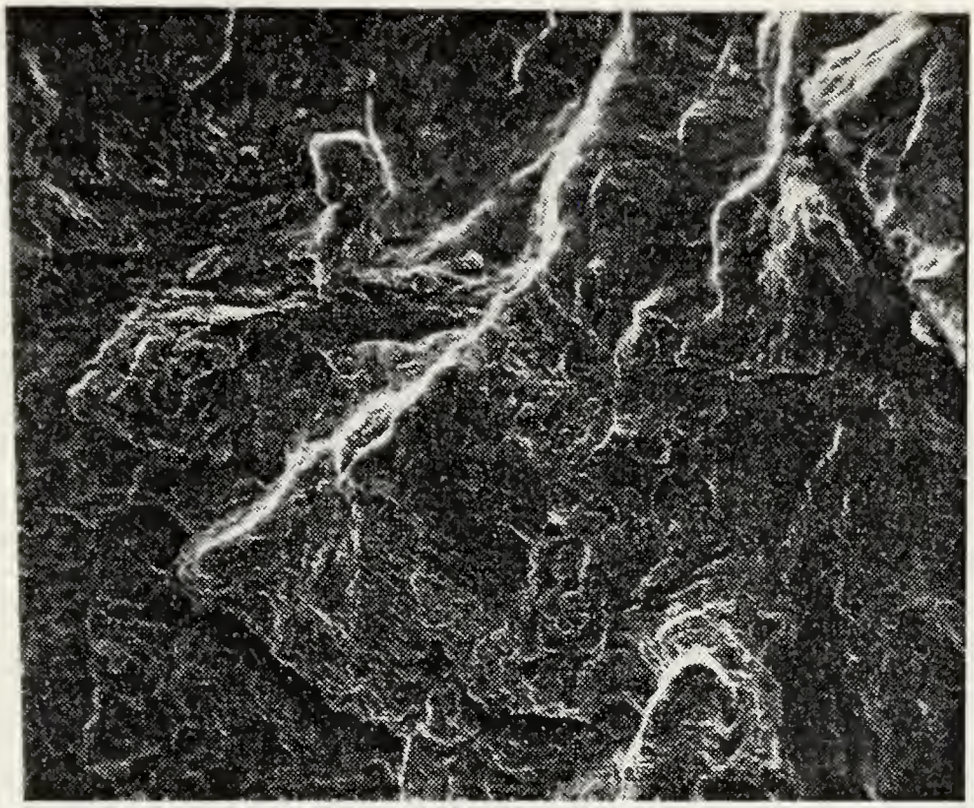

a) Compression - T+C Transition Region (265x)

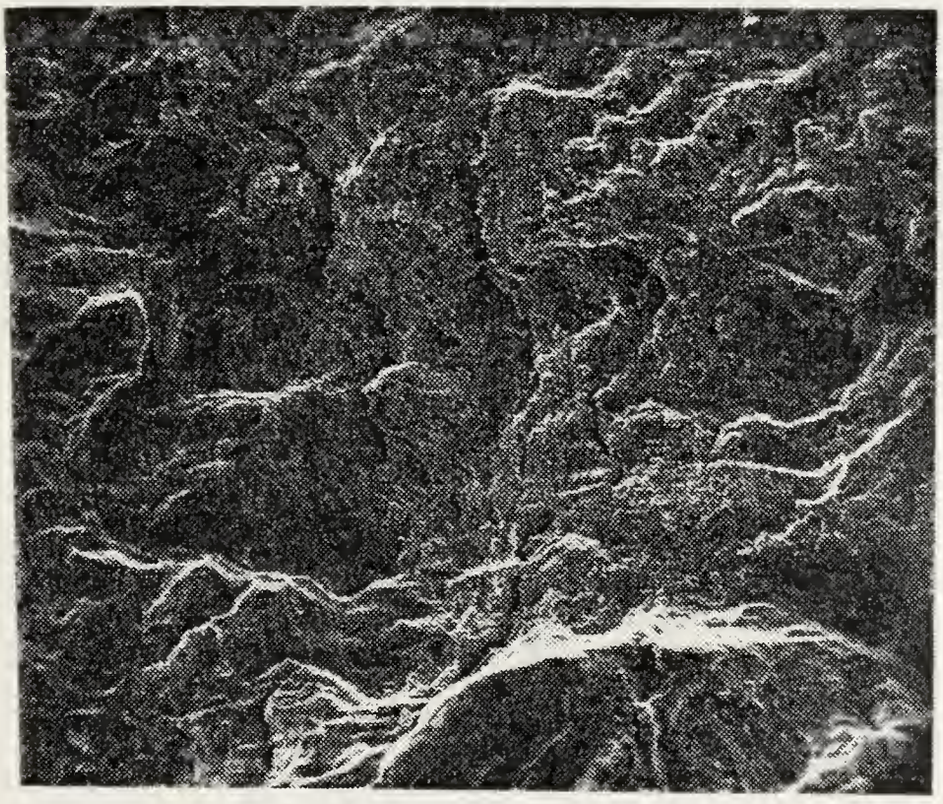

b) Tension - Compression Transition Region (265x)
Note "sticky" character of compression surface possibly denoting reweldment of the fracture surface

Figure 44. Surface Transition Regions for Normalized and Tempered Material in Vacuum. Specimen No. 13.

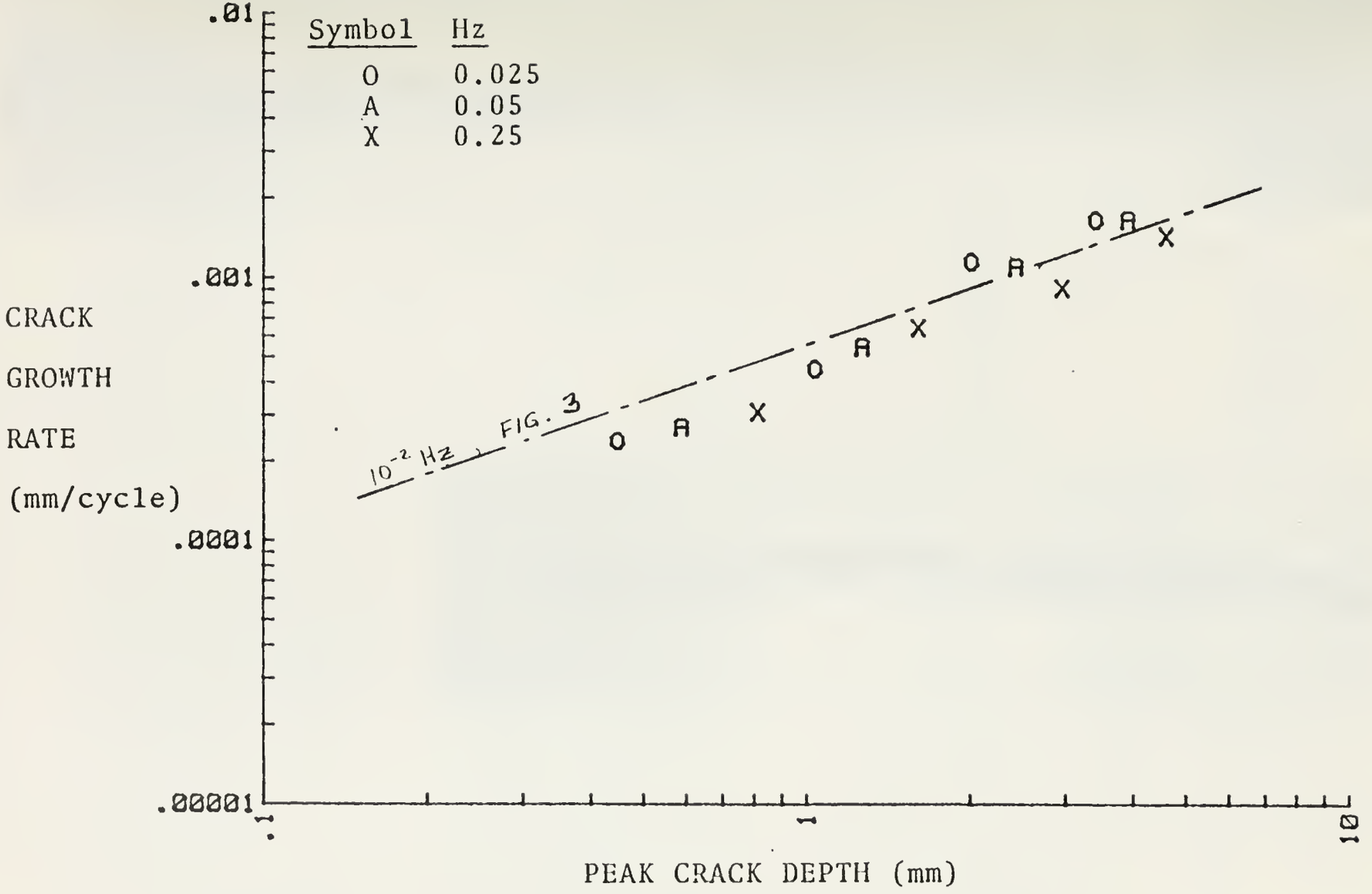

Figure 45. Continuous Cycling Data at High Frequency. Annealed Material Tested at 0.2% Plastic Strain Range.

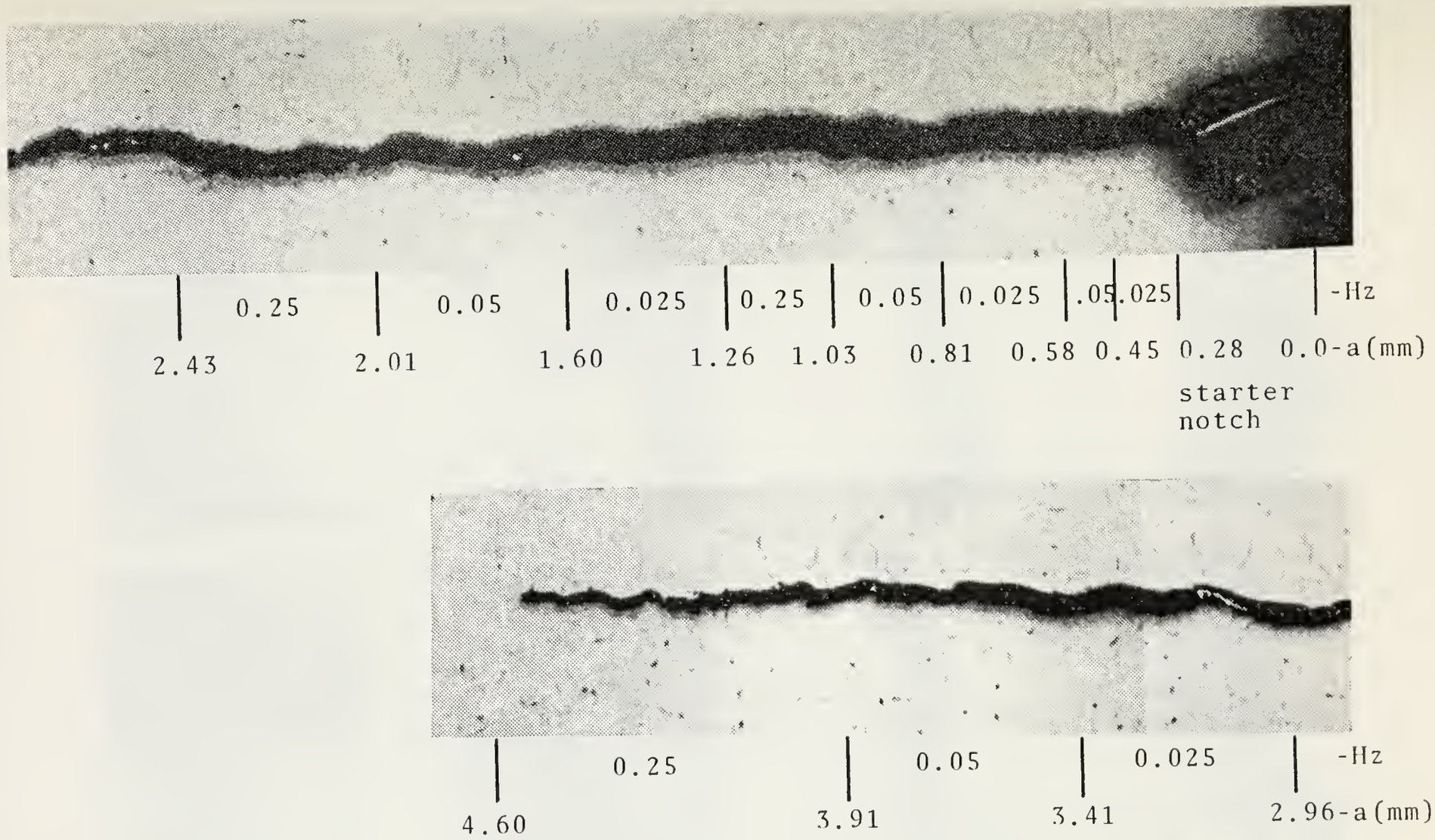

Figure 46. Crack Profile of Annealed Material with Cycling at Various High Frequencies in Air. Specimen No. 12 (64x).

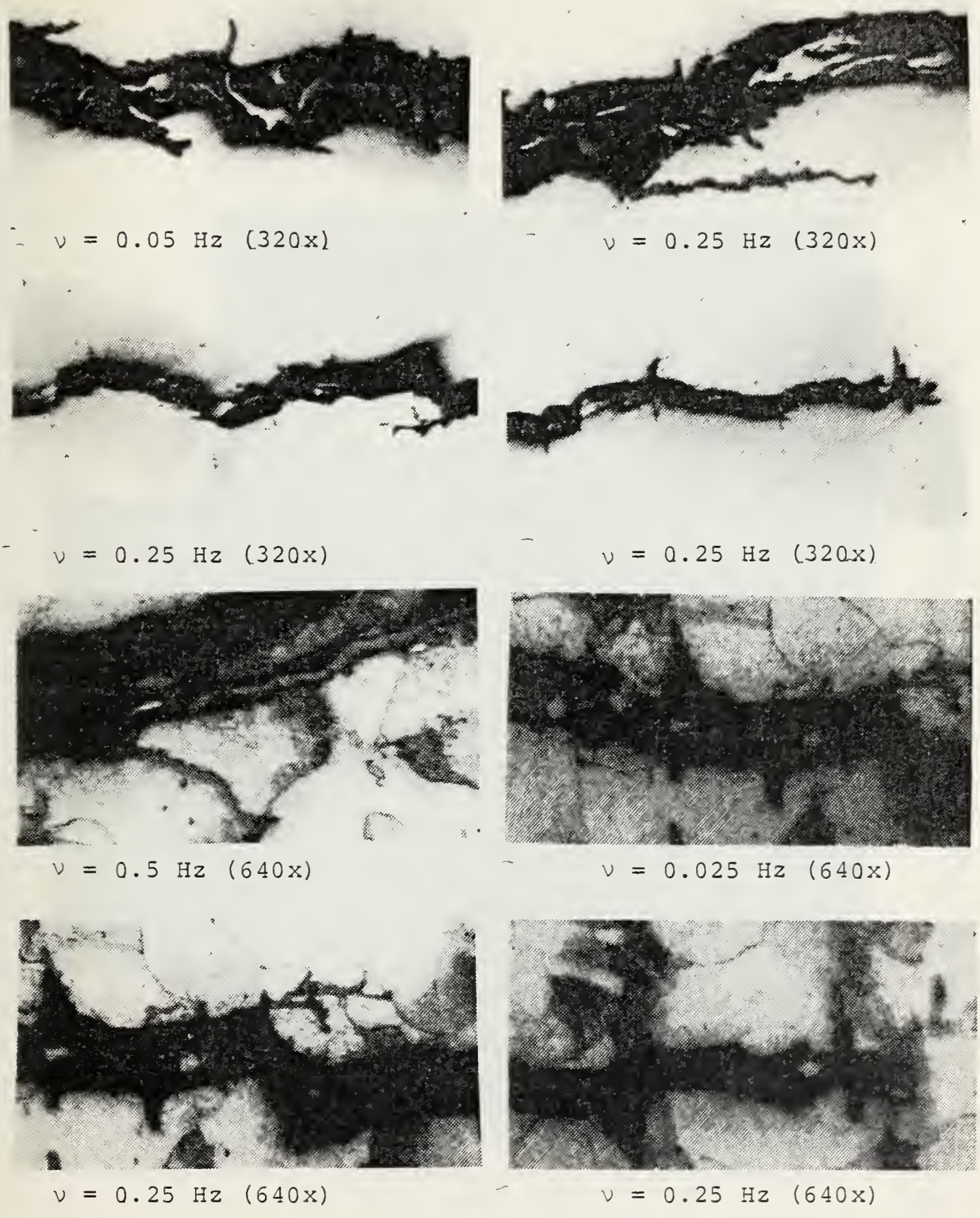

Figure 47. Frequency Effects in Annealed Material. Continuous Cycling in Air. Specimen No. 12.

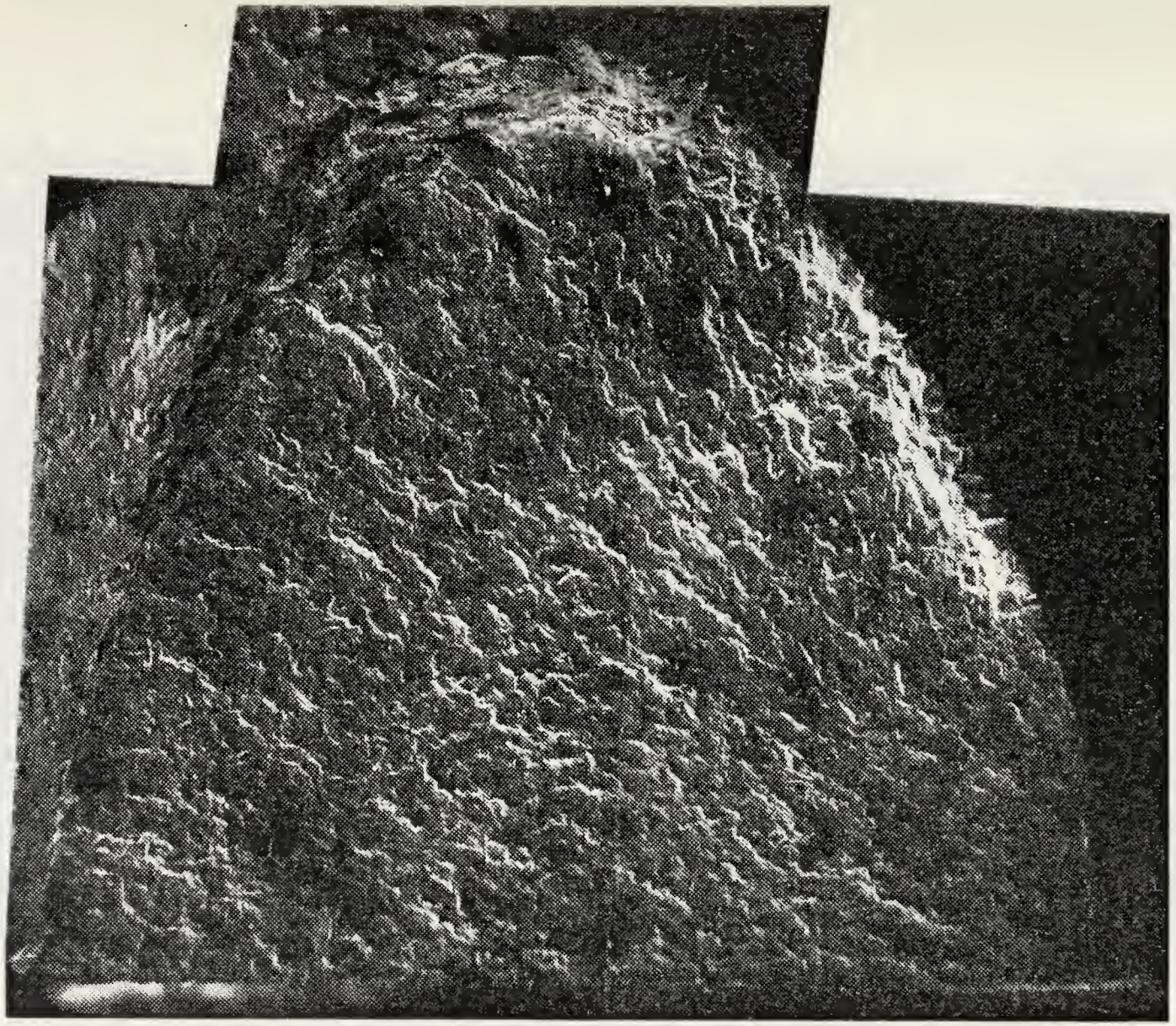

Figure 48. 1/2 Fracture Surface of Annealed Material Subjected to Changing Frequencies in Air. Specimen No. 12 (26x).

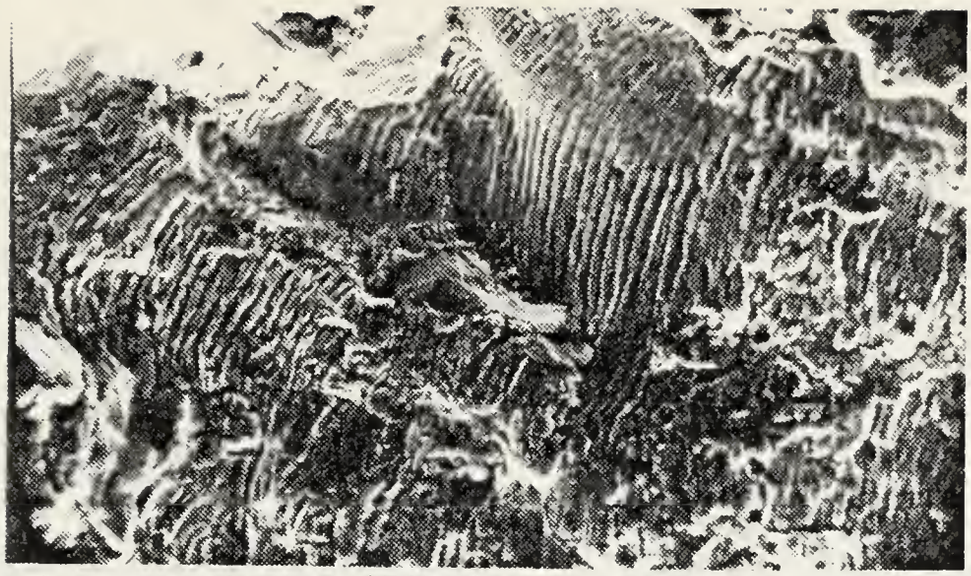

a) ν = 0.25 Hz (730x)

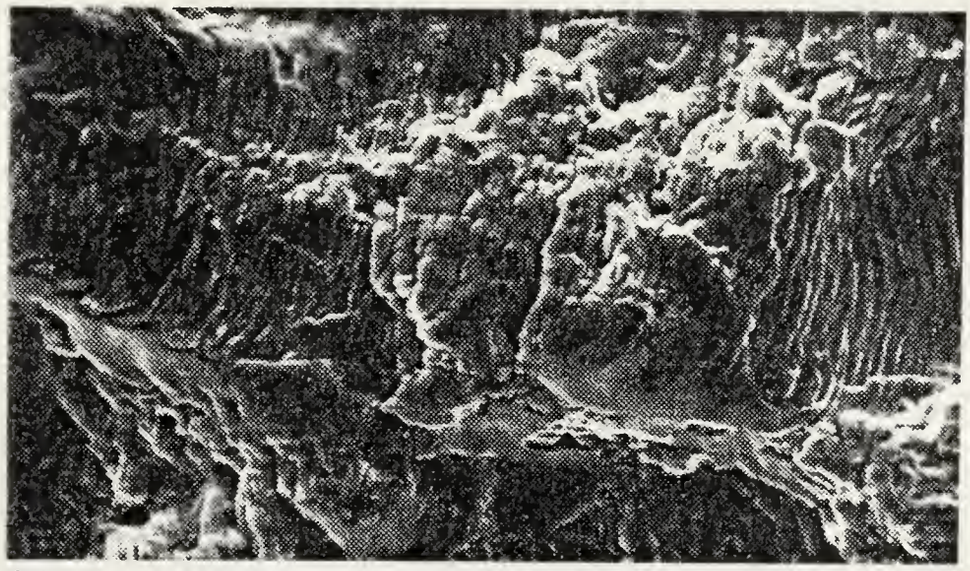

b) ν = 0.05 Hz (770x)

c) ν = 0.025 Hz (665x)

Figure 49. Fractographs of Annealed Material Continuously Cycled at Various Frequencies in Air. Specimen No. 12.

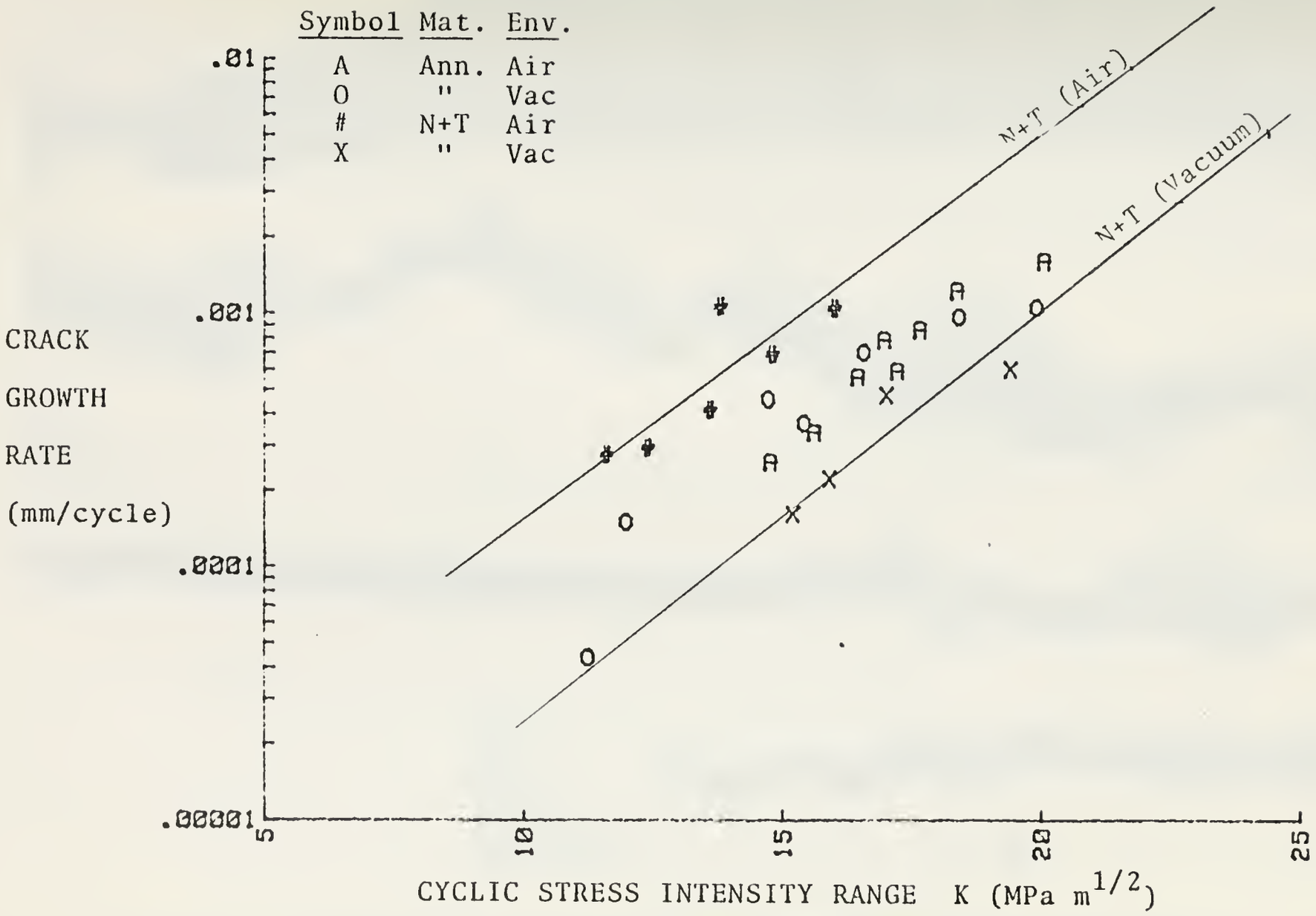

Figure 50. LEFM Data. Continuous Cycling at 10^{-2} Hz.

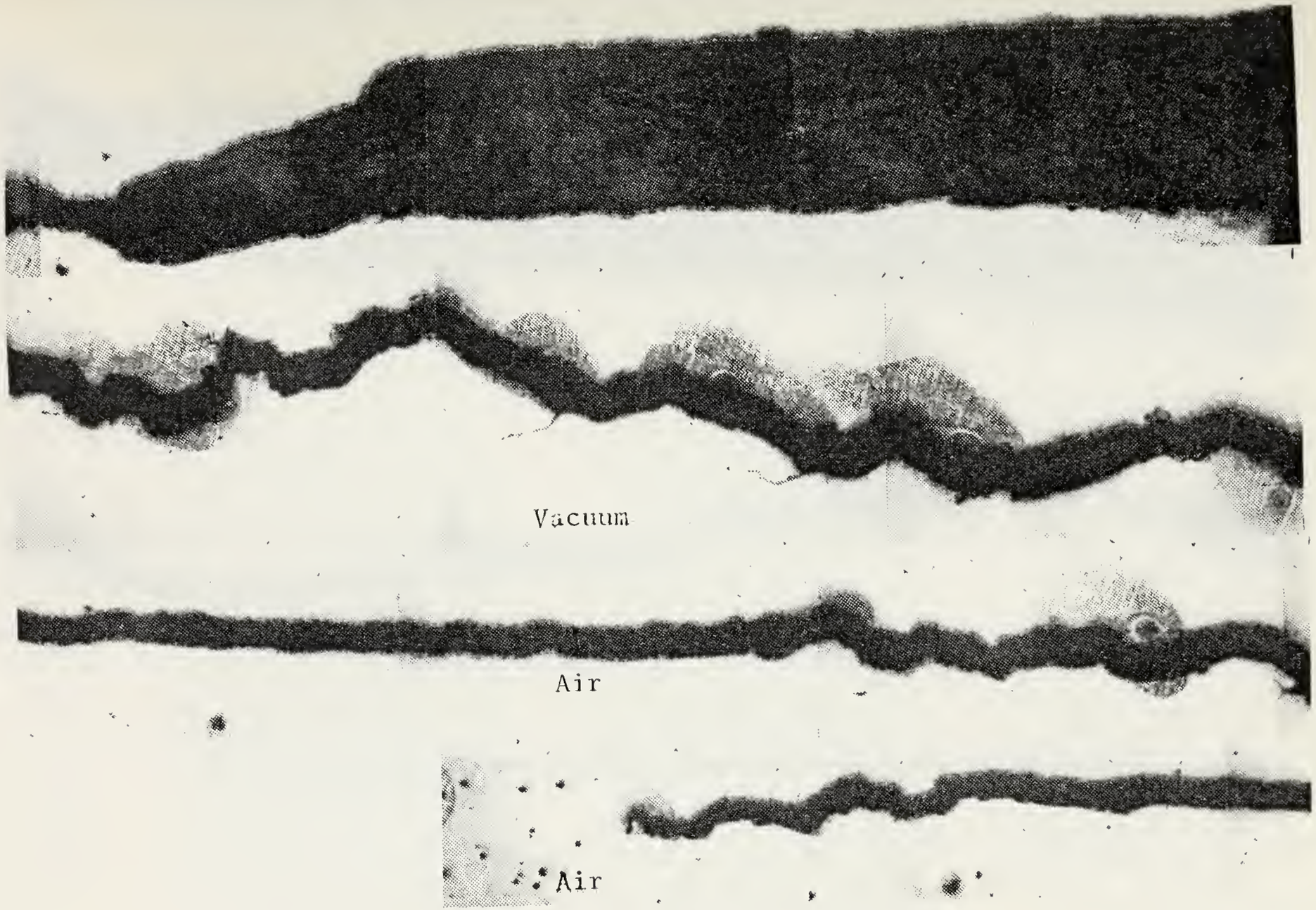

Figure 51. LEFM Crack Profile of Reannealed UKAEA Material (64x). Specimen No. 8.

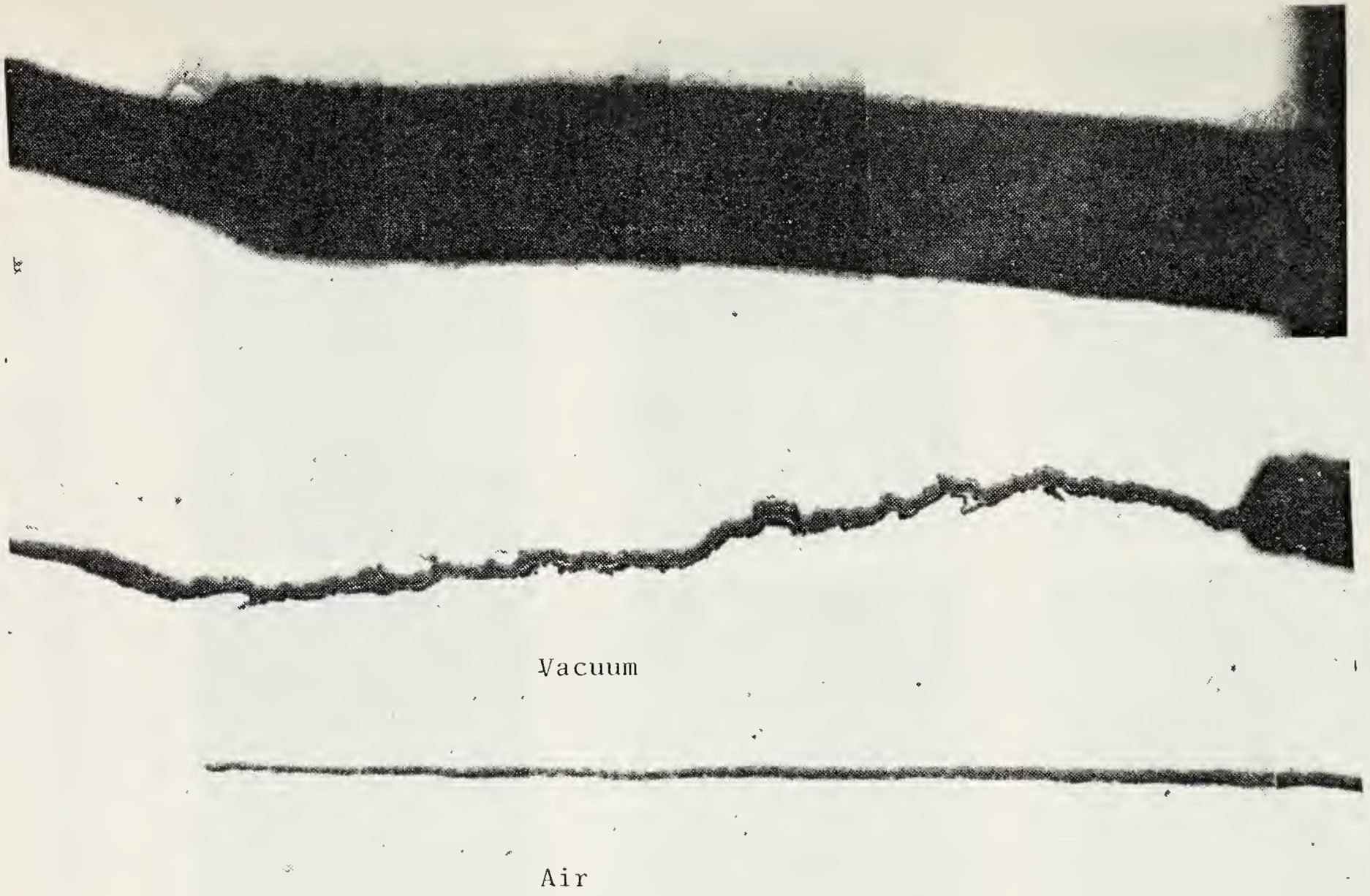

Figure 52. LEFM Crack Profile of Normalized and Tempered Material (64x). Specimen No. 10.

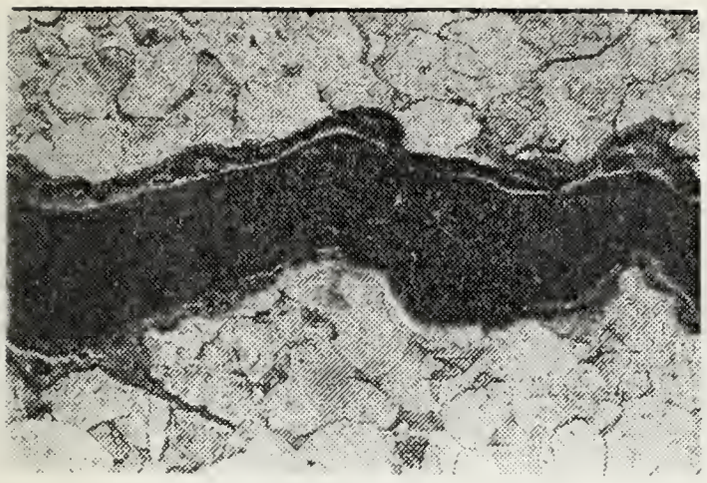

Vacuum Region (126x)

Vacuum Region (126x)

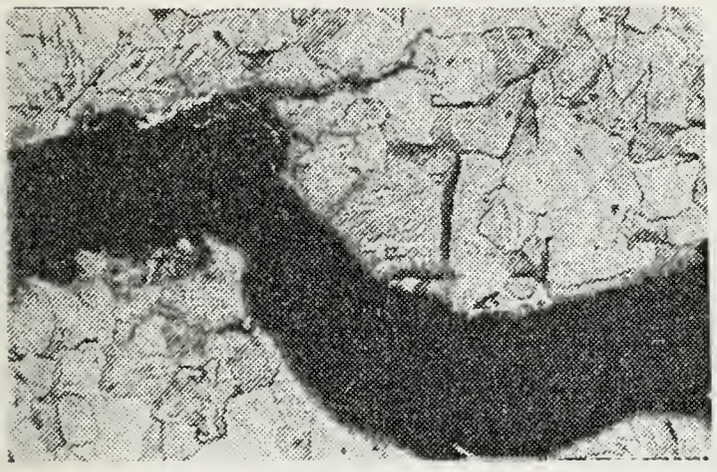

Vacuum Region (126x)

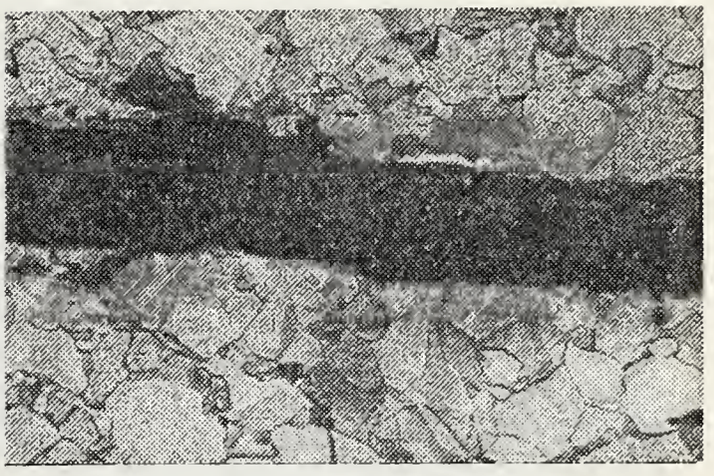

Vacuum Region (126x)

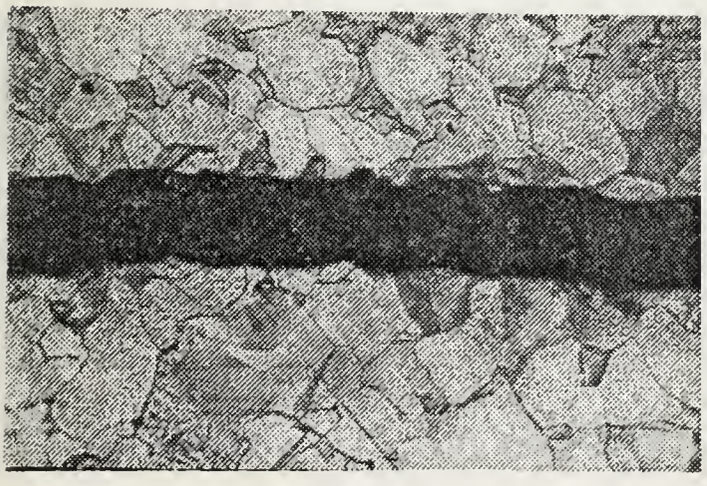

Air Region (126x)

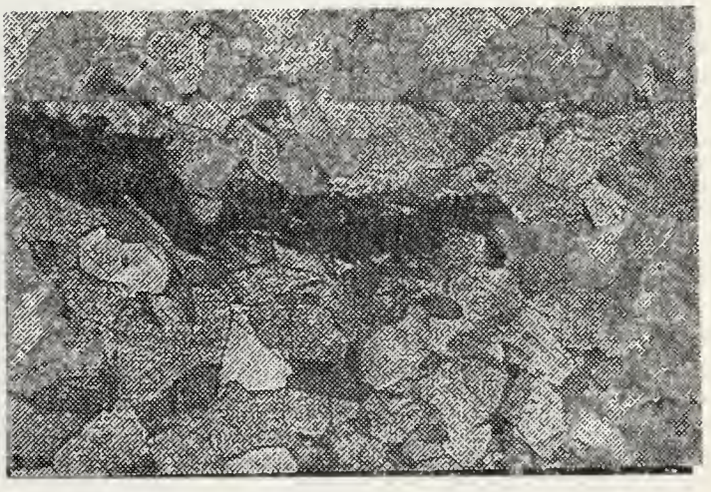

Air Region (126x)

Figure 53. LEFM Micrographs of Reannealed Material. Air and Vacuum Regions of the Crack are Shown. Specimen No. 8.

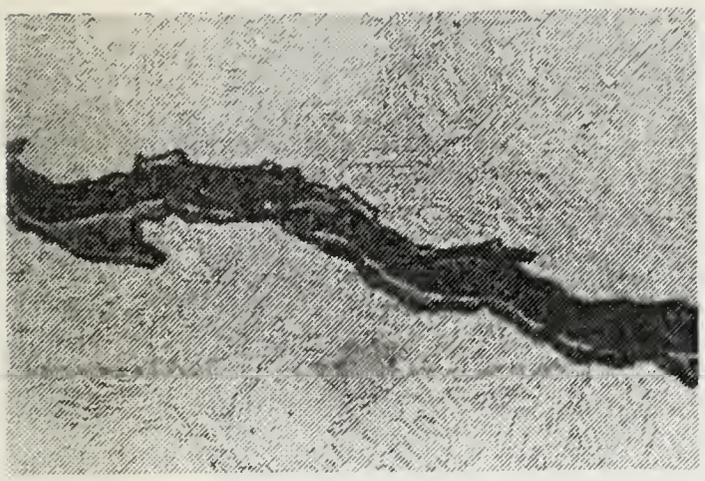

Vacuum Region (126x)

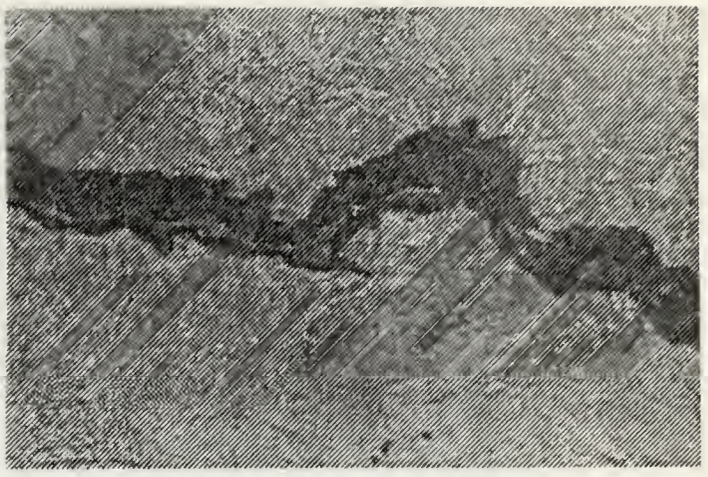

Vacuum Region (126x)

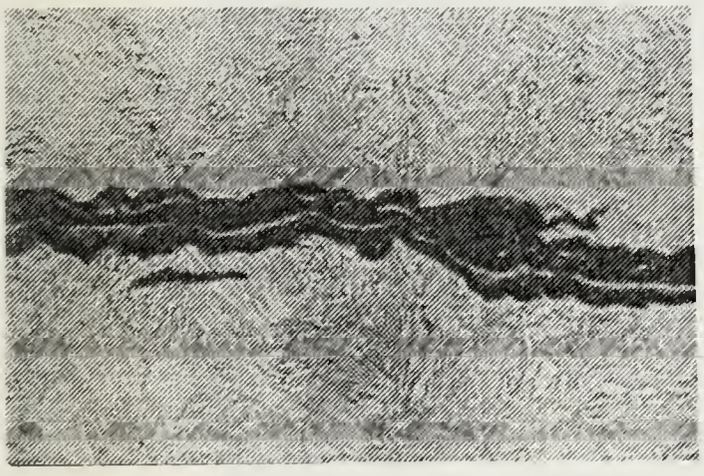

Vacuum Region (126x)

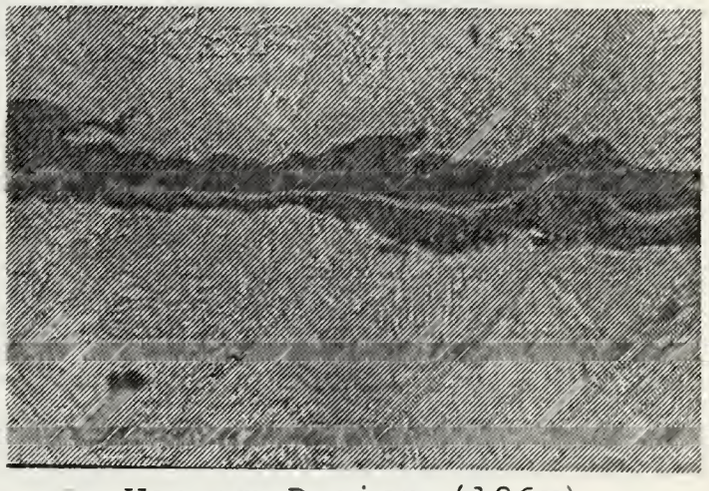

Vacuum Region (126x)

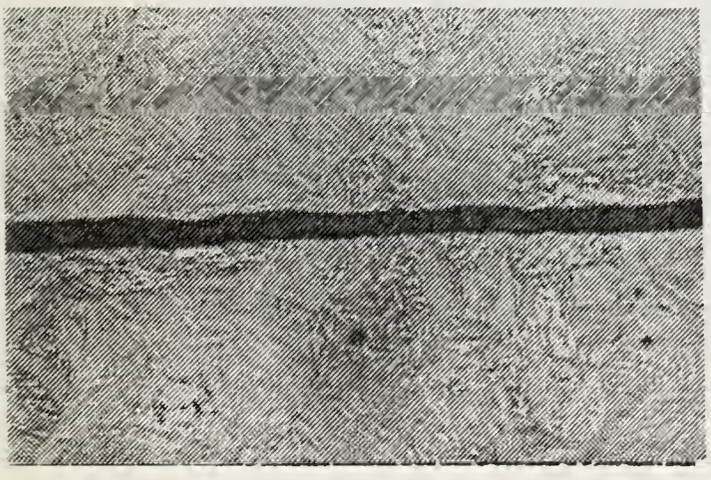

Air Region (126x)

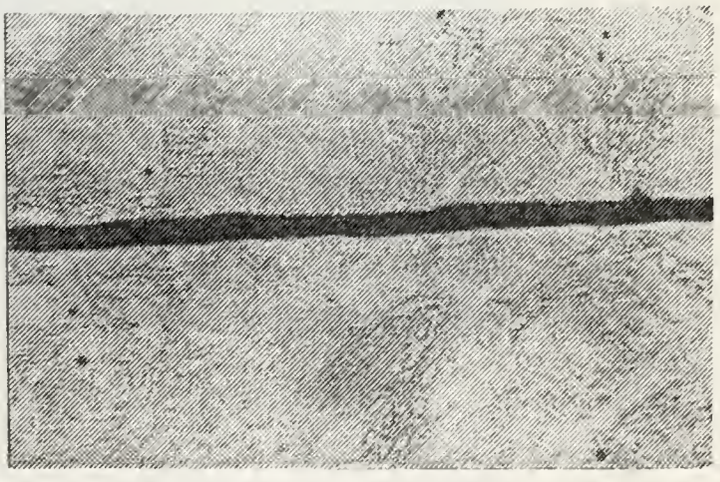

Air Region (126x)

Figure 54. LEFM Micrographs of Normalized and Tempered Material. Air and Vacuum Regions of the Crack are Shown. Specimen No. 10.

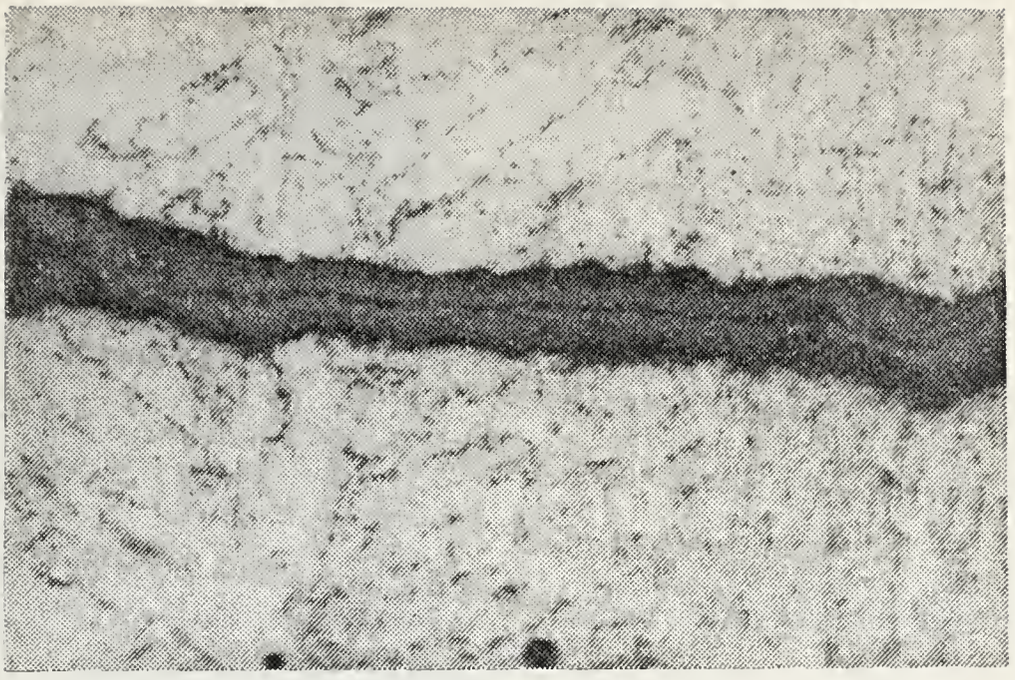

a) Air Region Near Crack Tip

b) Crack Tip (1500x). Crack Oxide Fills the Crack Tip.

Figure 55. LEFM Crack Tip in Normalized and Tempered Material. Specimen No. 10.

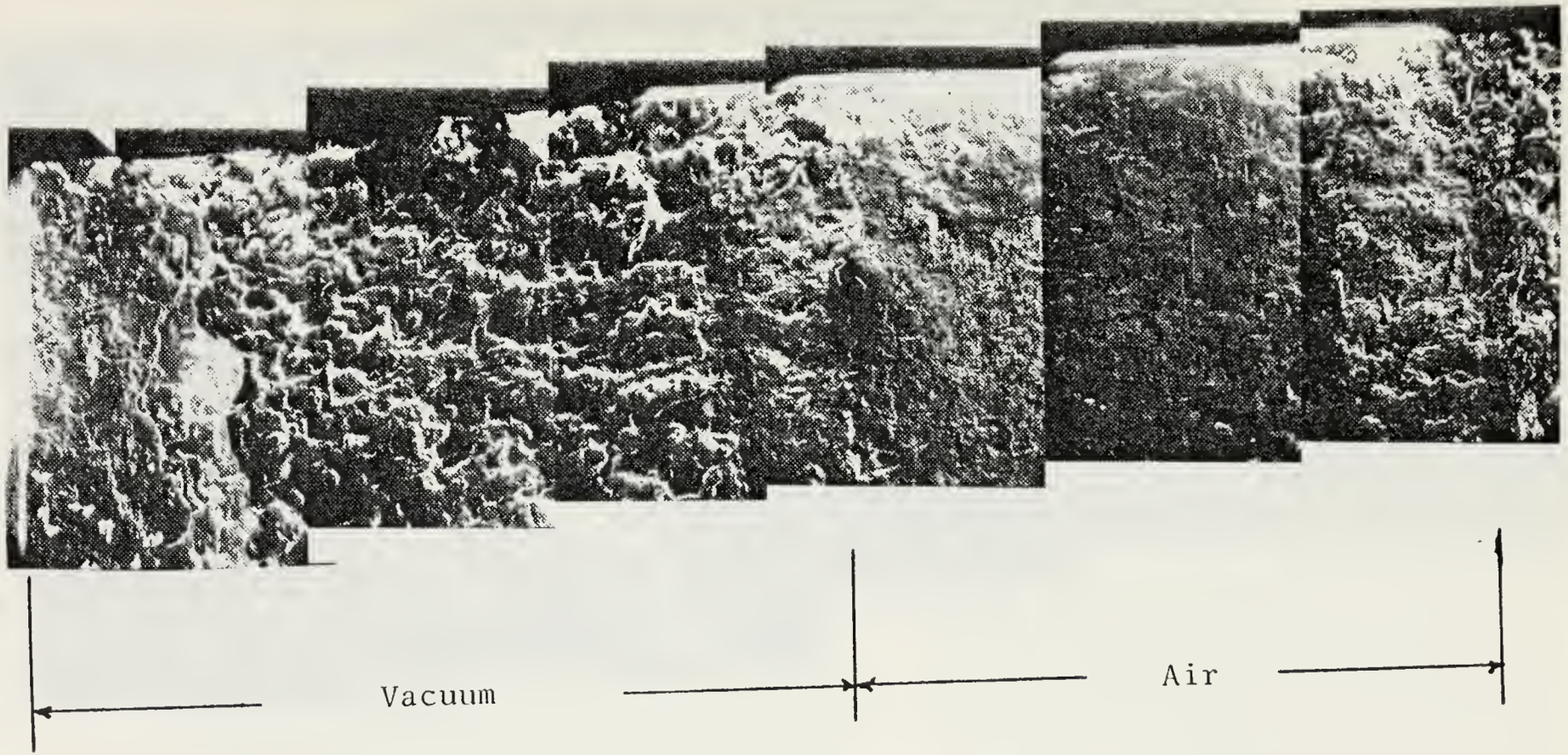

Figure 56. LEFM Fracture Surface of Annealed Material (18x). Specimen No. 8.

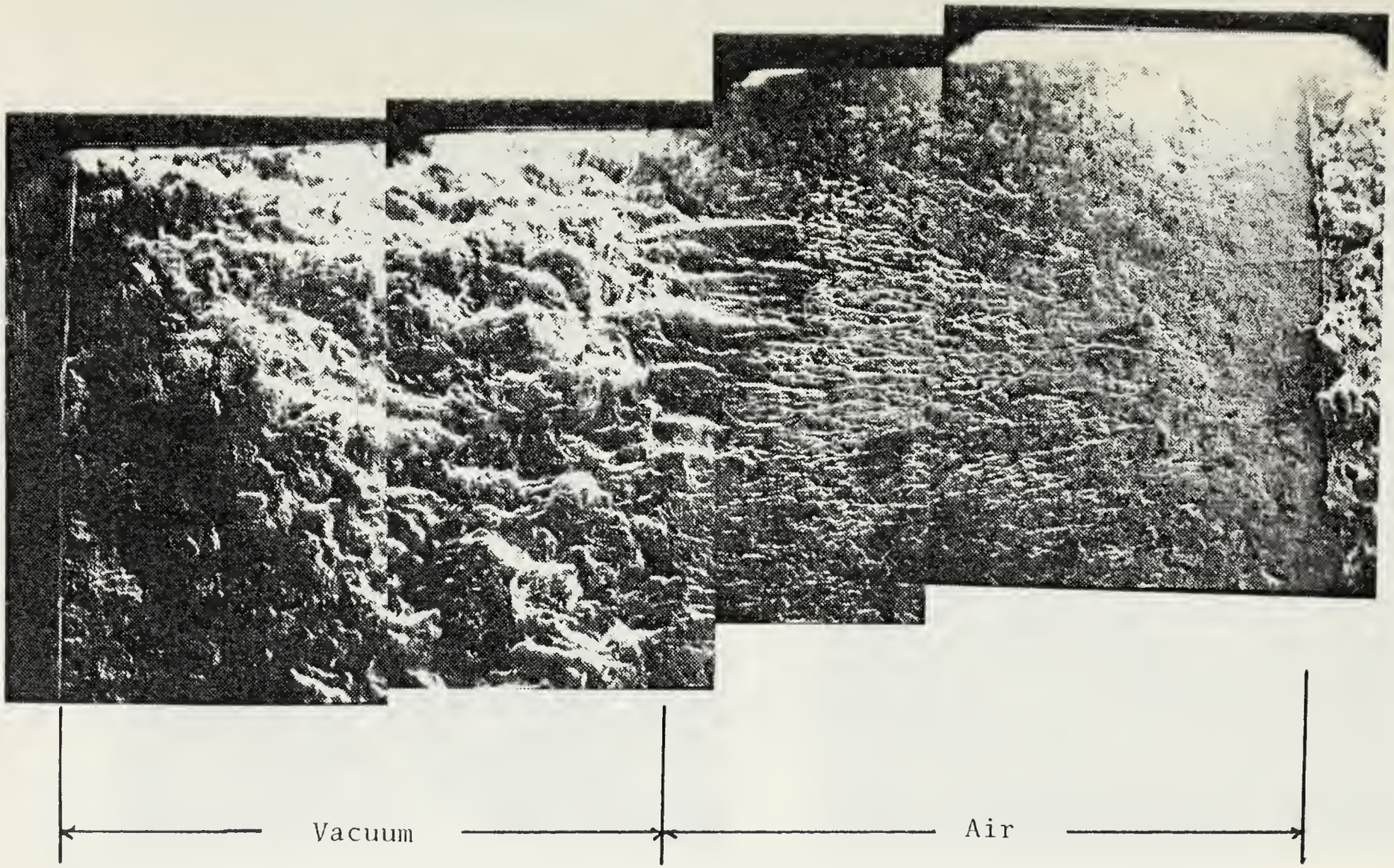

Figure 57. LEFM Fracture Surface of Normalized and Tempered Material (20x). Specimen No. 10.

a) Air Region Near End of Crack (600x)

b) Vacuum Region (600x)

Figure 58. LEFM Fractographs of Annealed Material. Vacuum and Air Regions are shown. Specimen No. 8.

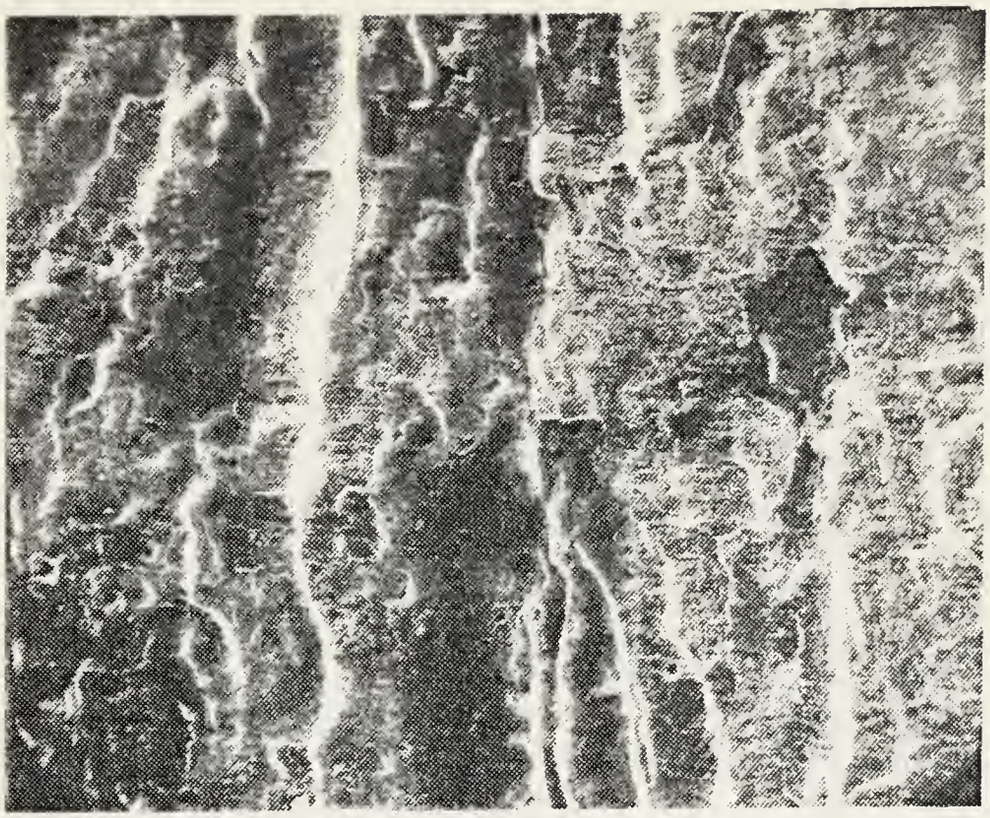

a) Vacuum Region (265x)

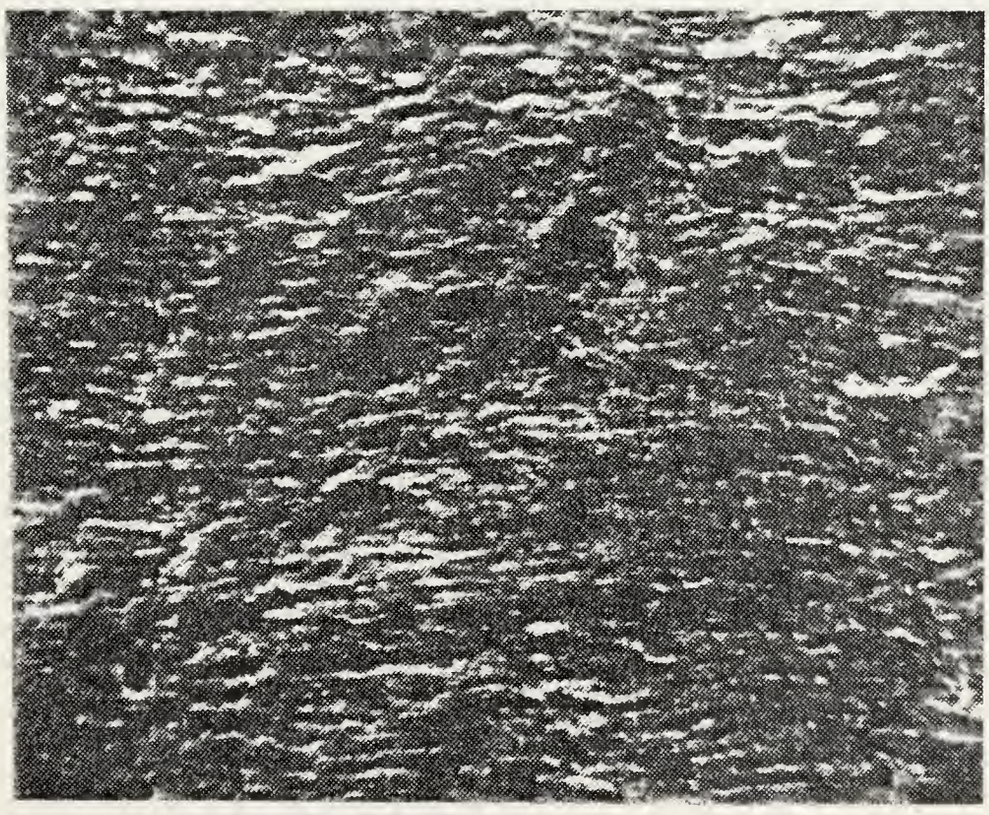

b) Air Region (1300x)

Figure 59. LEFM Fractographs of Normalized and Tempered Material. Vacuum and Air Regions are shown. Specimen No. 10.

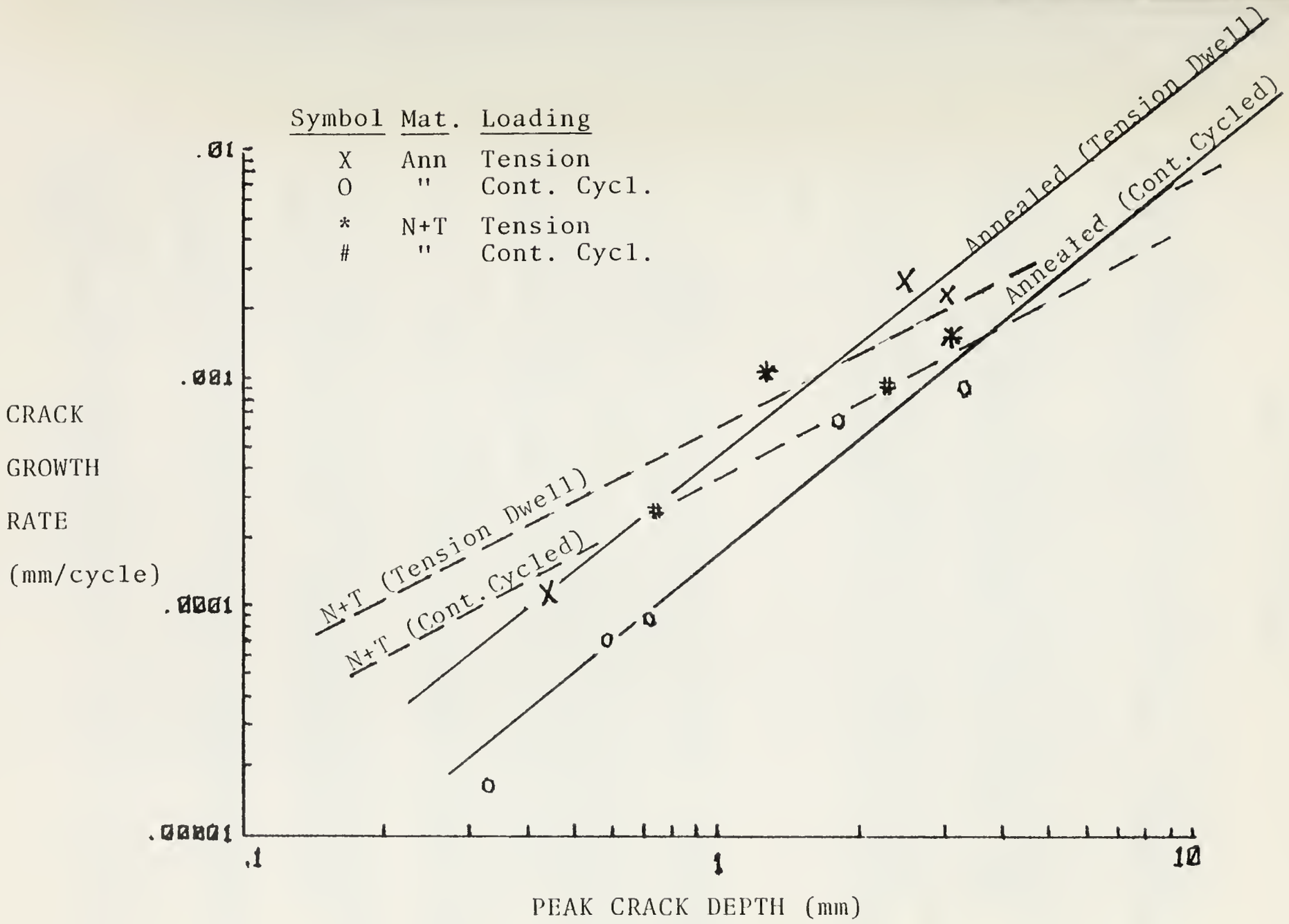

Figure 60. A Comparison of Tension Dwell and Continuous Cycling Data In Vacuum To Show The Effect of Creep in HSF.

LIST OF REFERENCES

1. W. B. Jones, J. A. Van Den Avyle, "Substructure and Strengthening Mechanisms in 2.25 Cr - 1 Mo Steel at Elevated Temperatures," Metallurgical Transactions A, Vol. 11A, p. 275, 1980.

2. C. R. Brinkman, "Creep-Fatigue Effects in Structural Materials Used in Advanced Nuclear Power Generating Systems," Proceedings of the 27th Sagamore Army Materials Research Conference, July 14-18, 1980.

3. R. H. Cook, R. P. Skelton, "Environmental-Dependence of the Mechanical Properties of Metals at High Temperature," International Metallurgical Reviews, Vol. 19, p. 199, 1974.

4. Ibid.

5. Ibid.

6. L. F. Coffin, "High Temperature Fatigue," Transactions of the American Society of Metals, Vol. 56, p. 339, 1963.

7. D. J. White, "Effect of Environment and Hold Time on the High Strain Fatigue Endurance of 1/2 Percent Molybdenum Steel," Proceedings of Institution of Mechanical Engineers, Vol. 184, p. 223, 1969.

8. D. C. Lord, L. F. Coffin, Jr., "Low Cycle Fatigue Hold Time Behavior of Cast Rene 80," Metallurgical Transactions, Vol. 4, p. 1647, July 1973.

9. J. R. Haigh, R. P. Skelton, C. E. Richards, "Oxidation-Assisted Crack Growth During High Cycle Fatigue of a 1 Cr-Mo-V Steel at 500C," Materials Science and Engineering, Vol. 26, p. 167-174, 1976.

10. R. P. Skelton, "Crack Growth During High Strain Fatigue of 0.5 Cr-Mo-V Steel at 825 °K," Material Science Engineering, Vol. 32, p. 211-219, 1978

11. H. Teranashi, A. J. McEvily, "The Effect of Oxidation on Hold Time Fatigue Behavior of 2.25 Cr - 1 Mo Steel," Metallurgical Transactions, Vol. 10A, p. 1806, November 1979.

12. R. P. Skelton, J. R. Haigh, "Fatigue Crack Growth Rates and Thresholds in Steels Under Oxidizing Conditions," Materials Science and Engineering, Vol. 36, p. 17-25, 1978.

13. C. R. Brinkman, J. P. Strizak, M. K. Booker, C. E. Jaske, "Time-Dependent Strain Controlled Fatigue Behavior of Annealed 2 1/4 Cr - 1 Mo Steel for use in Nuclear Steam Generator Design," Journal of Nuclear Materials, Vol. 62, pp. 181-204, 1976.

14. K. D. Challenger, A. K. Miller, C. R. Brinkman, "An Explanation for the Effect of Hold Periods on the Elevated Temperature Fatigue Behavior of 2.25 Cr - 1 Mo Steel," Journal of Engineering Materials and Technology, Vol. 103, p. 7-14, 1981.

15. K. D. Challenger, A. K. Miller, R. L. Langdon, "Elevated Temperature Fatigue with Hold Time in a Low Alloy Steel: A Predictive Correlation," Journal of Materials for Energy Systems, Vol. 3, p. 51-61, 1981.

16. C. A. Zapffe, C. O. Worden, "Fractographic Registrations of Fatigue," Trans. of ASM, Vol. 43, p. 958, 1951.

17. P. J. E. Forsyth, D. A. Ryder, "Some Results Derived from the Microscopic Examination of Crack Surfaces," Aircraft Engineering, Vol. 32, p. 96, April 1960.

18. P. J. E. Forsyth, D. A. Ryder, "Some Results of the Examination of Aluminum Alloy Specimen Fracture Surfaces," Metallurgical, Vol. 63, p. 117, March 1961.

19. R. W. Hertzberg, Deformation and Fracture Mechanics of Engineering Materials, p. 480, Wiley, 1976.

20. R. P. Skelton, J. I. Bucklow, "Cyclic Oxidation and Crack Growth During High Strain Fatigue of Low Alloy Steel," Metal Science, Vol. , p. 64-70, Feb. 1978.

21. R. P. Skelton, K. D. Challenger, "Effect of Environment and Dwell During Fatigue Crack Growth of 2 1/4 Cr - 1 Mo at 525C," Central Electricity Generating Board Memo, Nov. 1982.

INITIAL DISTRIBUTION LIST

		No. Copies
1.	Defense Technical Information Center Cameron Station Alexandria, Virginia 22314	2
2.	Library, Code 0142 Naval Postgraduate School Monterey, California 93940	2
3.	Department Chairman, Code 69 Department of Mechanical Engineering Naval Postgraduate School Monterey, California 93940	1
4.	Professor K. D. Challenger, Code 69Ch Department of Mechanical Engineering Naval Postgraduate School Monterey, California 93940	5
5.	Lt. John S. Kamen, USN 17 Kent Place Cos Cob, Connecticut 06870	4

Thesis
K1244 Kamen
c.1 The effects of environment and dwell on high temperature fatigue crack growth of 2 1/4 Cr - 1 Mo steel.